12-23-64
126

SECRET
CONFIDENTIAL

UNCLASSIFIED

MASTER

NAA-SR-8617
VOLUME II
SNAP REACTOR,
SNAP PROGRAM
M-3679 (36th Ed.)
COPY 126 OF 280
129 PAGES
SERIES A

SNAP TECHNOLOGY HANDBOOK
VOLUME II
HYDRIDE FUELS AND CLADDINGS
(Title Unclassified)

Compiled and Edited By
G.F. BURDI

Contributors
H.W. CARPENTER
L.B. LUNDBERG
L.R. STEELE
J.D. WATROUS

ATOMICS INTERNATIONAL
A DIVISION OF NORTH AMERICAN AVIATION, INC.
P.O. BOX 309 CANOGA PARK, CALIFORNIA

CONTRACT: AT(11-1)-GEN-8
ISSUED: NOVEMBER 15, 1964

DISCLAIMER

[redacted] [redacted]

LEGAL NOTICE

This report was prepared as an account of Government sponsored work. Neither the United States, nor the Commission, nor any person acting on behalf of the Commission:

A. Makes any warranty or representation, express or implied, with respect to the accuracy, completeness, or usefulness of the information contained in this report, or that the use of any information, apparatus, method, or process disclosed in this report may not infringe privately owned rights; or

B. Assumes any liabilities with respect to the use of, or for damages resulting from the use of information, apparatus, method, or process disclosed in this report.

As used in the above, "person acting on behalf of the Commission" includes any employee or contractor of the Commission, or employee of such contractor, to the extent that such employee or contractor of the Commission, or employee of such contractor prepares, disseminates, or provides access to, any information pursuant to his employment or contract with the Commission, or his employment with such contractor.

Printed in USA **Price** $2.45 **Available from the**

U. S. Atomic Energy Commission
Technical Information Extension,
P. O. Box 1001
Oak Ridge, Tennessee.

Please direct to the same address inquiries covering the procurement of other classified AEC reports.

[redacted] [redacted]

DISTRIBUTION

SYSTEMS FOR NUCLEAR AUXILIARY POWER (SNAP)-REACTOR SNAP PROGRAM M-3679 (36th Ed.)

	Copy No.
Aerojet-General Corporation (NASA)	1-6
Aerojet-General Corporation, Sacramento	7
Aerojet-General Nucleonics	8
Aeronautical Systems Division	9-10
Aerospace Corporation	11
Aerospace Test Wing (AFSC)	12
Air Force Surgeon General	13
Air Force Weapons Laboratory	14-15
AiResearch Manufacturing Company, Phoenix	16
Army Ballistic Research Laboratories	17
Army Missile Command	18
Army Nuclear Defense Laboratory	19
ARO, Inc.	20
Air University Library	21
Argonne National Laboratory	22
Army Combat Developments Command	23
Astropower, Inc.	24
Avco Corporation	25
Battelle Memorial Institute	26
Bendix Corporation (AF)	27
Brookhaven National Laboratory	28
Bureau of Naval Weapons	29-30
Bureau of Ships	31-32
Bureau of Yards and Docks	33
California Patent Group	34
Central Intelligence Agency	35
Chicago Patent Group	36
Defense Atomic Support Agency, Sandia	37
Department of the Army	38
Director of Defense Research and Engineering (OAP)	39
Edgerton, Germeshausen and Grier, Inc. Goleta	40
Foreign Technology Division (AFSC)	41
General Atomic Division	42
General Dynamics/Astronautics (AF)	43
General Dynamics/Fort Worth	44
General ElectricCompany, Cincinnati	45
General Electric Company (FPD)	46-47
General Electric Company (MSVD)	48
General Electric Company, Richland	49-50
General Electric Company, San Jose	51
General Electric Company, San Jose (AF)	52
General Technologies Corporation	53
Institute for Defense Analysis	54
Ion Physics Corporation	55
Jet Propulsion Laboratory	56-57
Johns Hopkins University (APL)	58
Lockheed-Georgia Company	59
Lockheed Missiles and Space Company	60
Los Alamos Scientific Laboratory	61
Martin-Marietta Corporation, Denver	62
Monsanto Dayton Laboratory	63
Mound Laboratory	64
NASA Ames Research Center	65
NASA Goddard Space Flight Center	66-67
NASA Langley Research Center	68
NASA Lewis Research Center	69-72
NASA Manned Spacecraft Center	73
NASA Marshall Space Flight Center	74
NASA Scientific and Technical Information Facility	75-77
National Aeronautics and Space Administration, Washington	78-79
NASA Western Operations Office	80
Naval Air Development Center	81
Naval Ordnance Laboratory	82-83
Naval Postgraduate School	84
Naval Radiological Defense Laboratory	85
Naval Research Laboratory	86-87
Naval Underwater Ordnance Station	88
Navy Marine Engineering Laboratory	89
New York Operations Office	90
New York Operations Office, Canel Project Office	91
North American Aviation, Inc., Downey	92
Nuclear Metals, Inc.	93
Office of Naval Research	94-95
Office of the Assistant General Counsel For Patents (AEC)	96
Office of the Chief of Engineers	97
Office of the Chief of Naval Operations	98-100
Office of the Chief of Naval Operations (OP-03EG)	101-102
Office of the Chief of Transportation	103
Phillips Petroleum Company (NRTS)	104-107
Pratt and Whitney Aircraft Division	108
Pratt and Whitney Aircraft Division (NASA)	109
Rand Corporation	110
Republic Aviation Corporation	111
Sandia Corporation	112
School of Aerospace Medicine	113
Union Carbide Corporation (ORNL)	114-121
USAF Headquarters	122
University of California, Livermore	123
Westinghouse Electric Corporation, Lima (AF)	124
Westinghouse Electric Corporation, (NASA)	125
Division of Technical Information Extension	126-165
AI Library (Includes 2 copies to CPAO, 2 copies to AEC, Washington, 2 copies to COO)	166-280

INSERT LATEST PAGES. DESTROY SUPERSEDED PAGES.

LIST OF EFFECTIVE PAGES

NOTE: The portion of the text affected by the changes is indicated by a vertical line in the outer margin of the page.

TOTAL NUMBER OF PAGES IN THIS PUBLICATION IS 129 CONSISTING OF THE FOLLOWING:

*The asterisk indicates pages changed, added, or deleted by the current change

ADDITIONAL COPIES OF THIS PUBLICATION MAY BE OBTAINED FROM ATOMICS INTERNATIONAL

A A

CONTENTS

CONTENTS

TABLES

TABLES

FIGURES

FIGURES

FIGURES

FIGURES

ABSTRACT

This report contains currently available property data on zirconium and yttrium hydride fuels and associated cladding (Hastelloy N, X, and R-235, Rene 41, TD Nickel, and TZM) and coating materials. Also included is a brief description and status summary of SNAP 2, 8, and 10A fuel elements. This handbook is one of three being compiled under the direction of the Atomics International SNAP General Supporting Technology Program. NAA-SR-8617, Vol I, issued August 1, 1964, contains information on the current status of the Liquid Metals Technology. NAA-SR-8617, Volume III, to be published, will contain information on refractory fuels and claddings.

INTRODUCTION

Since the nuclear fuel is the heart of any reactor system, a thorough knowledge of relevant fuel and cladding properties is a fundamental requirement of effective reactor design. The purpose of this Handbook is to collect most of the available property and performance data and present this information in a consistent and systematic form as an aid to engineers designing compact nuclear reactors. To facilitate the addition of information, a loose-leaf format has been adopted. Periodic revisions will be performed to incorporate current property data in this SNAP TECHNOLOGY HANDBOOK.

The reader needing more information on zirconium hydrides than what is given in this handbook is referred to "Bibliographical Survey of Uranium-Zirconium Studies," by A. W. Barsell, L. D. Montgomery, and J. T. Roberts, report NAA-SR-9525.

1.0 ZIRCONIUM ALLOY HYDRIDES

1.1 PHYSICOCHEMICAL PROPERTIES

1.1.1 Physical

1.1.1.1 Phase Diagram

The binary zirconium-hydrogen system has been studied extensively (one of the earliest surveys of work conducted on this system was compiled by Gilbert[1.1]), while the ternary zirconium-uranium-hydrogen system has been studied on a much smaller scale. A composite zirconium-hydrogen phase diagram is shown in Figure 1.1.1, based upon work performed and/or summarized by Libowitz[1.2] and Beck.[1.3] One major controversial area includes the two phase $\delta + \epsilon$ region, which is bounded by dotted lines; recent investigations have shown that the transformation from $\delta + \epsilon$ is martensitic in nature, thus prohibiting the presence of a two phase region. Due to inhomogeneities most metallographic and x-ray investigations show the coexistence of the two phases in the dotted region.

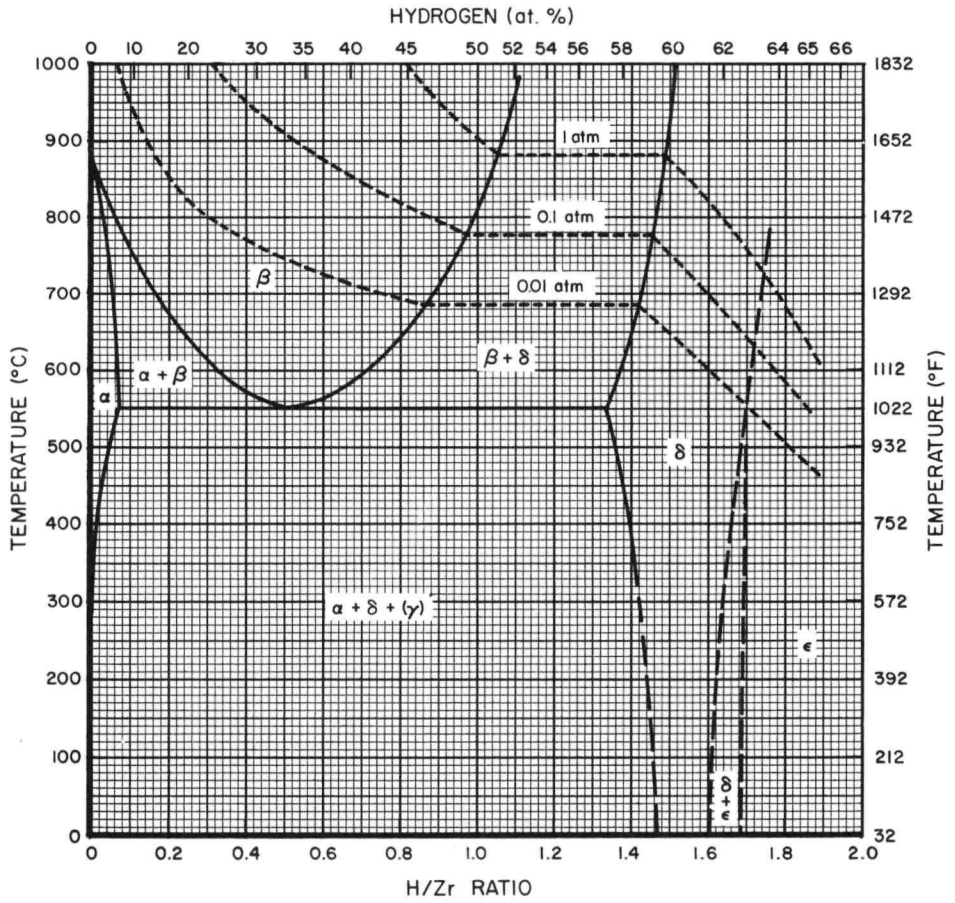

8-11-64 7569-01647

Figure 1.1.1. Zirconium-Hydrogen Phase Diagram

A second controversial area is the presence of a γ phase within the $\alpha + \delta$ region. Beck[1.3] claims that γ is a metastable decomposition product of δ produced by a diffusion controlled shear mechanism. Work by Sidhu[1.4] using neutron diffraction studies of ZrH_x confirms the existence of

the γ phase at temperatures below 265°C. Sidhu claims that the hydrogen atoms in the FCT (face-centered-tetragonal) γ phase takes on ordered positions in the zirconium lattice while the FCC (face-centered-cubic) δ phase contains the hydrogen in random positions. Motz[1.5] also confirms the existence of the FCT phase at these temperatures, but his phase diagram interpreting the information is incorrect. In the ϵ phase the apparent maximum hydrogen content is approximately 1.986 H/Zr with the reason for this lack of stoichiometry from ZrH_2 not completely understood.[1.2]

The ternary zirconium-uranium-hydrogen system has been studied using elevated temperature x-ray diffraction[1.6] and pressure-temperature-composition relationships.[1.6, 1.7, 1.8] Both types of studies result in the same general conclusions that at elevated temperatures a second beta (β) phase, probably uranium rich, forms which in turn decomposes at higher hydrogen levels to the delta (δ) hydride and finely precipitated elemental uranium. Also boundaries for the zirconium-hydrogen α, δ, and ϵ phases are relatively unaffected by the addition of uranium; therefore, the basic zirconium-hydrogen phase diagram may be used in these regions.

1.1.1.2 Crystal Structure

Only a small amount of hydrogen is soluble in the close-packed-hexagonal (CPH) α phase zirconium which causes an expansion of the lattice.[1.3] The high temperature body-centered-cubic (BCC) β phase has a much higher solubility for hydrogen than before any transformation occurs. The δ phase hydride has a FCC lattice which remains relatively constant in size at all compositions.[1.3, 1.9] The FCT ϵ phase has continuously changing lattice dimensions. Figure 1.1.2 illustrates the above facts.

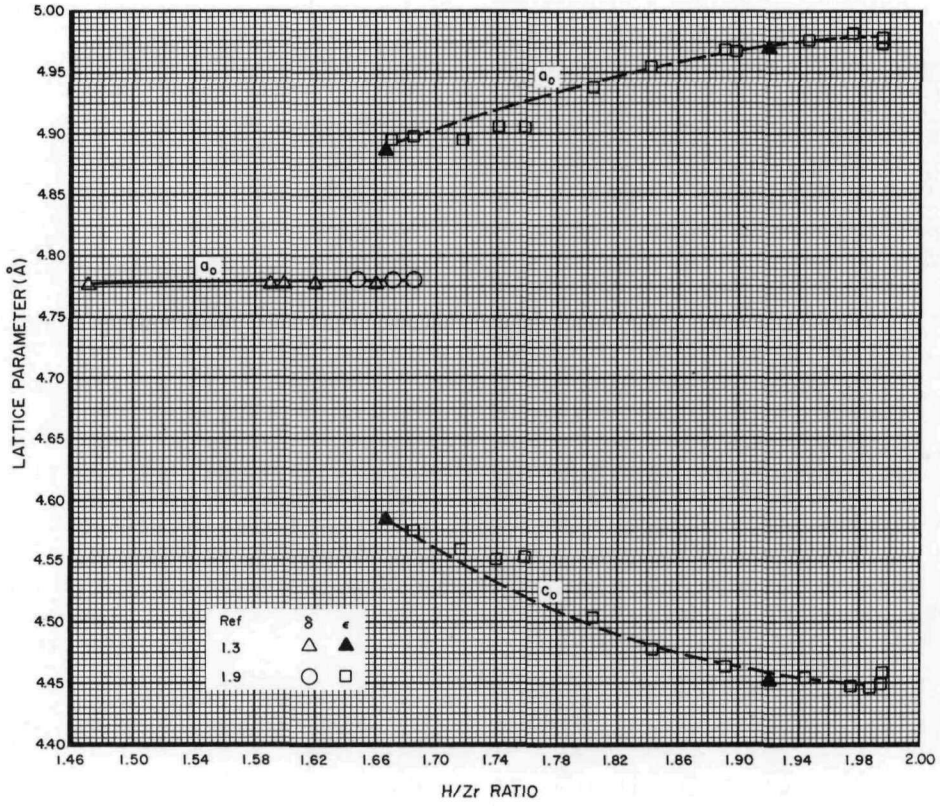

8-11-64 7569-01648

Figure 1.1.2. Lattice Dimensions of Zirconium-Hydrogen System

Structure of the γ phase has been indexed as both a body-centered-tetragonal (BCC)[1.3] and a FCT structure,[1.10] both of which are the same structure with a $\sqrt{2}$ relationship between the A_o lattice dimension. Table 1.1.1 lists some specific lattice parameters. Lattice dimensions for δ and ϵ phases are also shown in Figure 1.1.2.

TABLE 1.1.1

LATTICE PARAMETERS OF ZIRCONIUM-HYDROGEN SYSTEM

Phase	Structure	H/Zr Ratio	a_o (A)	c_o (A)	Density (gm/cm^3)	Reference
α	CPH	H Saturated	3.2335	5.1520	6.494	1.3
γ	FCT	~1.0	4.5957	4.9686	5.837	1.3
γ	FCT	Not Stated	4.61	4.975	5.79	1.10
δ	FCC	1.59	4.7783	-	5.650	1.3
δ	FCC	1.667	4.7808	-	5.645	1.3
δ	FCC	1.646	4.7808	-	5.645	1.9
δ	FCC	1.670	4.7812	-	5.645	1.9
δ	FCC	Not Stated	4.78	-	5.65	1.10
ϵ	FCT	1.667	4.886	4.582	5.640	1.3
ϵ	FCT	1.670	4.8925	4.5823	5.625	1.9
ϵ	FCT	1.920	4.971	4.452	5.624	1.3
ϵ	FCT	1.945	4.9754	4.4531	5.613	1.9
ϵ	FCT	2.00	4.964	4.44	5.66	1.10

1.1.1.3 Density

The density of zirconium hydride as a function of hydrogen content was obtained from Reference 1.11. The curves for the fuel compositions shown in Figure 1.1.3 were calculated by assuming that the densities of the components do not change when they are mixed together. All compositions are given with respect to the unhydrided fuel (H = 0). The cross hatched areas in the figure represent a range determined by the amounts of α, δ, and γ phase zirconium obtained upon cooling during the production process.

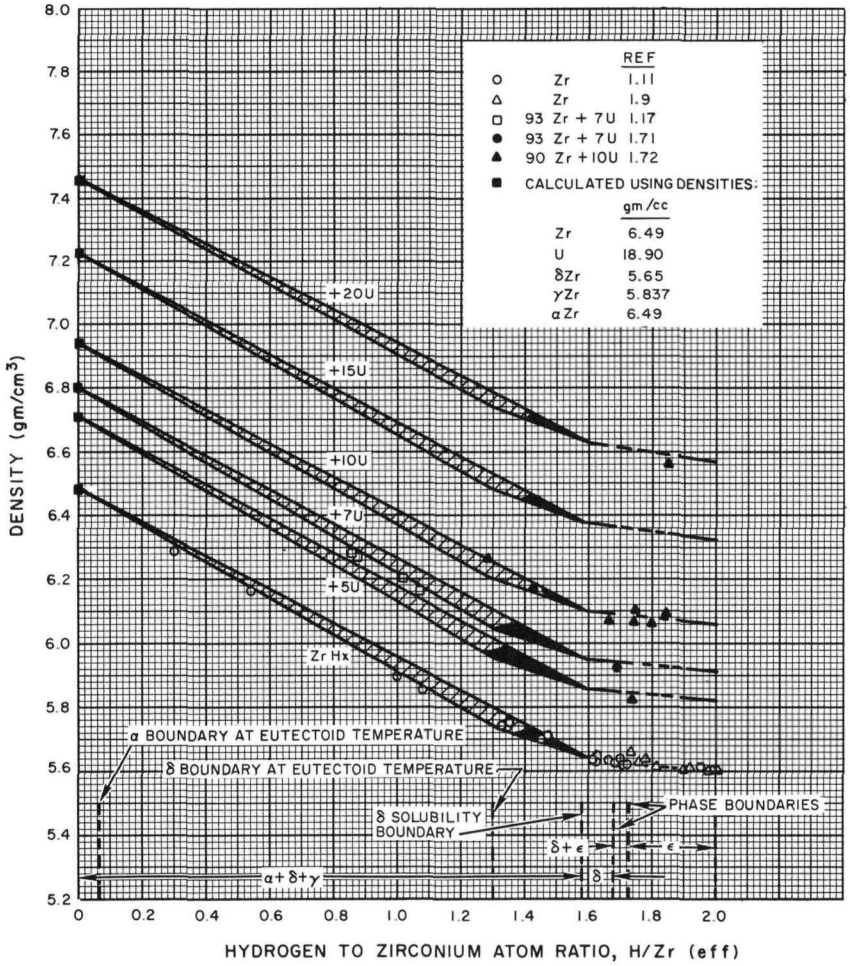

8-14-64 7569-01649

Figure 1.1.3. Room Temperature Density of ZrH Fuel (Ref 1.72)

1.1.1.4 Hydrogen Density

The concentration of hydrogen in the fuel, expressed as the number of hydrogen atoms per cubic centimeter multiplied by 10^{-22}, is called N_H. Figure 1.1.4 shows the dependence of N_H on the atom ratio of hydrogen to metal. This curve is based on the densities of the fuels shown in Figure 1.1.3. At a given value of hydrogen-to-metal-atom ratio, each of the fuels have approximately the same N_H.

In order to convert the H/Zr(eff)* ratios to the H/M† ratios use the following conversion coefficients: for 7% U, H/M = 0.972 H/Zr(eff); 10% U, H/M = 0.959 H/Zr(eff); 15% U, H/M = 0.937 H/Zr(eff); and 15% U, 6.5% Hf, H/M = 0.906 H/Zr(eff). Each conversion coefficient is the ratio of zirconium atoms (not tied up with carbon) to total metal atoms in the fuel.

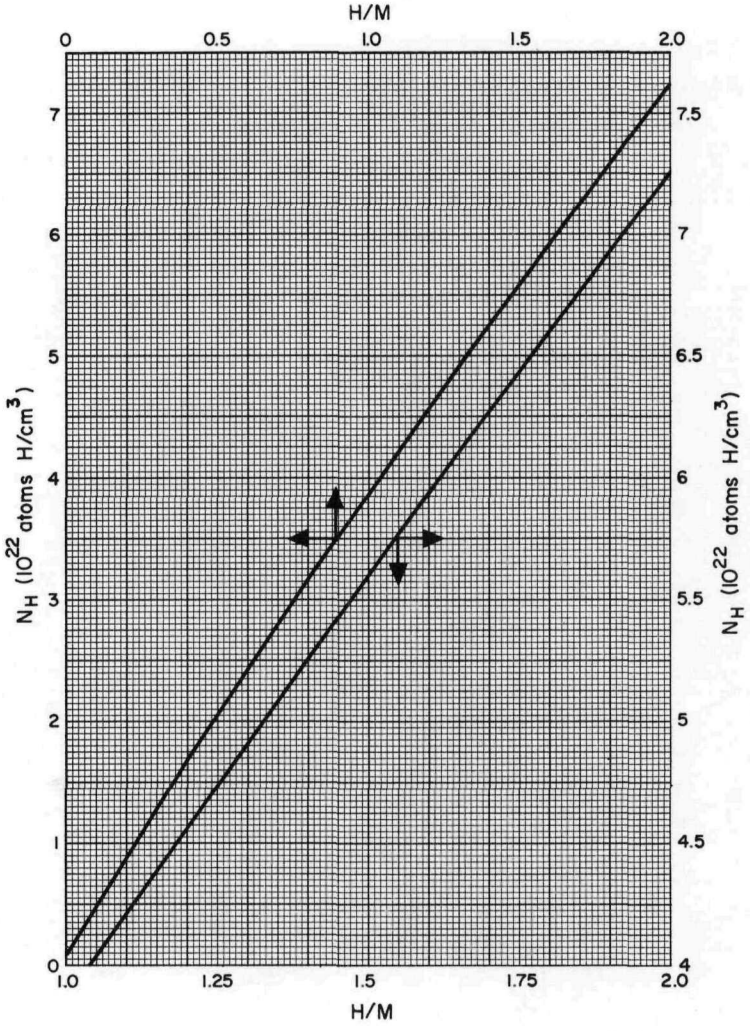

8-14-64 7569-01650

Figure 1.1.4. Hydrogen Density of Zirconium Hydride Fuel at Room Temperature

*H/Zr(effective) atom ratio is understood to mean that the zirconium atoms tied up with carbon (ZrC) is not included in this ratio, as originally outlined in Ref 1.62.
†H/M is the hydrogen-to-metal atom ratio.

1.1.1.5 Conversion Formulas

To convert from the wt % H to the H/Zr_{total} ratio use,

$$H/Zr_{total} = \frac{90.496\ (\text{wt \% H})}{100 - (\text{wt \% H} + \text{wt \% C} + \text{wt \% U})} \quad \ldots(1)$$

Any carbon in the fuel may be present as ZrC. The H/Zr (eff) ratio in the zirconium hydride is obtained by using,

$$H/Zr(\text{eff}) = \frac{90.496\ (\text{wt \% H})}{100 - 8.595\ (\text{wt \% C}) - (\text{wt \% U}) - (\text{wt \% H})} \quad \ldots(2)$$

All compositions in these formulas should be based on the unhydrided fuel. If the wt % of any constituent is known on the basis of hydrided fuel, it can be converted to the unhydrided basis by dividing by the quantity (1 - wt % H/100).

To convert H/Zr_{total} to H/Zr(eff) use,

$$H/Zr(\text{eff}) = H/Zr_{total}\left[\frac{100 - (\text{wt \% H} + \text{wt \% C} + \text{wt \% U})}{100 - (\text{wt \% H} + 8.595\ \text{wt \% C} + \text{wt \% U})}\right] \quad \ldots(3)$$

1.1.2 Electrical

1.1.2.1 Electrical Resistivity

Table 1.1.2 shows the resistivity of zirconium hydride as a function of temperature and composition. As hydrogen is added to zirconium, resistivity increases until a composition of 1.60 H/Zr(eff) is reached. Upon further addition of hydrogen, resistivity decreases. The increase with temperature for all compositions, including the fuel, is almost linear.

TABLE 1.1.2

ELECTRICAL RESISTIVITY OF ZIRCONIUM HYDRIDE
ρ(micro-ohm-cm)

Hydride H/Zr(eff)	Temperature °C								Ref
	25	100	200	300	400	500	600	700	
0.67 - 1.04	55	68	87	105	122	137	-	-	1.12
1.48	65.0	73	89	105	-	-	-	-	1.13
1.54	69.1	-	-	-	-	-	-	-	1.14
1.59	76.4	-	-	-	-	-	-	-	1.14
1.62	74.7	-	-	-	-	-	-	-	1.14
1.63	72.2	-	-	-	-	-	-	-	1.14
1.64	66.6	-	-	-	-	-	-	-	1.14
1.65	63.0	69	80	91	102	114	125	138	1.13
1.81	54.7	-	-	-	-	-	-	-	1.14
1.90	41.9	-	-	-	-	-	-	-	1.14
1.96	25.2	-	-	-	-	-	-	-	1.14
1.70 (15% U, 6.5% Hf)	62.3	71	81.2	91.0	100.3	-	-	-	1.15

TABLE 1.1.3

HALL COEFFICIENT, R_H, 10^{-5} cm^3/coulomb (Ref 1.14)

Sample	Temperature, °K		
	4.2	77	300
$ZrH_{1.54}$	+29.9	+37.3	+34.8
$ZrH_{1.59}$	-	-	+39.0
$ZrH_{1.62}$	-	-	+39.0
$ZrH_{1.63}$	-	+11.2	+21.2
$ZrH_{1.64}$	+39.8	+39.8	+42.0
$ZrH_{1.74}$	-	-32.2	-17.7
$ZrH_{1.81}$	-48.7	-50.4	-39.0
$ZrH_{1.87}$	-	-52.0	-45.8
$ZrH_{1.90}$	-	-66.0	-61.2
$ZrH_{1.96}$	-	-65.9	-67.9

1.1.2.2 Hall Coefficient[1.14]

Values for Hall coefficients of various samples of zirconium hydride are given in Table 1.1.3. A negative Hall coefficient is indicative of majority electron conduction and a positive value is evidence for majority hole conduction.

1.1.3 Thermal

1.1.3.1 Thermal Conductivity

The thermal conductivity of zirconium hydride has been measured, but the data scatter considerably. Only that from Ref 1.15 and 1.16 are shown in Figure 1.1.5, and the data for 0.83 and 1.3 H/Zr(eff) above 1000°F has been discarded because of the large concentration gradients in the test samples. The data for 1.5 H/Zr(eff) indicate that k decreases with temperature. Since the conductivity of uranium increases with temperature, the conductivity of fuel may increase, decrease, or remain constant with temperature depending upon the uranium content. The k for the fuel shown in Figure 1.1.5 increases with temperature above 500°F. Toy and Vetrano[1.17] reported a uniform value of 13 ± 1 Btu/hr-ft-°F for the 90Zr+10U hydride fuel with H/Zr(eff) of 1.7 in the temperature range of 200 to 1200°F.

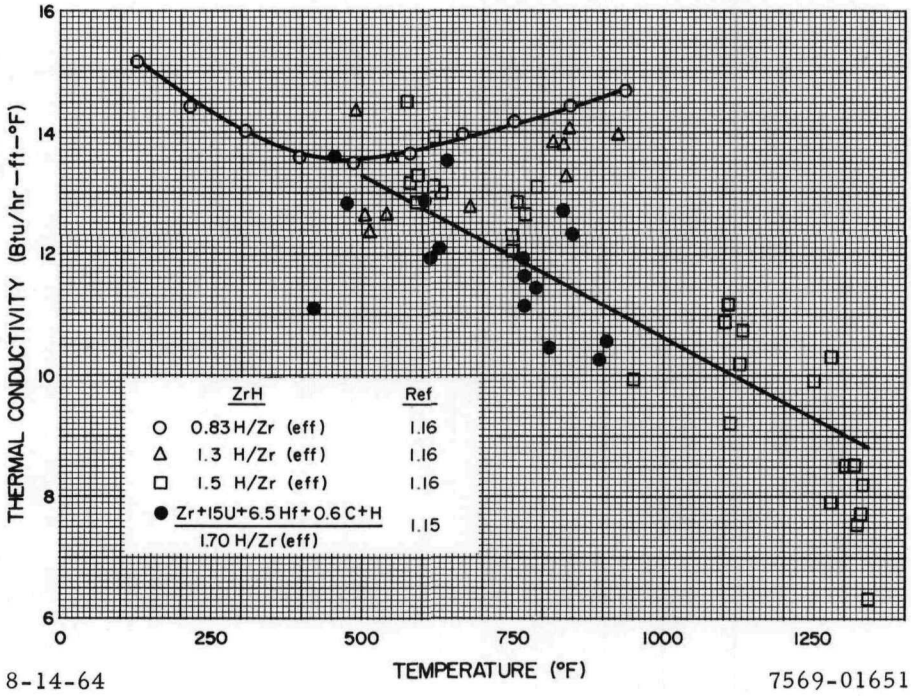

Figure 1.1.5. Thermal Conductivity

1.1.3.2 Specific Heat

The relationship of specific heat to temperature for various compositions of zirconium hydride is shown in Figure 1.1.6. Specific heat increases with hydrogen content; however, abrupt changes are noted at the transition temperature where a phase transformation occurs (1022°F) for H/Zr(eff) < 1.3. No data should be extracted from this figure in the region illustrated by the broken lines, because no measurements were taken during a phase transformation. Since material that goes through a transition is of little use as a fuel, additional data for H/Zr(eff) less than one, reported in Ref 1.12 and 1.16, are not shown here.

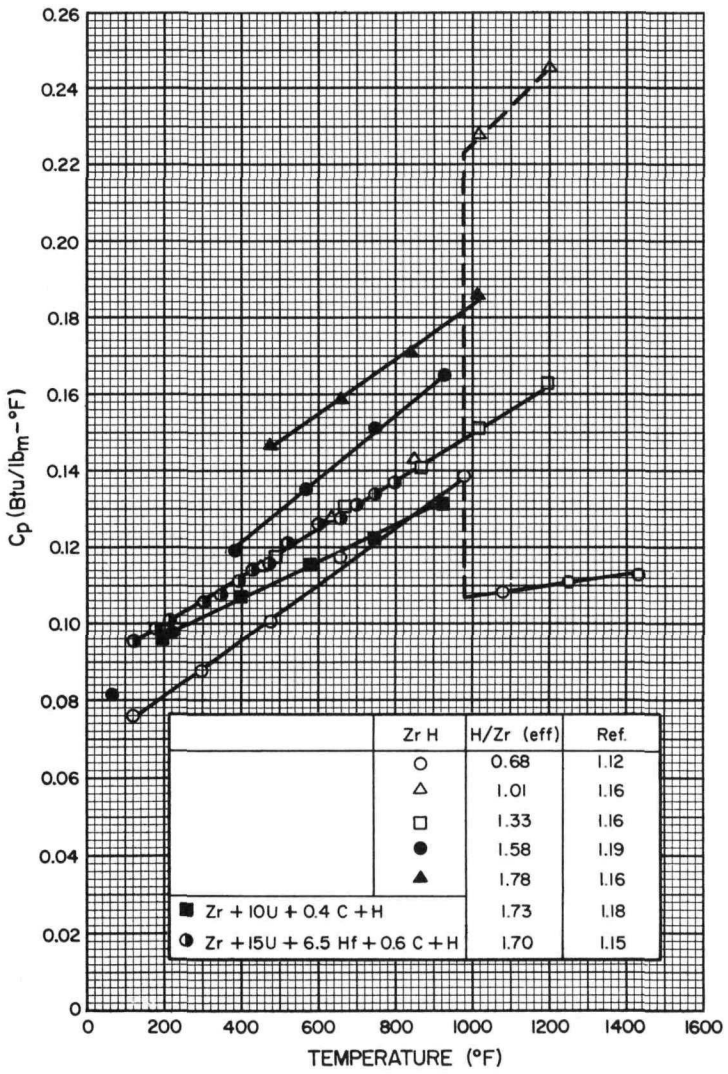

8-14-64 7569-01652

Figure 1.1.6. Specific Heat of Zirconium Hydride Materials

1.1.3.3 Thermal Expansion

The linear thermal expansion of some compositions of zirconium hydride fuel is shown in Table 1.1.4. Since there is an abrupt change in size accompanying a change in phase, values for β-phase hydrides are not reported here. Data on these may be obtained from References 1.16 and 1.20.

TABLE 1.1.4

THERMAL EXPANSION OF ZIRCONIUM HYDRIDE FUEL

Material	H/Zr(eff)	Linear Expansion, $\Delta\ell/\ell$, 10^{-3} in./in., From RT to Temperature, °C (°F)						Ref
		200 (392)	400 (752)	500 (932)	600 (1112)	700 (1292)	800 (1472)	
Zr	0.70	1.2	3.2	4.6	-	-	-	1.16
Zr	1.01	1.2	3.4	5.0	-	-	-	1.16
Zr	1.54	1.2	3.4	4.9	5.6	7.6	9.6	1.16
Zr	1.70	1.13	3.29	4.55	6.09	7.59	-	1.20
Zr	1.83	1.2	3.4	4.9	6.6	-	-	1.16
Zr+7U	0.6 - 1.2	1.11	3.19	4.78	-	-	-	1.20
Zr+7U	1.58	1.18	3.36	4.53	5.83	7.26	8.90	1.20
Zr+7U	1.7 - 1.8	1.18	3.36	4.68	6.10	7.57	9.48	1.20
Zr+15U+6.5Hf	1.70	1.35	3.65	4.90	-	-	-	1.21

1.1.3.4 Thermal Shock[1.22]

Initial thermal shock tests of zirconium hydride fuel were performed in February 1959. In this test a 3/8 in. OD by 2 in. long fuel cylinder (90% Zr + 10% U with $N_H = 6$) was heated to 1300°F in an evacuated silica capsule. The sample was then quenched by crushing the capsule in an ice-brine. Metallographic examination of samples showed that the quench produced many fine hair-line cracks.

Additional thermal shock tests on a similar fuel were performed in late 1959. These experiments consisted of dropping cylinders of fuel, 1/4 in. OD by 2-1/2 in. long, from a furnace at 1200°F into a stagnant pool of eutectic NaK. The temperature of the NaK was reduced on each successive run until 300°F was reached. No cracking or other observable effect on the sample was seen.

In February 1962, small plates (1 by 1 by 0.22 in. and 2 by 4 by 0.22 in.) of fuel were thermally shocked. The three smaller plates were bonded to stainless steel on both 1 by 1 in. surfaces, while the two larger plates were stainless steel clad on all surfaces. The thermal shock consisted of three cycles of heating to 1100°F and quenching into water. Four of the five samples showed evidence of cracks across the thin portion of the fuel, but the other sample showed no cracks.

1.1.4 Chemical

1.1.4.1 Thermodynamic Functions

The following data on $ZrH_{2.000}$ at 298.15°K have been reported.[1.23]

C_p = 7.396 ± 0.015 cal/deg/mole

$S°$ = 8.374 ± 0.02 cal/deg/mole

$H°-H_o°$ = 1284.1 ± 2 cal/mole

$(F°-H_o°)/T$ = -4.067 ± 0.01 cal/deg/mole

Free energy of formation = -30.9 ± 2 kcal/mole

TABLE 1.1.5

HEAT OF FORMATION

H/Zr(eff)	ΔH, kcal/mole
1.5	43.5
1.6	41.2
1.7	39.5
1.8	38.4
1.9	37.8

The heat formation may be obtained from dissociation pressure measurements when the data are expressed in the form $p = Ae^{-\Delta H/RT}$. According to Raymond,[1.24] this ΔH is a function of H/Zr(eff) in the delta and epsilon phases as shown in Table 1.1.5.

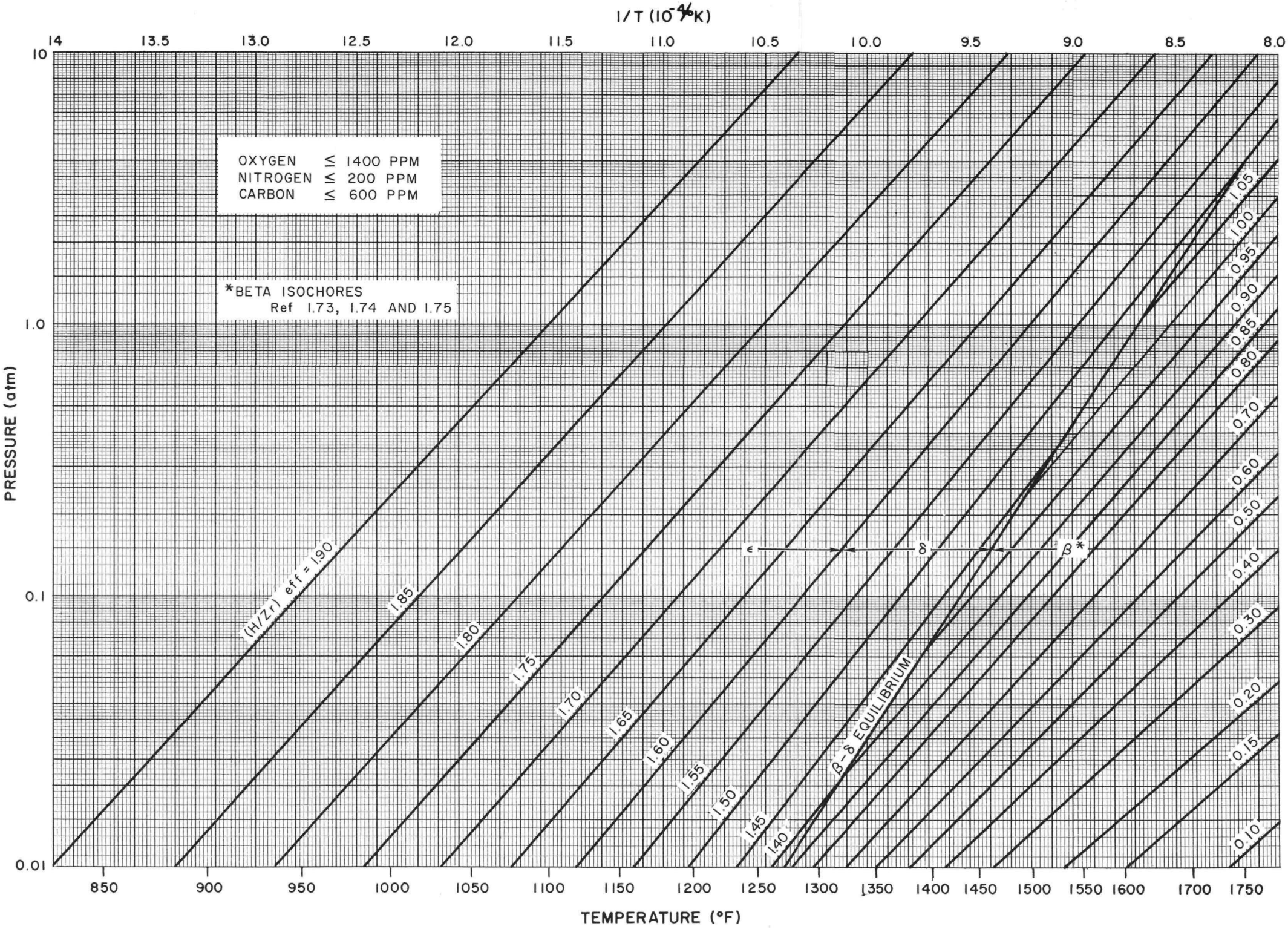

8-14-64 7569-01653

Figure 1.1.7. Dissociation Pressure Isochores of Zirconium Hydride (Ref 1.24)

BLANK

1.1.4.2 Hydrogen Dissociation Pressure

Raymond[1.24] carefully determined the hydrogen dissociation pressures of unfueled δ and ϵ phase zirconium hydride. His data are presented in Figure 1.1.7 in terms of curves obtained from data by the method of least-squares. The expression that best fits the experimental data in the δ and ϵ regions is (p in atms and T in °K):[1.24]

$$\ln p = -3.8415 + 38.6433\ H/Zr(eff) - 34.2639\left[H/Zr(eff)\right]^2 + 9.281\left[H/Zr(eff)\right]^3 + \frac{10^3}{T}\left\{-31.2982 + 23.5741\ H/Zr(eff) - 6.0280\left[H/Zr(eff)\right]^2\right\} \quad \ldots(1)$$

Comparison of Raymond's data with the data presented by Libowitz[1.27] showed excellent agreement; however, with the earlier work by Atkins[1.7] conflict occurred in the H/Zr(eff) range of 1.55 to 1.75. Since hydrogen dissociation pressures are independent of the uranium content (U≤10 wt %) in fueled zirconium hydride, Raymond's data was compared to Johnson's data[1.25, 1.26] (somewhat scattered) on fueled zirconium hydride.* In general, agreement was noticeable, but Raymond's data was somewhat higher above a H/Zr(eff) of 1.65. Raymond's data is considered to be the most reliable and should be used.

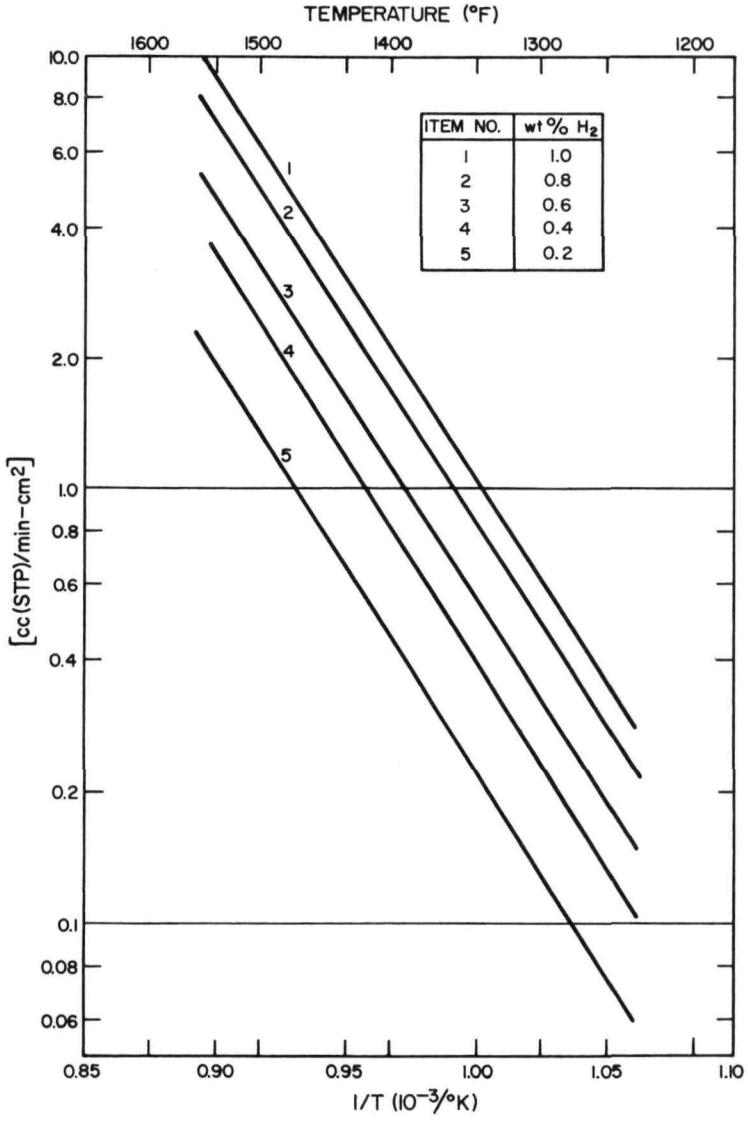

8-14-64 7569-01654

Figure 1.1.8. Effect of Temperature and Hydrogen Content on the Hydrogen Escape Rate of Bare Zirconium Hydride (Ref 1.64, 1.65)

An equation that closely approximates Raymond's data and can be used more easily than equation (1) is given below (p in atms and T in °K)

$$p = \left[\frac{H/Zr(eff)}{1.97 - H/Zr(eff)}\right]^3 \times e^{\left[(13.6 - \frac{19{,}800}{T})\right]} \quad \ldots(2)$$

If no impurities existed in hydrided zirconium (fueled or unfueled), 2.0 would appear in equation (2) instead of 1.97.

1.1.4.3 Hydrogen Loss From Bare Zirconium Hydride

Under nonequilibrium conditions hydrided metal can lose hydrogen. Figure 1.1.8 presents results reported by Huffine[1.64, 1.65] on the hydrogen escape rates of zirconium hydride. Later studies[1.66] have shown that the escape rate is dependent upon the amount of

*It should be noted that Johnson gives his weight percentages in terms of hydrided material, instead of the usual practice of giving it in terms of unhydrided material.

oxidizing that has occurred on the sample's surface. In testing samples with $N_H = 4$, 3 to 4% was lost after 100 hours at about 1150°F, whereas none was apparently lost from samples at 1350°F. Oxidation was slight at 1150°F, but at 1350°F a barrier was formed to sufficiently eliminate hydrogen from escaping. Actually the oxidation appeared to drive the hydrogen further into the material.

1.1.4.4 Hydrogen Redistribution Due to a Temperature Gradient

If a gap exists between the fuel rod and cladding, hydrogen will travel through this gap to equalize the surface dissociation pressure along the fuel rod's length.[1.28] Figure 1.1.9, obtained from the following equation (with p and T in units of atm and °K, respectively);

$$p = \left[\frac{H/Zr(eff)}{1.97 - H/Zr(eff)}\right]^3 \times e^{\left[13.6 - \frac{19,800}{T}\right]} \qquad \ldots(1)$$

may be used to graphically determine the equilibrium redistribution of hydrogen.

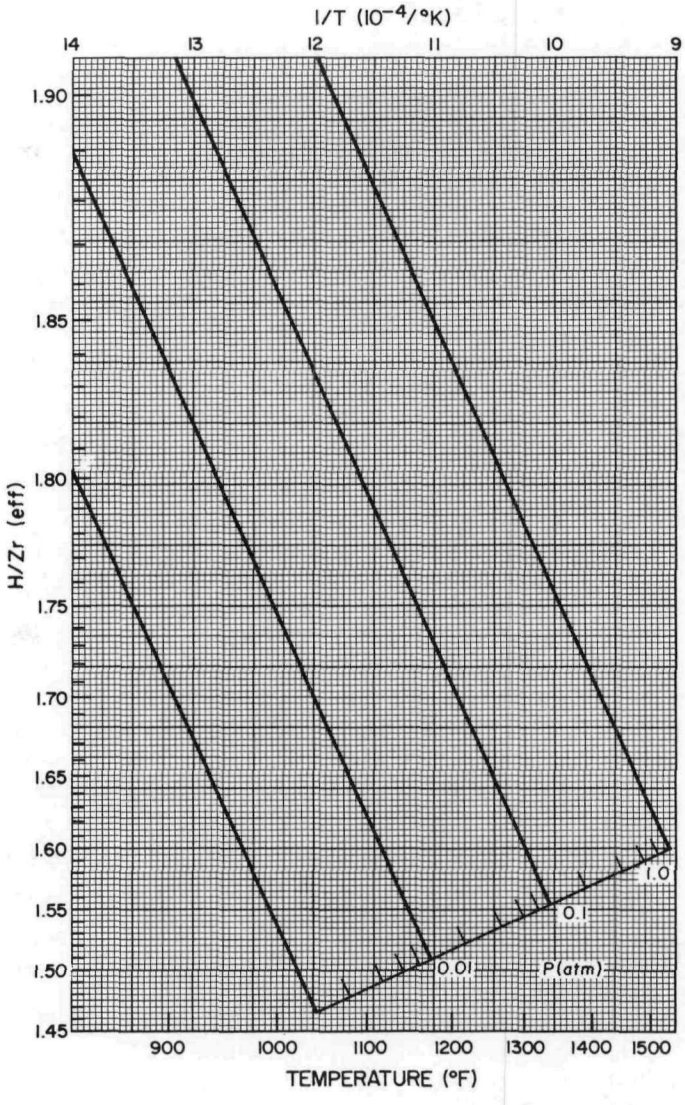

8-14-64 7569-01655

Figure 1.1.9. Graphical Estimate of Concentration in a Fuel Element Containing a Gap

First, divide the fuel element into equal axial segments and assign an average segment temperature to each. Place tracing paper over Figure 1.1.9 and draw full height vertical lines corresponding to the average temperature of each segment. For the first trial choose the value for gap pressure corresponding to the total $H/Zr(eff)_o$, before redistribution, and the average temperature of the full fuel element. Draw this assumed gap pressure line. Read off the values of the estimated H/Zr(eff) for each segment at the intersections of the pressure line with the temperature lines. If the average of these segment values, say $H/Zr(eff)_1$, is not equal to the initial overall concentration, $H/Zr(eff)_o$, reiterate by choosing a gap pressure corresponding to $H/Zr(eff)_o$ and the temperature determined by the intersection of $H/Zr(eff)_1$ and the previous gap pressure line. This second trial should give an average H/Zr(eff) very close to $H/Zr(eff)_o$. If this is not satisfactory, a third trial may be made.[1.63]

In the absence of any free surface (gap) which allows hydrogen to flow from the hot surface to the cold surface, hydrogen redistribution will be controlled by thermal diffusion. The equation which governs the equilibrium distribution may be expressed[1.30, 1.31] as;

$$\frac{-d \ln\left[H/Zr(eff)\right]}{dT} = \frac{Q^*}{\left[H/Zr(eff)\right] RT^2 \left\{d(\ln p)/d\left[H/Zr(eff)\right]\right\}_T} \qquad \ldots(2)$$

By substituting the expression for the equilibrium dissociation pressure:

$$p = \left[\frac{H/Zr}{1.97 - H/Zr(eff)}\right]^3 e^{\left[13.6 - \frac{19,800}{T}\right]} \qquad \ldots(3)$$

into (2), one obtains

$$\frac{-d \ln\left[H/Zr(eff)\right]}{dT} = \frac{Q^*}{RT^2} = \left[\frac{1.97 - H/Zr(eff)}{3(1.97)}\right]$$

Integrating,

$$\left[\frac{1.97}{H/Zr(eff)} - 1\right] e^{Q^*/3RT} = K \text{ (a constant)} \qquad \ldots(4)$$

Knowing the temperature distribution and the concentration at one point, one may determine the concentration at any other point.

It has been found that for linear temperature gradient axially, or for a linear temperature gradient with respect to the square of the radius radially, the average value of H/Zr(eff) occurs approximately at the temperature defined by:

$$\left(\frac{1}{T}\right)_{ave} = 1/2\left(\frac{1}{T_{min}} + \frac{1}{T_{max}}\right) \qquad \ldots(5)$$

This relationship may be used to determine the value for K.

The above relationship may be substituted into the expression for K to obtain;

$$H/Zr(eff) = \frac{1.97}{1 + \left[\frac{1.97}{H/Zr(eff)} - 1\right] e^{\left[\frac{Q^*}{6R}\left(\frac{1}{T_{min}} + \frac{1}{T_{max}} - \frac{2}{T}\right)\right]}} \qquad \ldots(6)$$

which gives the hydrogen concentration at any temperature (in °K) between T_{max} and T_{min}.[1.63] The

Heat of Transport, Q^*, for β phase zirconium hydride[1.31] was found to vary somewhat linearly with temperature. Values ranged from 7,000 cal/mole at 900°K to 12,000 at 1130°K. The value of Q^* for δ phase has not yet been measured in the absence of diffusion via the surface. Since Q^* has not been measured for all phases, equation (6) should be used with extreme caution and with the insight that this equation may give incorrect values of concentration until Q^* is measured accurately.

A computer code,[1.29] HYREP, which uses the dissociation pressure correlation of Raymond,[1.24] has been written to calculate hydrogen redistribution with or without a gap existing between the fuel rod and cladding. Two main assumptions were used in HYREP; (1) no loss of hydrogen from the element, and (2) constant hydrogen pressure exists along the length of the element ($\partial p/\partial L = 0$).

1.1.4.5 Hydrogen Diffusion Coefficient

Experimental values of the diffusion coefficient of hydrogen through delta-phase zirconium hydride are shown in Figure 1.1.10. The data from any one source scatter little from a straight line, but there is little agreement in the data from different sources. This disagreement may be due to different experimental techniques and surface conditions of the samples.

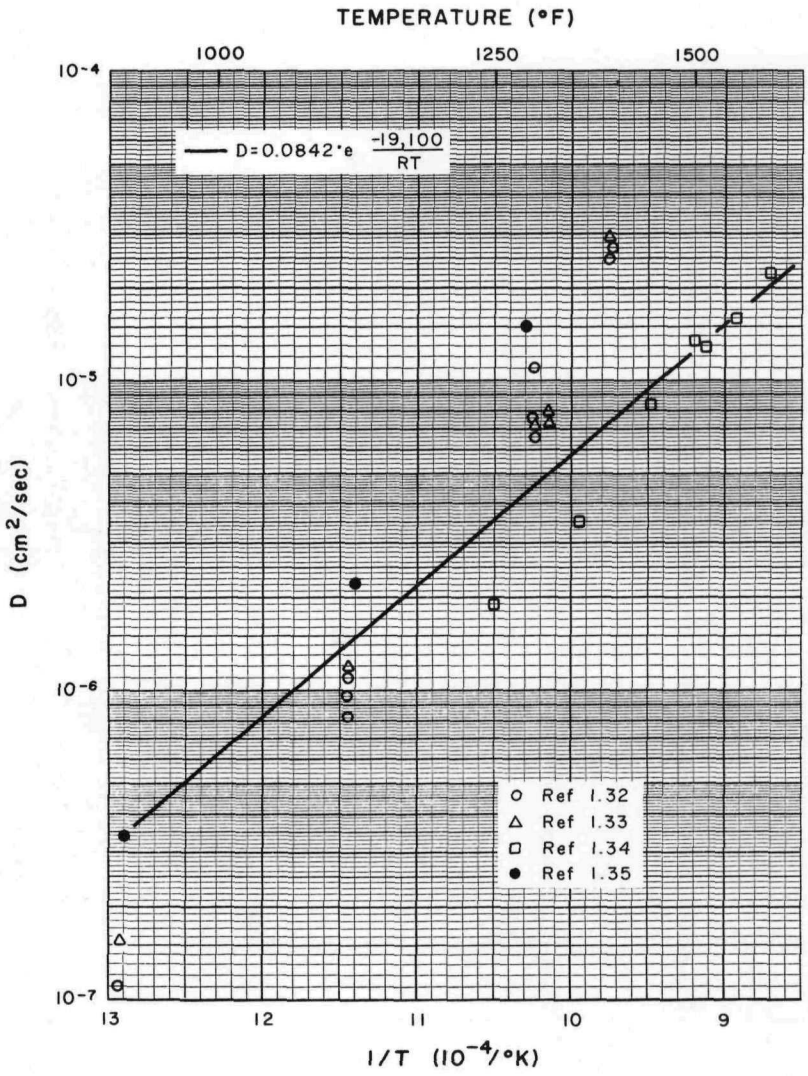

8-14-64 7569-01656

Figure 1.1.10. Hydrogen Diffusion Coefficient

The dotted line represents a theoretical estimate[1.36] which indicates the most accurate evaluation of the data. Additional investigation is needed in this area.

1.1.4.6 Fuel Rod Transient Hydrogen Concentration

In some applications the dissociation pressure of zirconium hydride is sufficiently high that hydrogen will escape from the surface unless it is contained. The transient average concentration of hydrogen, C_{ave}, in a cylindrical bare fuel rod is shown in Figure 1.1.11 as a function of time, t, diffusion coefficient, D, and radius of the element, r. The initial concentration of hydrogen is represented by C_o, while the final or equilibrium concentration is C_{eq}. The curve was plotted by using the solution to the transient concentration of a cylinder.[1.38] It does not consider any change in the diffusion coefficient during the transient.

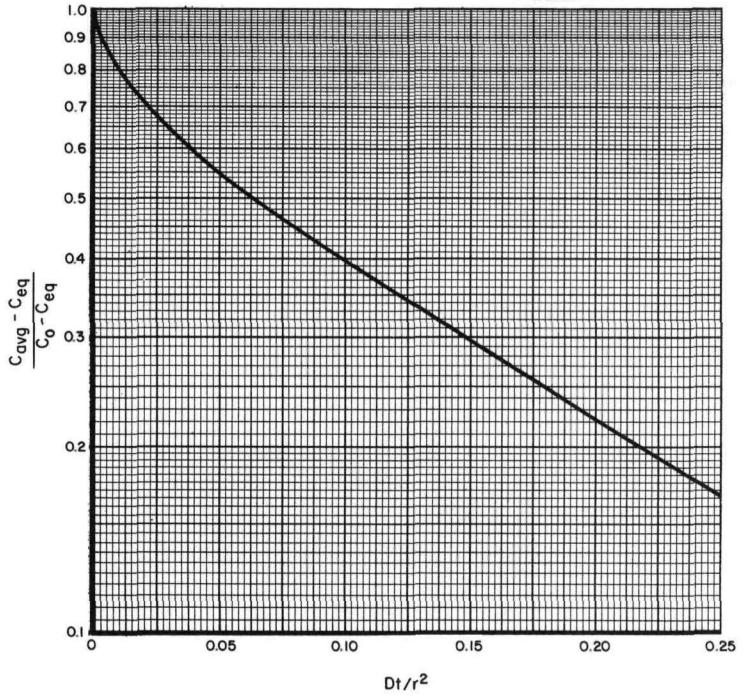

8-11-64 7569-1552a

Figure 1.1.11. Concentration of Hydrogen in Bare Fuel Rods Under Transient Conditions

This plot may also be used for the hydriding of a cylinder. In this case C_{eq} is larger than either C_o or C_{ave}.

1.1.4.7 Hydrogen Loss Rate for a Cylindrical Bare Fuel Rod

Figure 1.1.12 is a plot of the slope of the curve shown in Figure 1.1.11. It gives the rate of change in the average concentration of hydrogen in the bare fuel element as a function of time.

Figure 1.1.12. Transient Rate of Hydrogen Loss

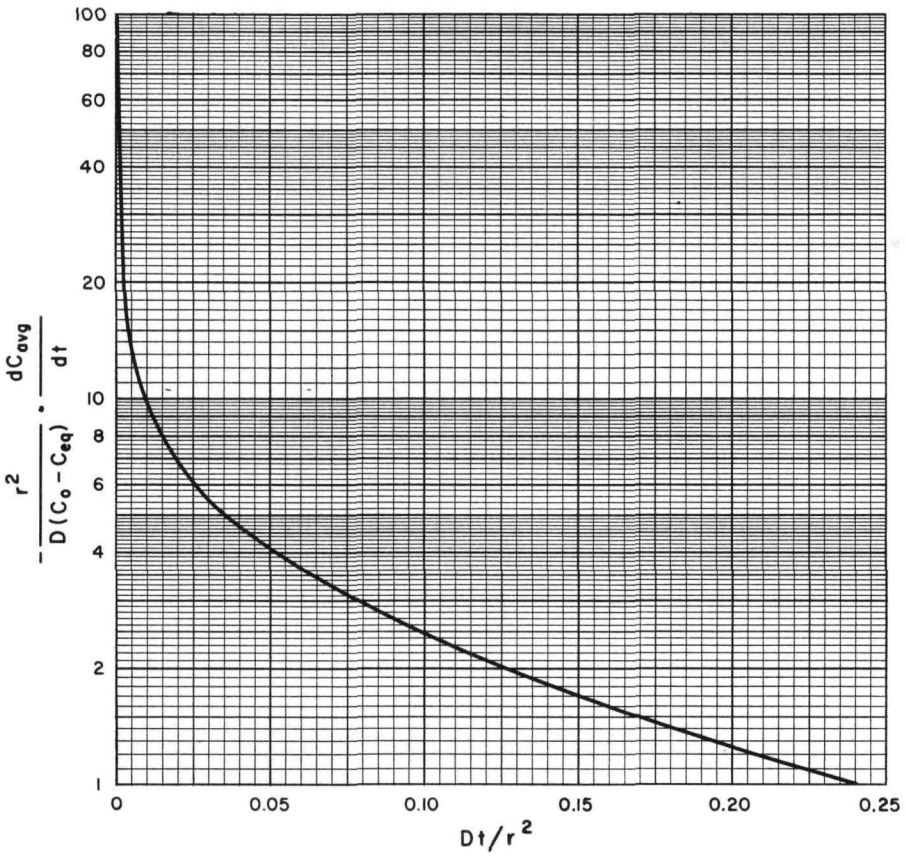

8-14-64 7569-01657

TABLE 1.1.6

COMPATIBILITY OF ZIRCONIUM HYDRIDE FUEL

Hydrided Fuel H/Zr(eff) = 1.6	Material	Temperature (°F) - Time (hr)	Results	Ref
Zr + 7%U	347 SS	1200 - 216	Surface oxidized 2μ diffusion layer	1.39
Zr + 10%U	Hastelloy B	1200 - 216	Diffusion layer formed	1.39
Zr + 10%U	Inconel X	1200 - 216	Diffusion layer formed	1.39
Zr + 10%U	Molybdenum	1200 - 210	No diffusion or reaction	1.39
Zr + 10%U	Gold	1200 - 216	130μ diffusion zone	1.39
Zr + 7%U	Molybdenum	1500 - 190	No diffusion or reaction	1.39
Zr + 7%U	Hastelloy B	1500 - 190	45μ diffusion zone	1.39
Zr + 10%U	Inconel X	1500 - 190	70μ diffusion zone	1.39
Zr + 7%U	Nickel	1600 - 360	225μ diffusion zone	1.39
Zr + 7%U	Inconel X	1600 - 360	100μ diffusion zone	1.39
Zr + 7%U	Molybdenum	1600 - 360	20μ diffusion zone	1.39
Zr + 7%U	Molybdenum	1300 - 235	No diffusion or reaction	1.39
Zr + 7%U	Inconel X	1300 - 235	12μ diffusion zone	1.39
Zr + 10%U	Chromized Hastelloy	1450 - 513	8μ diffusion layer	1.40
Zr + 10%U (modified)	Bare Hastelloy N	1450 - 320	64μ diffusion layer	1.40
Zr + 15%U	304 SS	570 - 400 (boiling water at 1230 psi and pH = 7)	No reaction of metal to fuel or metal to fuel in water	1.41
Zr + 15%U	346 SS	570 - 400 (boiling water at 1230 psi and pH = 7)	No reaction of metal to fuel. Slight reaction of metal, fuel and water	1.41

1.1.4.8 Compatibility

Table 1.1.6 is a compilation of the compatibility of zirconium hydride fuel with various solid materials at several different temperatures.

Corrosion rate of fuel under the environment of the last 2 samples in the table was 353 mg/dm^2/mo with a penetration of less than 2 mils.

1.2 MECHANICAL PROPERTIES

1.2.1 Short Time

1.2.1.1 Tensile Properties

In general, the zirconium hydrides and the zirconium alloy hydrides in the hydrogen composition region of the present SNAP 2/10A designs—H/Zr(eff) = 1.4 to 2.0—are brittle materials. Some ductility is obtained at elevated temperatures, but even at the maximum temperatures for which data are available, the fuel is still classed as a brittle material. The tensile behavior of the fuel is closely connected with the phase relationships found in the basic reference system, namely, the zirconium-hydrogen system. The data in Table 1.2.1 represent the tensile properties of zirconium + 8 wt % uranium hydrides.

TABLE 1.2.1

ELEVATED TEMPERATURE TENSILE PROPERTIES OF ZIRCONIUM + 8 wt % URANIUM HYDRIDES[1.42]

Temperature (°F)	Hydrogen Content (H/Zr effective)	0.2% Offset Yield Strength (psi)	Ultimate Tensile Strength (psi)	Young's Modulus, E (10^6 psi)
700	0.84	-	16,600	10.6
800	0.86	-	14,400	10.7
1000	0.87	12,800	20,900	8.6

Figure 1.2.1 represents data for unfueled zirconium hydride and gives an indication of the ultimate tensile strength of the fuel materials over the hydrogen composition range from 0 to 2 H/Zr(eff) values at 1112°F (600°C).

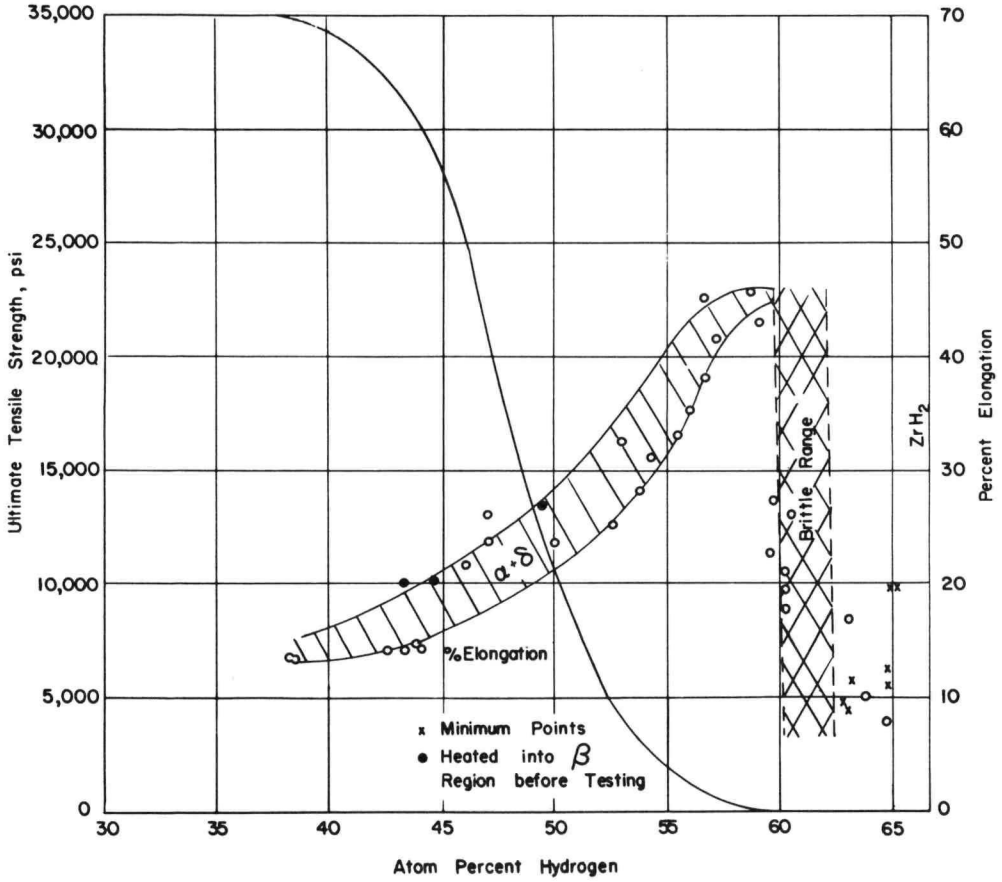

8-13-64 7569-01722

Figure 1.2.1. Ultimate Tensile Strength and Percent Elongation of Zirconium Hydride at 600°C (Ref 1.11)

The stress-strain diagrams in Figure 1.2.2 indicate the tensile behavior of 0.84 to 0.86 H/Zr(eff) hydrides of a zirconium +8 wt % uranium fuel alloy. This alloy is similar to the Zr + 10U alloy with respect to the mechanical properties of its hydrides.

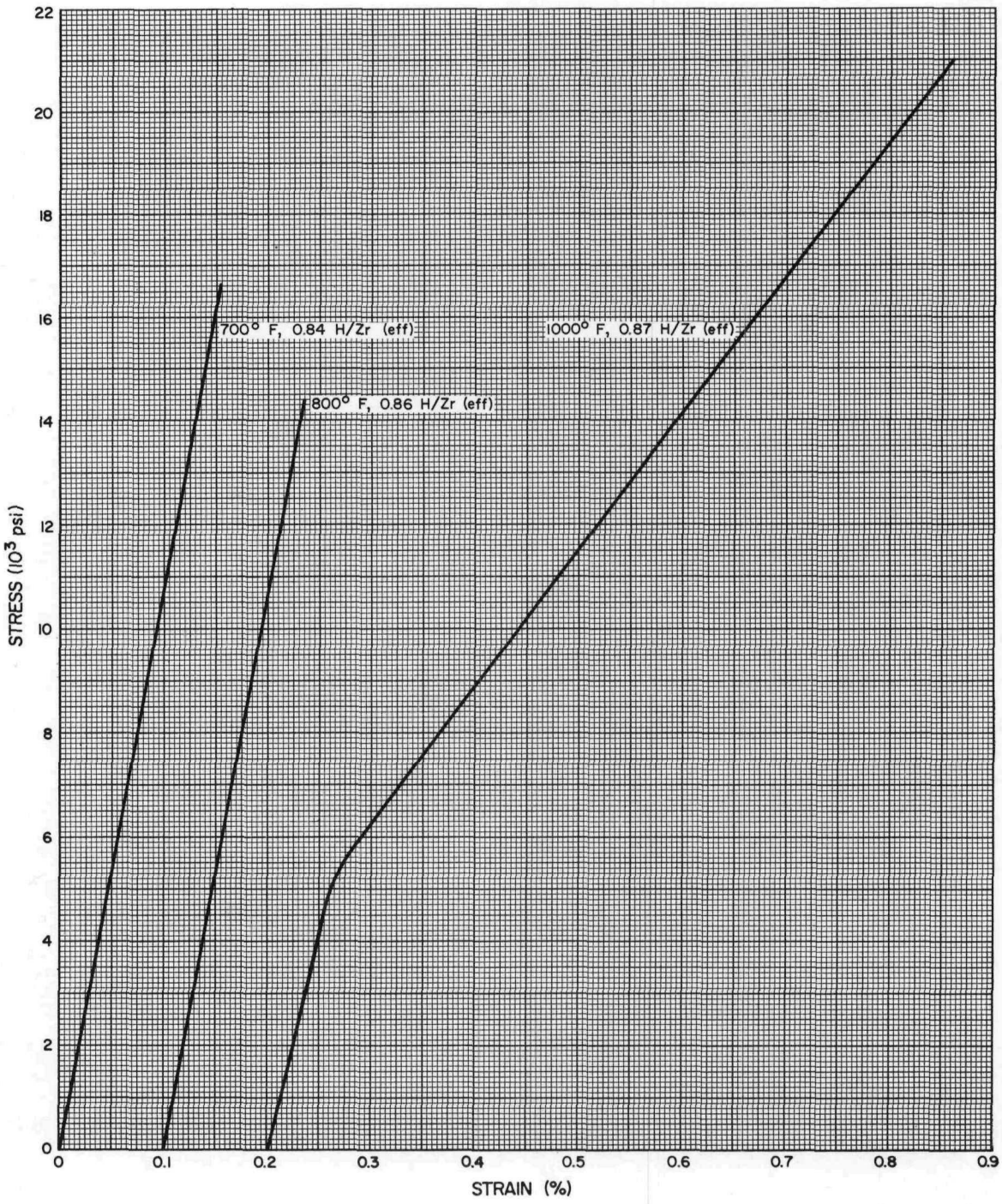

8-14-64

7569-01659

Figure 1.2.2. Elevated Temperature – Stress-Strain Diagrams for Zr + 8 wt % U Hydride (Ref 1.42)

Figures 1.2.3 through 1.2.6 illustrate typical stress-strain diagrams for Zr + 10U alloy hydrides at various H/Zr(eff) ratios and carbon contents. The "X" at the end of each curve indicates the failure point.

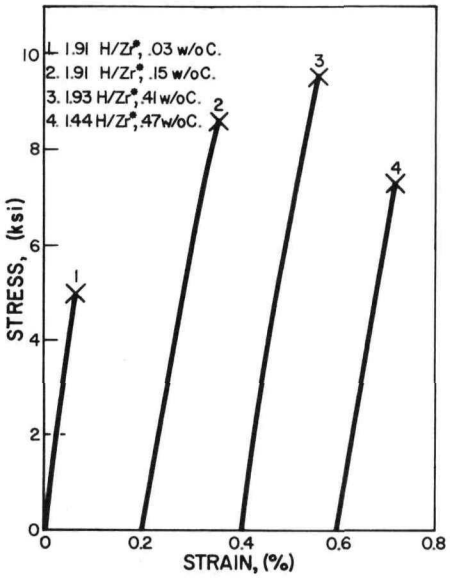

3-24-64 7568-1544

Figure 1.2.3. Room Temperature Stress-Strain Diagram for Zr + 10 U Hydride (Ref 1.43)

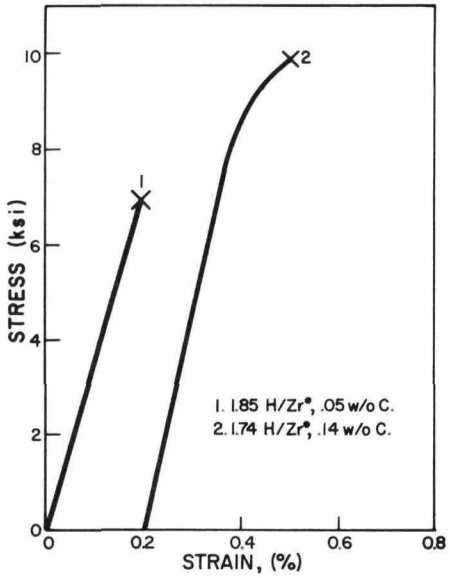

3-24-64 7546-1544

Figure 1.2.4. 1250°F Stress-Strain Data on Zr + 10 U Hydride (Ref 1.43)

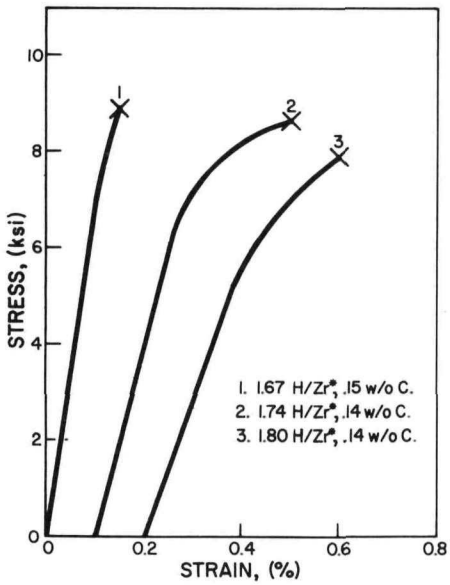

3-24-64 7568-1544

Figure 1.2.5. 1350°F Stress-Strain Data for Zr + 10 U Hydride (Ref 1.43)

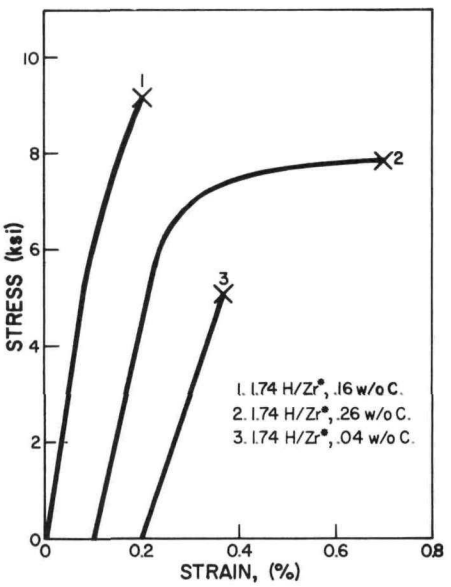

3-24-64 7568-1544

Figure 1.2.6. 1450°F Stress-Strain Data for Zr + 10 U Hydride (Ref 1.43)

Figures 1.2.7 through 1.2.9 show the effect of carbon content on the ultimate tensile strength for Zr + 10 U alloy hydrides at various H/Zr(eff) ratios and temperatures.

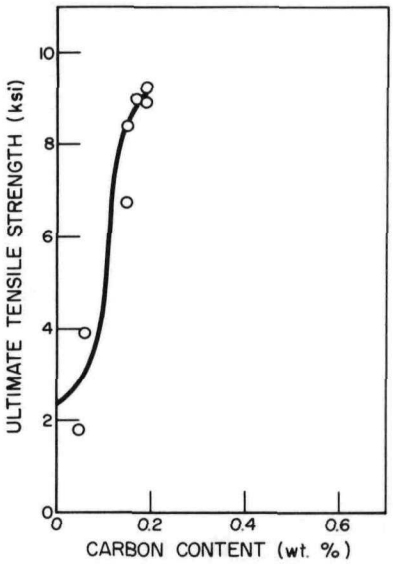

3-25-64 7568-1536

Figure 1.2.7. Room Temperature Ultimate Tensile Strength for Zr + 10 U, H/Zr (eff) = 1.82 to 1.85 (Ref 1.43)

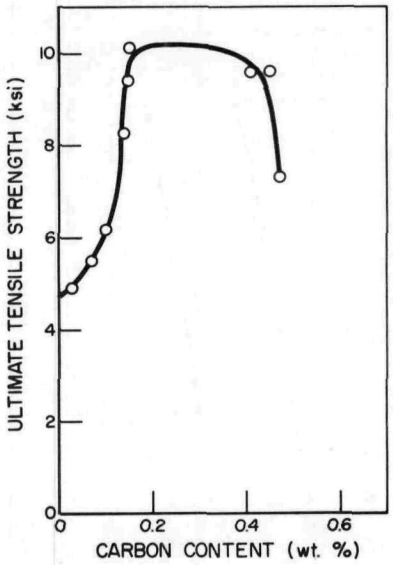

3-25-64 7568-1536

Figure 1.2.8. Room Temperature Ultimate Tensile Strength for Zr + 10 U, H/Zr (eff) = 1.89 to 1.94 (Ref 1.43)

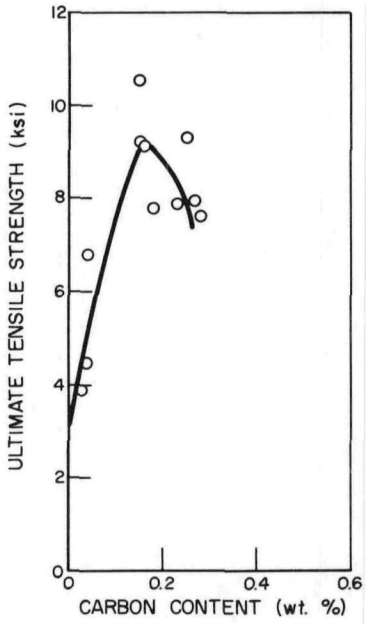

3-25-64 7568-1536

Figure 1.2.9. 1450°F Ultimate Tensile Strength for Zr + 10 U Alloy Hydrides (Ref 1.43)

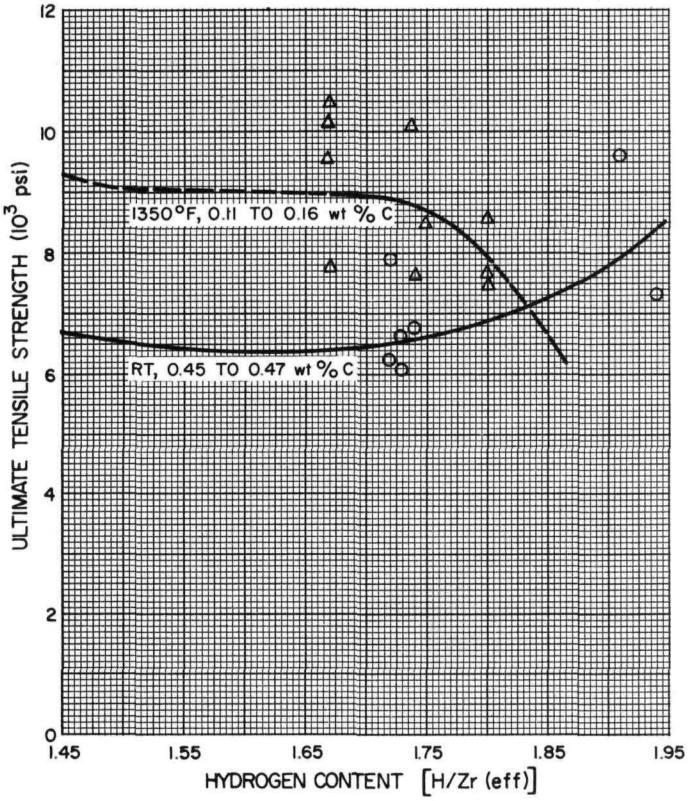

8-14-64 7568-1535A

In order to clearly illustrate the effect of hydrogen content and temperature on the ultimate tensile strength of Zr + 10 U alloy hydrides, Figures 1.2.10 and 1.2.11 are presented. Dotted lines indicate an extrapolation of existing data.

Figure 1.2.10. Effect of Hydrogen Content on the Ultimate Tensile Strength of Zr + 10 U Alloy Hydrides (Ref 1.43)

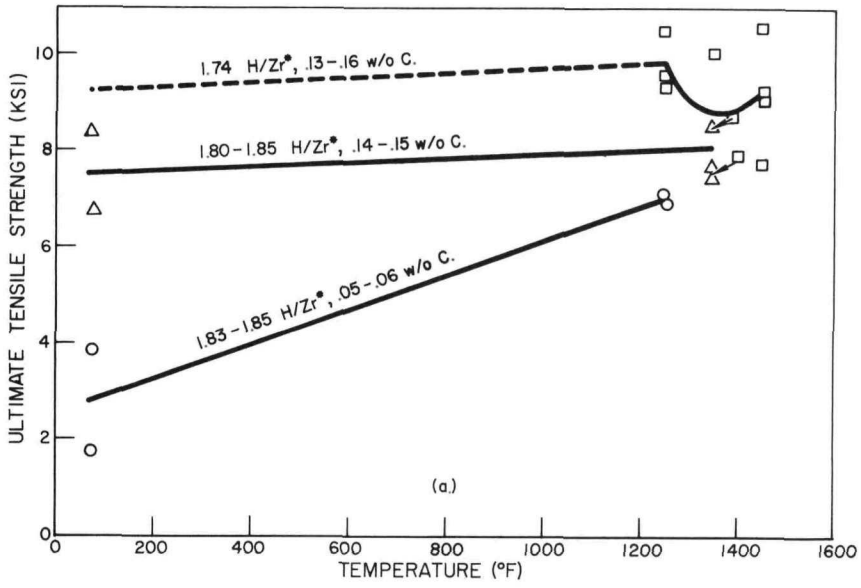

7568-1535

Figure 1.2.11. Effect of Temperature on the Ultimate Tensile Strength of Zr + 10 U Alloy Hydrides (Ref 1.43)

7568-1535

Variation of the Young's modulus of some Zr + 10 U alloy hydrides with carbon content is shown in Figure 1.2.12 for room temperature data and in Figure 1.2.13 for elevated temperature data.

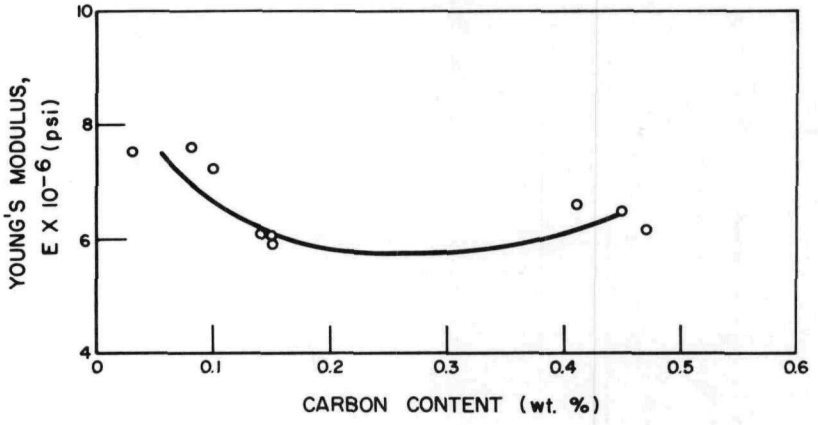

3-25-64 7568-1541

Figure 1.2.12. Room Temperature Young's Modulus Data for Zr + 10 U Alloy Hydrides (Ref 1.43)

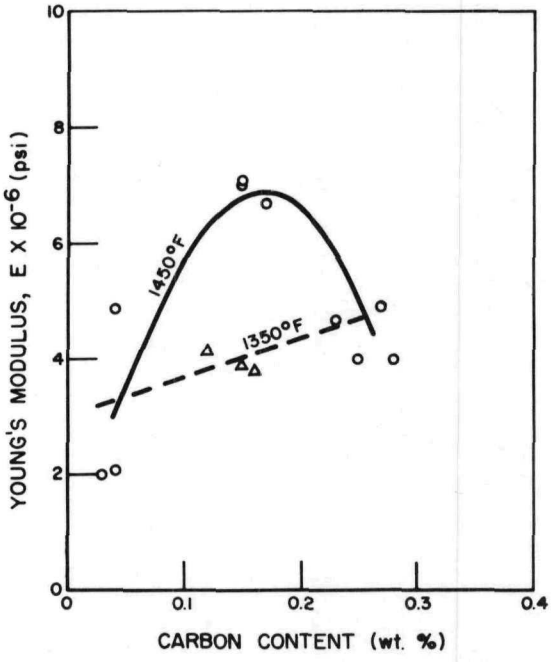

3-25-64 7568-1541

Figure 1.2.13. Elevated Temperature Young's Modulus Data for Zr + 10 U Alloy Hydrides (Ref 1.43)

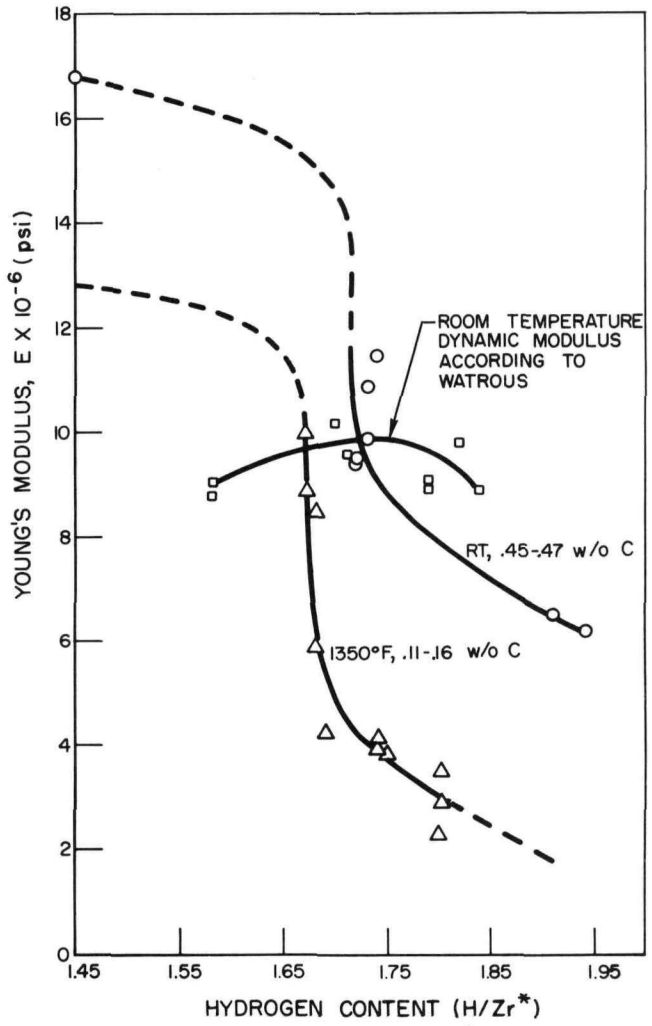

Figure 1.2.14. Effect of Hydrogen Content on the Young's Modulus (Ref 1.43)

Figures 1.2.14 and 1.2.15 are presented to illustrate the effect of hydrogen content and temperature, respectively, on the Young's modulus of Zr + 10 U alloy hydrides. The room temperature dynamic modulus data shown in Figure 1.2.14 are for Zr + 7 U alloy hydrides. However, Lundberg[1.44] feels that small changes in uranium weight percentages have very little effect on the Young's modulus. The cause for the difference in data at the same temperature is that one set of data represents a static Young's modulus while the other set represents a dynamic modulus.

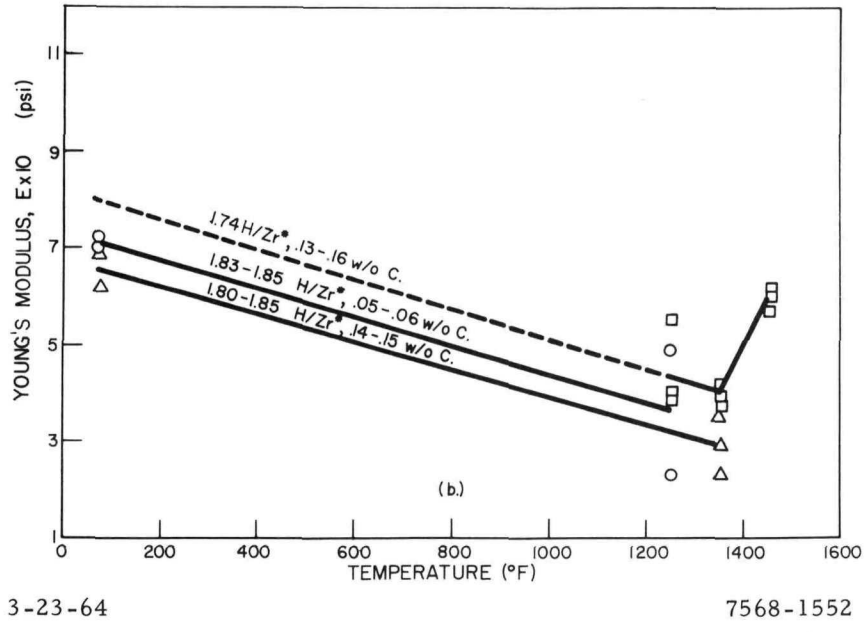

Figure 1.2.15. Effect of Temperature on the Young's Modulus (of Zr + 10 U Alloy Hydride (Ref 1.43)

1.2.1.2 Transverse Rupture Strength

It has been shown that the transverse rupture strength of a brittle material is equivalent to the ultimate tensile strength. Pears[1.46] has found that the true ultimate tensile strengths of both ATJ graphite and alumina are essentially equivalent to their flexural strengths. In general, as long as the material closely obeys Hooke's law all the way to failure, the flexural strength (transverse rupture strength) is 150 to 200% higher than the ultimate tensile strength obtained by methods normally used for metals and other basically ductile materials. The ultimate tensile strength values reported in the previous subsection were determined by these methods. With regard to the effects on the ultimate tensile strength by the compositional and temperature variables, the ductile material tensile test method does not appear to cloud the picture significantly. Estimates of the true ultimate tensile strength can be obtained by increasing the tensile test values by a factor of 150 or 200%. The larger factor will probably give the best estimates for conditions where the fuels are known not to obey Hooke's law all the way to failure.

TABLE 1.2.2

AVERAGE TRANSVERSE RUPTURE STRENGTH OF NON-FUELED ZIRCONIUM BASE-ALLOY HYDRIDES[1.47]

Alloy Addition (wt %)	Hydrogen Composition Range (H/M)		
	0.88 to 1.5	1.65 to 1.79	1.80 to 1.89
	Rupture Strength (psi)		
None	16,000	9,000	9,000
2.3 Nb	38,000	18,000	20,000
3.5 La	35,000	15,000	16,000
1.4 Cr	33,000	11,000	13,000

Transverse rupture strength data have been obtained on non-fueled zirconium and zirconium-base alloy hydrides and are summarized in Table 1.2.2, while data on fueled hydrides are summarized in Table 1.2.3.

TABLE 1.2.3

AVERAGE TRANSVERSE RUPTURE STRENGTH OF ZIRCONIUM-URANIUM ALLOY HYDRIDES

Uranium Content (wt %)	Carbon Content (wt %)	Temperature (°F)	Hydrogen Composition Range H/Zr(eff)			Ref
			0.92 to 1.6	1.72 to 1.86	1.87 to 1.97	
			Rupture Strength (psi)			
7	0.02	77	--	18,000	18,000	1.47
10	0.02	77	20,000	16,000	16,000	1.47
10	0.4	78	20,000	--	--	1.48
10	0.02	500	20,000	16,000	16,000	1.47
10	0.5	500	39,300	--	--	1.48
10	0.4	950	27,700	--	--	1.48
10	0.02	1000	43,000	20,000	24,000	1.47
10	0.02	1200	--	15,000	23,000	1.47

1.2.1.3 Compressive Properties

Room temperature compressive mechanical properties have been determined for both fueled and non-fueled zirconium base alloy hydrides and also for unalloyed zirconium hydrides. Table 1.2.4 contains data for unalloyed zirconium hydrides, zirconium-niobium, zirconium-lanthanum, and zirconium-chromium alloy hydrides and unmodified zirconium + 7 wt % and 10 wt % uranium fueled hydrides.

TABLE 1.2.4

COMPRESSIVE STRENGTH AND APPARENT COMPRESSIVE YIELD STRENGTH OF ZIRCONIUM-BASE ALLOY HYDRIDES AT ROOM TEMPERATURE[1.47]

Alloy Addition (wt %)	Hydrogen Concentration (H/M)					
	0.80 to 1.50		1.60 to 1.80		1.80 to 1.89	
	Ultimate Strength (psi)	Yield Strength (psi)	Ultimate Strength (psi)	Yield Strength (psi)	Ultimate Strength (psi)	Yield Strength (psi)
None	20,000	13,000	20,000	13,000	19,000	13,000
2.2 Nb	>145,000	125,000	75,000	41,000	91,000	48,000
3.9 La	94,000	72,000	69,000	23,000	82,000	24,000
1.4 Cr	>145,000	>145,000	>145,000	102,000	>145,000	97,000
7 U (unmodified)	--	--	83,000	26,000	76,000	25,000
10 U (unmodified)	>145,000	116,000	43,000	25,000	44,000	25,000

Some recent data on the compressive properties of carbon modified Zr + 10 U hydride fuel materials are listed in Table 1.2.5. The proportional limit indicated in this table is similar to the apparent compressive yield strength given in Table 1.2.4.

Table 1.2.6 presents some additional data on Zr + 10 U in which two different hydriding methods were used. Some doubt exists on the Poisson's ratio data since it can not exceed the value of 0.50, which is the theoretical limit.

Typical compressive stress-strain diagrams for several carbon modified fueled materials are given in Figure 1.2.16.

TABLE 1.2.5

ROOM TEMPERATURE COMPRESSION PROPERTIES OF MODIFIED Zr + 10 U HYDRIDE FUELS (Ref 1.47)

Sample	H/Zr(eff)	Carbon wt %	Property Limit (psi)	Ultimate Compression Strength (psi)	0.2% Offset Compressive Yield Strength (psi)	Compressive Young's Modulus (10^6 psi)
254-B-17	1.70	0.04	30,000	68,000	31,000	4.8
254-B-18	1.81	0.05	29,000	73,000	34,000	3.9
254-B-16	1.85	0.045	29,000	65,000	31,000	4.7
253-C-11	1.62	0.12	33,000	107,000	39,000	4.9
253-B-1	1.64	0.14	31,000	104,000	36,000	4.4
253-C-15	1.68	0.115	36,000	104,000	41,000	4.1
253-C-14	1.76	0.13	28,000	113,000	37,000	5.0
253-B-14	1.76	0.125	34,000	119,000	39,000	4.7
255-A-17	1.64	0.26	41,000	110,000	48,000	5.1
255-A-16	1.74	0.21	33,000	118,000	36,000	4.8
255-A-18	1.80	0.29	39,000	126,000	43,000	5.0

TABLE 1.2.6

ADDITIONAL ROOM TEMPERATURE COMPRESSIVE ELASTIC PROPERTIES OF Zr + 10 U ALLOY HYDRIDES (Ref 1.43)

Carbon Content (wt %)	Hydrogen Content, H/Zr(eff)	Hydriding Method	Poisson's Ratio	Young's Modulus, E, 10^6 psi	Calculated Shear Modulus, G, 10^6 psi
0.02	1.79	(1)	0.50	5.43	1.81
0.02	1.82	(1)	0.55	6.26	2.02
0.04	1.76	(1)	0.52	8.80	2.89
0.04	1.82	(2)	0.45	6.26	2.15
0.11	1.68	(2)	0.40	6.26	2.23
0.29	1.85	(2)	0.38	7.00	2.53

(1) Precipitation Hydrided
(2) Production Hydrided

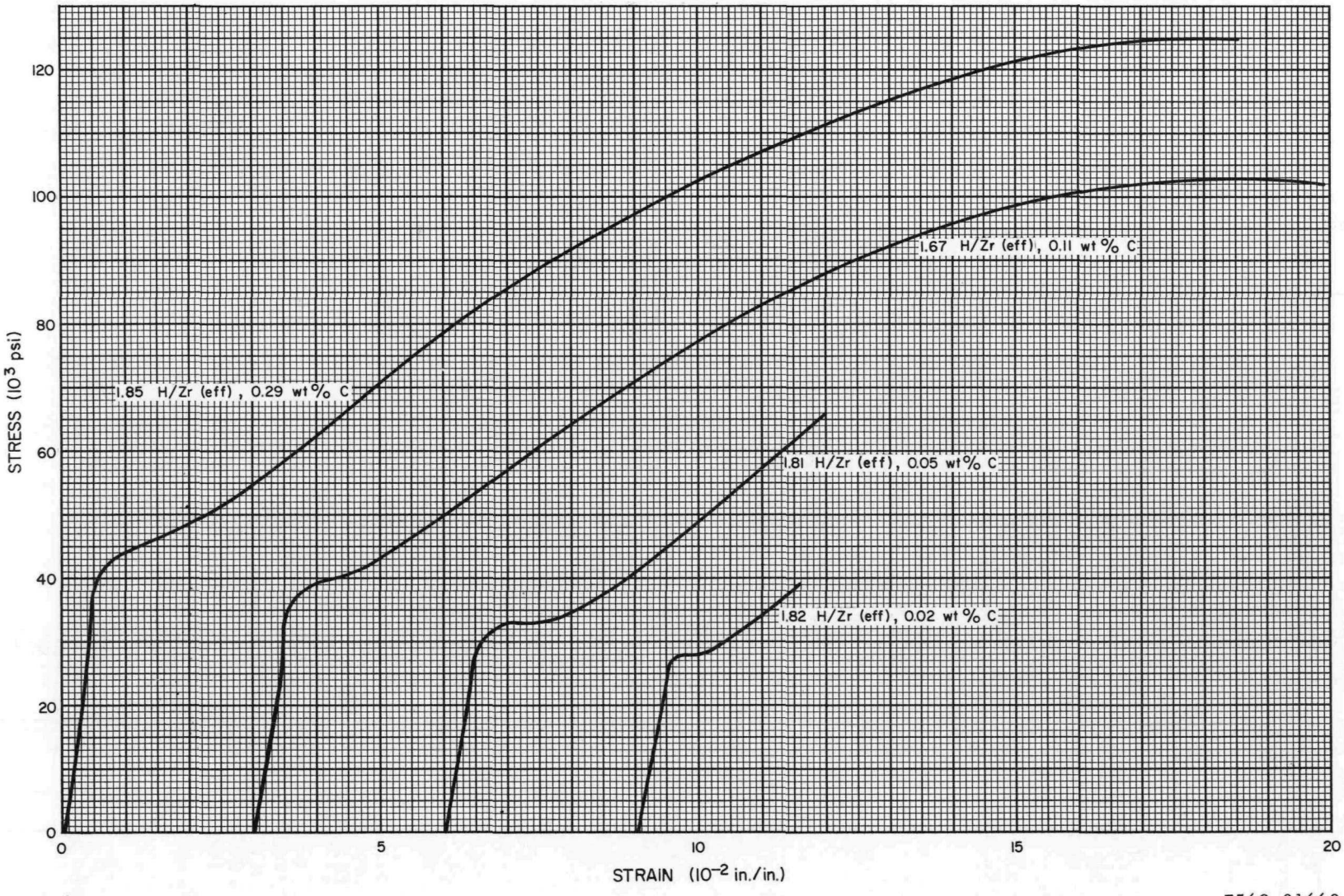

8-14-64

7569-01660

Figure 1.2.16. Typical Room Temperature Compressive Stress-Strain Diagrams for Zr + 10 U Alloy Hydrides (Ref 1.43)

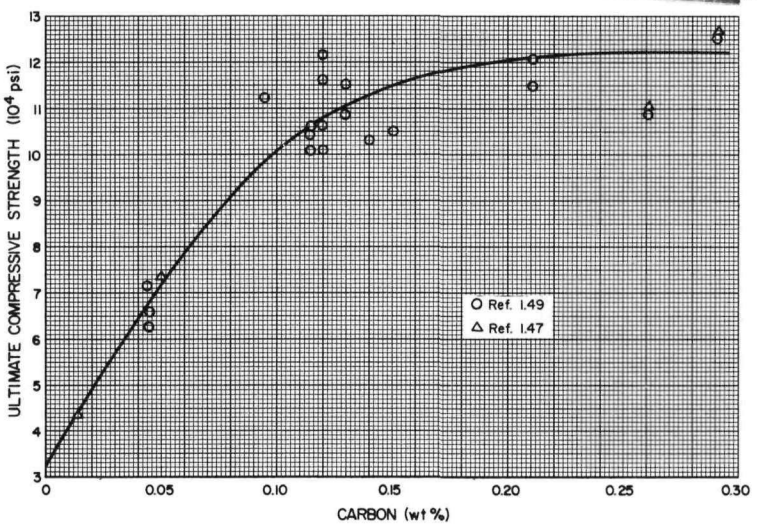

8-14-64 7569-01661

Figure 1.2.17. Room Temperature Ultimate Compressive Strength Data for Zr + 10 U Alloy Hydride Fuel (H/Zr(eff) = 1.67 to 1.85)

The room temperature ultimate compressive strength of the modified fueled hydrides increases quite rapidly with carbon content to about 0.15 wt % and then remains essentially constant above this carbon content level. Figure 1.2.17 illustrates this property effect.

As is typical for brittle materials, the Young's modulus of these fuel materials in compression are slightly lower than comparable values obtained from the tensile tests.

1.2.1.4 Hardness

Hardness data for Zr + 10 U alloy hydrides are given in Table 1.2.7.

The effect of hydrogen concentration on the hardness of unalloyed zirconium hydride is shown in Figure 1.2.18.

TABLE 1.2.7

HARDNESS DATA FOR ZIRCONIUM + 10 wt % URANIUM ALLOY HYDRIDES (Ref 1.50)

Composition		95% Confidence Limits Hardness Values (DPH-100 g load)
H/Zr(eff)	wt % Carbon	
1.60	0.15	205.6
1.60	0.40	186 to 210
1.65	0.02	214.0
1.65	0.15	188 to 222
1.65	0.35	167
1.65	0.40	164 to 182
1.65	0.50	146 to 162
1.70	0.02	163 to 185
1.70	0.40	149 to 165
1.70	0.50	154 to 166
1.70	0.55	178 to 202
1.75	0.15	145 to 159
1.75	0.45	131 to 193
1.75	0.55	143 to 147
1.80	0.15	140 to 156
1.80	0.35	133 to 147
1.85	0.15	142 to 166
2.00	0.15	144

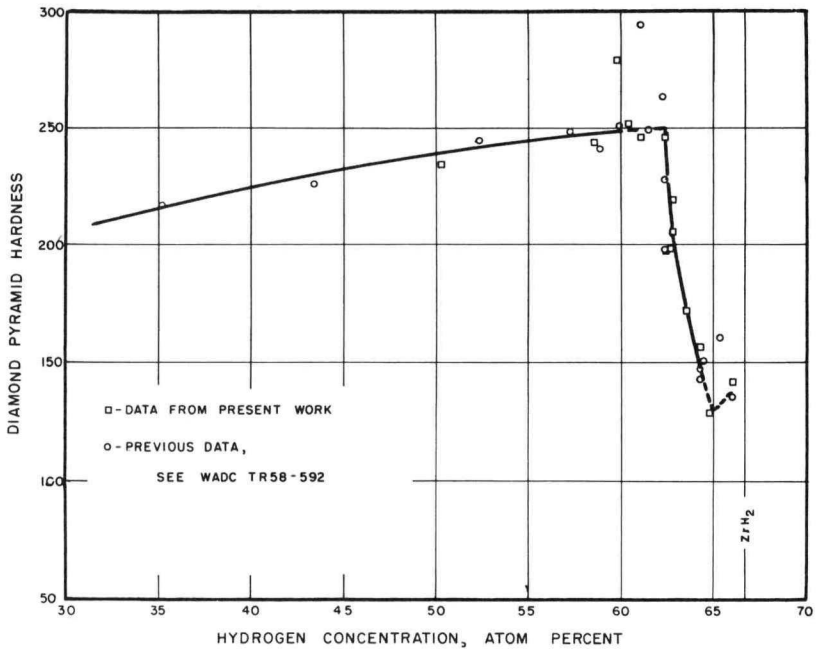

8-13-64 7569-01721

Figure 1.2.18. Effect of Hydrogen Content on Hardness of Zirconium Hydride (Ref 1.11)

1.2.1.5 Impact Strength

The SNAP fuels have a very low impact strength as can be noted from the charpy test data presented in Table 1.2.8. These data indicate that the impact strength of the fuel materials tend to increase with increasing carbon content and hydrogen content.

TABLE 1.2.8

CHARPY IMPACT DATA FOR ZIRCONIUM + 10 wt % URANIUM ALLOY HYDRIDES (Ref 1.50)

Composition		95% Confidence Limits Impact Values ($ft\text{-}lb/in^3$)
H/Zr(eff)	wt % Carbon	
1.60	0.15	0.370
1.60	0.40	0.368 to 0.392
1.65	0.02	0.350
1.65	0.15	0.362 to 0.372
1.65	0.35	0.450 to 0.490
1.65	0.40	0.411 to 0.527
1.65	0.50	0.466 to 0.516
1.70	0.02	0.359 to 0.371
1.70	0.40	0.421 to 0.511
1.70	0.50	0.483 to 0.529
1.70	0.55	0.505
1.75	0.15	0.390 to 0.440
1.75	0.45	0.463 to 0.473
1.75	0.55	0.510
1.80	0.15	0.417 to 0.441
1.80	0.35	0.473 to 0.523
1.85	0.15	0.404 to 0.500
2.00	0.15	0.440

1.2.2 *Long Time*

1.2.2.1 Stress-rupture

Stress-rupture data under tension are presented in Figures 1.2.19, 1.2.20, and 1.2.21 for zirconium hydrides with N_H values of 2.70, 3.45, and 4.0, respectively.

Preliminary data on fueled zirconium hydride[1.52] indicates that materials with hydrogen contents high enough to place them in the δ-ϵ phase region of the zirconium-hydrogen system have much better stress-rupture properties. The single data point presented in Figure 1.2.21 was used to form this preliminary conclusion.

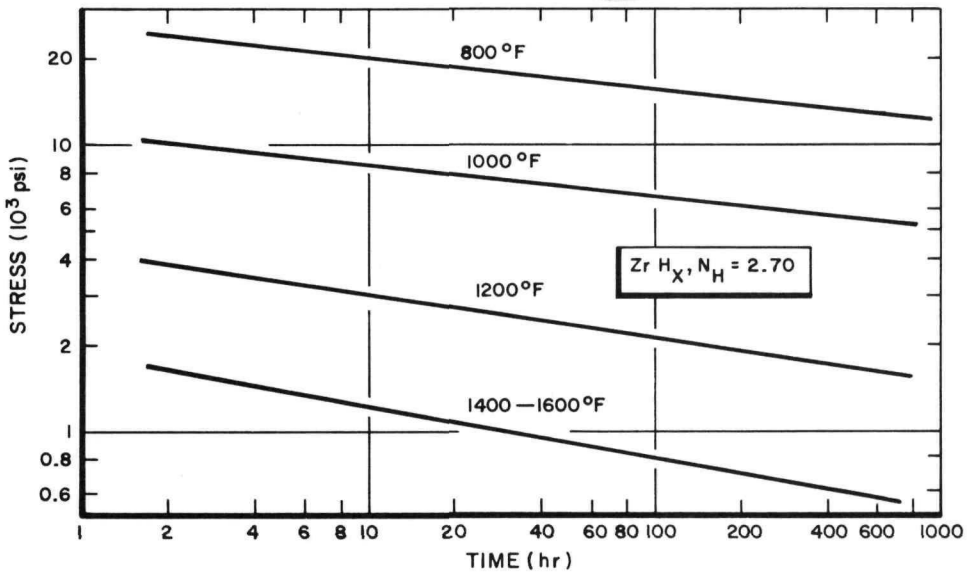

8-10-64

7569-01663

Figure 1.2.19. Stress-rupture Strength of Zirconium Hydrides Where ZrH, N_H = 2.70 (Ref 1.51)

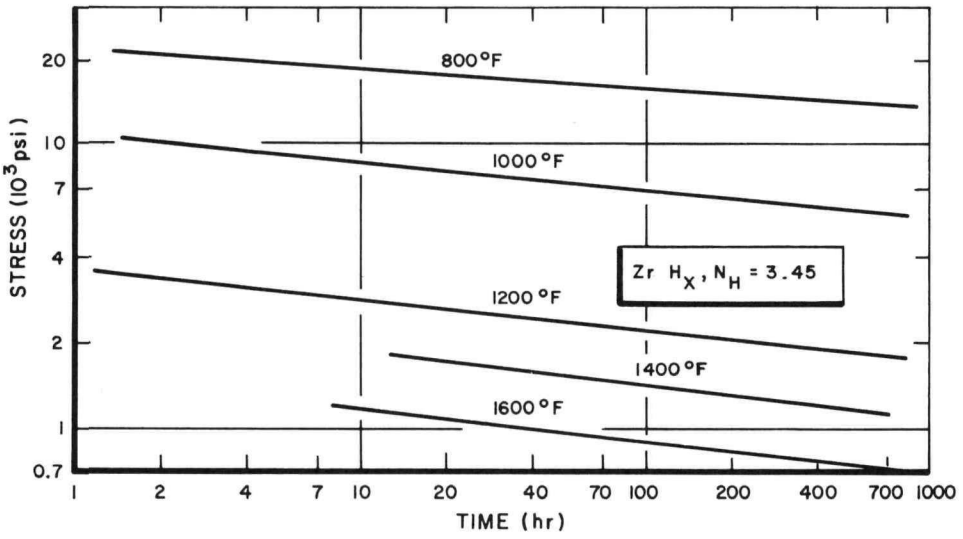

Figure 1.2.20. Stress-rupture Strength of Zirconium Hydrides Where ZrH, N_H = 3.45 (Ref 1.51)

8-10-64

7569-01664

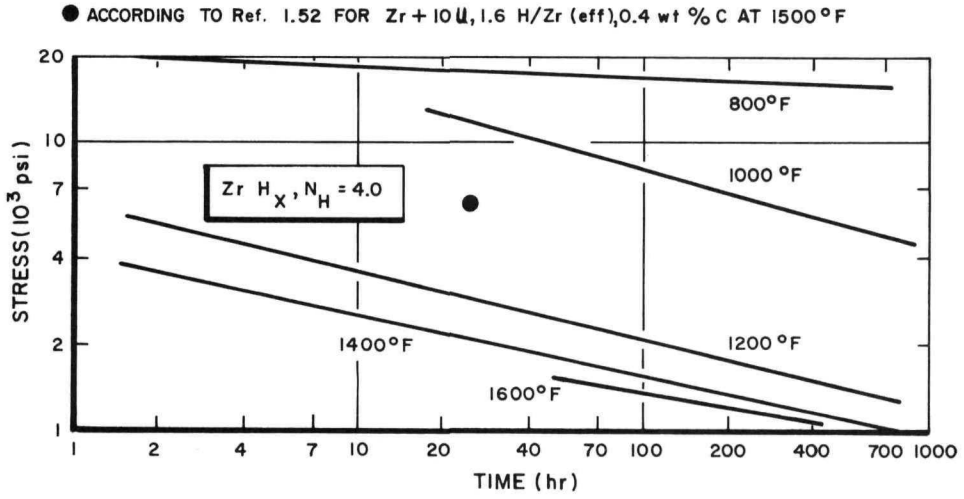

Figure 1.2.21. Stress-rupture Strength of Zirconium Hydrides Where ZrH, N_H = 4.0 (Ref 1.51)

8-10-64

7569-01665

TABLE 1.2.9

RESULTS OF SOME TENSILE CREEP TESTS ON MODIFIED (Zr + 10 U ALLOY HYDRIDES) SNAP FUELS[1.52]

Test Parameters					Minimum Creep Rate (hr^{-1})
Temperature (°F)	H_2 Pressure (psia)	H/Zr(eff)	Carbon Content (wt %)	Tensile Stress (psi)	
1400	19.5	1.67	0.4	3100	7×10^{-8}
1400	19.5	1.67	0.4	4000	6×10^{-6}
1400	31.2	1.76	0.4	4000	7×10^{-6}
1450	31.8	1.67	0.4	4000	2×10^{-5}
1500	25.7	1.60	0.3	4000	2×10^{-5}
1500	25.7	1.60	0.3	6000	2×10^{-4}

1.2.2.2 Creep

A few tensile creep tests have been performed on some modified fueled samples and are presented in Table 1.2.9. These data admittedly do not represent a very clear or thorough picture of the creep behavior of the SNAP fuels having hydrogen content of 1.6 H/Zr(eff) or greater; however, by comparing these data with the data in Figures 1.2.22 and 1.2.23, which are minimum creep rate data under tensile stress for Zr + 8 U alloy hydride with H/Zr(eff) = 1, it can be seen that steady state (minimum) creep rates expected for these materials are orders of magnitude lower than for fuels in the region of H/Zr(eff) = 1.

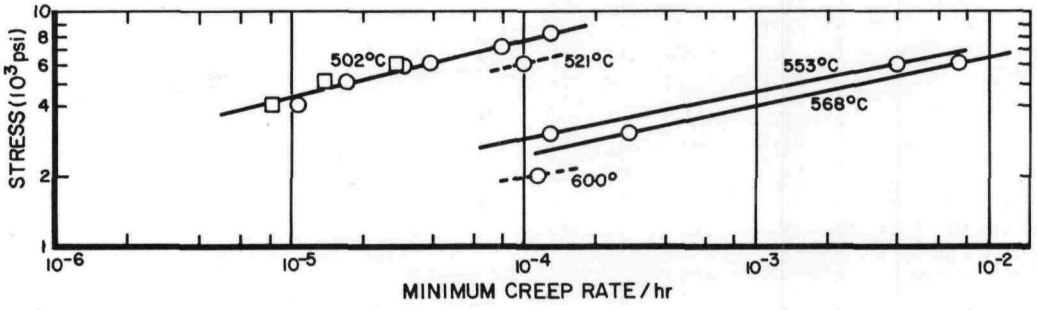

8-10-64 7569-01666

Figure 1.2.22. Minimum Creep Rate vs Stress at Various Temperatures for a Zirconium-Hydrogen-Uranium (Atom Ratio 1:1:0.03) Alloy (Ref 1.53)

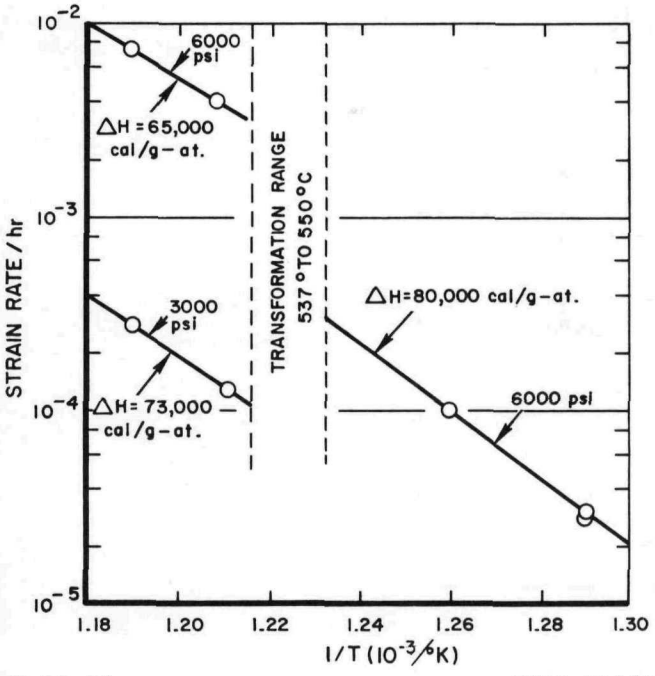

8-10-64 7569-01667

Figure 1.2.23. Minimum Creep Rate of a Zirconium-Hydrogen-Uranium (Atom Ratio 1:1:0.03) Alloy (Zr + 8 U) vs the Reciprocal of the Absolute Temperature at 3000 and 6000 psi (Ref 1.53)

1.3 IRRADIATION PROPERTIES

1.3.1 Nuclear - Cross Sections

In Figure 1.3.1 is shown the thermal macroscopic absorption and scattering cross sections for zirconium hydride as a function of H/Zr (eff). This curve is based on given microscopic cross sections[1.54] and the density given in Figure 1.1.3.

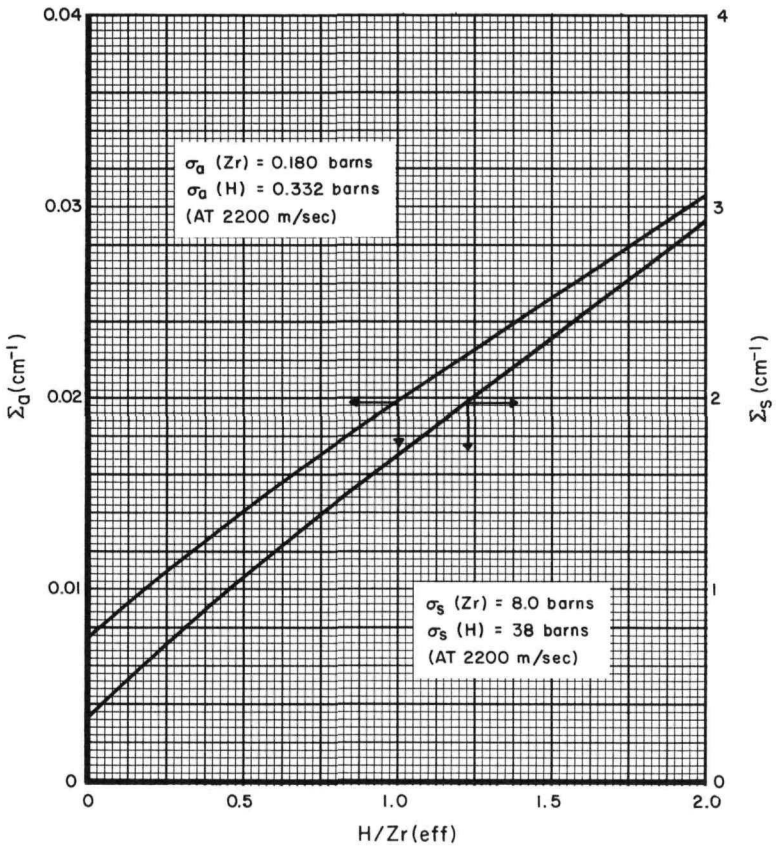

8-12-64 7569-01668

Figure 1.3.1. Neutron Absorption and Scattering Cross Sections

1.3.2 Radiation Behavior

1.3.2.1 Volume Changes

Experimental data[1.55, 1.68] have shown that the density of zirconium hydride fuel decreases during irradiation. This decrease in density ($\Delta\rho/\rho_{final}$) or fractional increase in volume ($\Delta V/V_{initial}$) is a function of the percentage of metal atoms fissioned, b, the temperature of the sample during irradiation, and possibly the time of irradiation Steele[1.57] used the model of Greenwood et al.[1.56] for material having a low volume increase resulting in the surface tension forces controlling the fission gas bubbles and obtained the following semi-empirical equation:

$$\frac{\Delta V}{V_{initial}}(\%) = b^{1.5}\left(\frac{T}{1000}\right)^{1.5} e^{\left(9.80 - \frac{17,400}{T}\right)}, \qquad \ldots(1)$$

where b and T, the "effective temperature," are in units of metal at. % and °R, respectively. Unfortunately only three data points[1.55] (on unmodified Zr+10U hydrided material) were available for use to obtain the above equation. The "effective temperature" was computed by making the temperature history a series of plateaus. The first plateau goes from zero burnup until the maximum temperature is reached. Each successive plateau goes from the previous maximum until the successive lower maximum temperature occurs. By applying the swelling relationship to each plateau, a single temperature which gives the same change in volume as the series of plateaus may be obtained. Steele did not include growth - a volume increase due to the increase in the number of atoms in the fuel - in deriving the generalized equation prior to data fitting. Experimental data are lacking in this area, especially below 1300°F where growth may contribute a very large portion of the volume increase.

Miller[1.69] estimated swelling of modified and unmodified Zr+10U hydride fuel (N_H = 6.5) due to irradiation by the following experimental equation:

$$\frac{\Delta V}{V_{initial}}(\%) = \left(1.2 \times 10^6\right) b^2 \, e^{-22{,}600/\overline{T}_{max}} + 1.0\, b \qquad \ldots(2)$$

where b and T_{max}, the averaged peak fuel temperature, are in units of metal at. % and °R respectively. Modified[1.68] and unmodified[1.55] fuel data were used to obtain the above information. The last term of this equation attempts to take in consideration volume increases due to growth.

Zogran[1.67] modified a model presented by Barnes[1.70] for fuel swelling at elevated temperatures in which bubbles are in vacancy equilibrium (1/2 absolute melting temperature) and obtained the following semi-empirical equation:

$$\frac{\Delta V}{V_{initial}}(\%) = \overline{T}\, b^{1.25} (t \ln t)^{0.25} \, e^{\left(3.7 - \frac{22{,}500}{\overline{T}}\right)} \qquad \ldots(3)$$

where b, t (irradiation time), and $\overline{T}$ (the locational and time averaged fuel temperature) are in units of metal at. %, hr, and °R, respectively. The data used to obtain the above equation were carefully selected from modified Zr + 10U hydride fuel data.[1.68]

The above three equations are illustrated in Figures 1.3.2 and 1.3.3 for an irradiation time of 10,000 hr and two burnup values, 0.4 and 2.0 metal at. %, respectively. Considerable differences exist between the three equations at temperatures around 1500°F and below 1200°F. These differences exist due to the fact that no reliable experimental data are available. Additionally, the data that do exist in the temperature range of 1200 to 1500°F are quite scattered and scarce. Additional experiments need to be performed with greater care, and the results examined very carefully and accurately. Therefore, until such data become available, the above equations should be used with extreme care and only as a guide.

1.3.2.2 Structure Changes

Unfueled, unclad zirconium hydride (N_H = 5.6) shows no effect of radiation other than increasing the number of small voids and microfissures which develop during thermal cycling. No detectable failures of zirconium hydride have been attributed to radiation damage.[1.58, 1.59, 1.60]

Fueled, clad zirconium hydride (N_H = 6.0, 10 wt % U) have been irradiated to determine the effect of radiation on SNAP 8 fuel as a function of temperature and burnup. Observations thus far indicate no apparent microstructure change on the hydrided zirconium-uranium alloy due to radiation.[1.61]

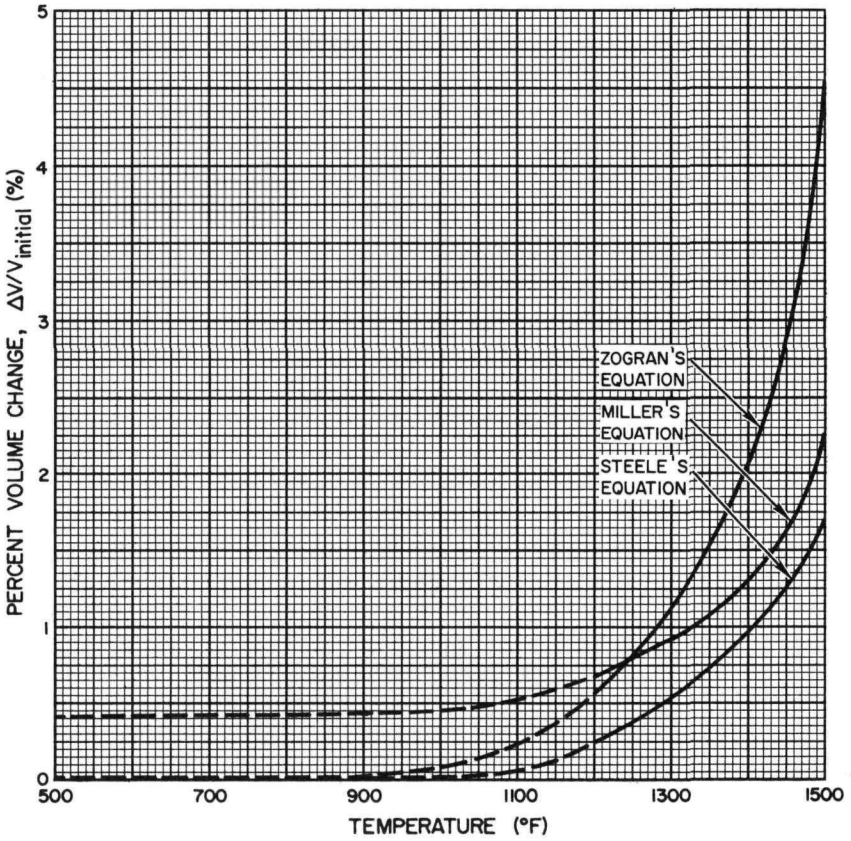

Figure 1.3.2. Comparison of Fuel Swelling Equations Under 0.4 Metal at.% and 10,000 Hr Irradiation Conditions

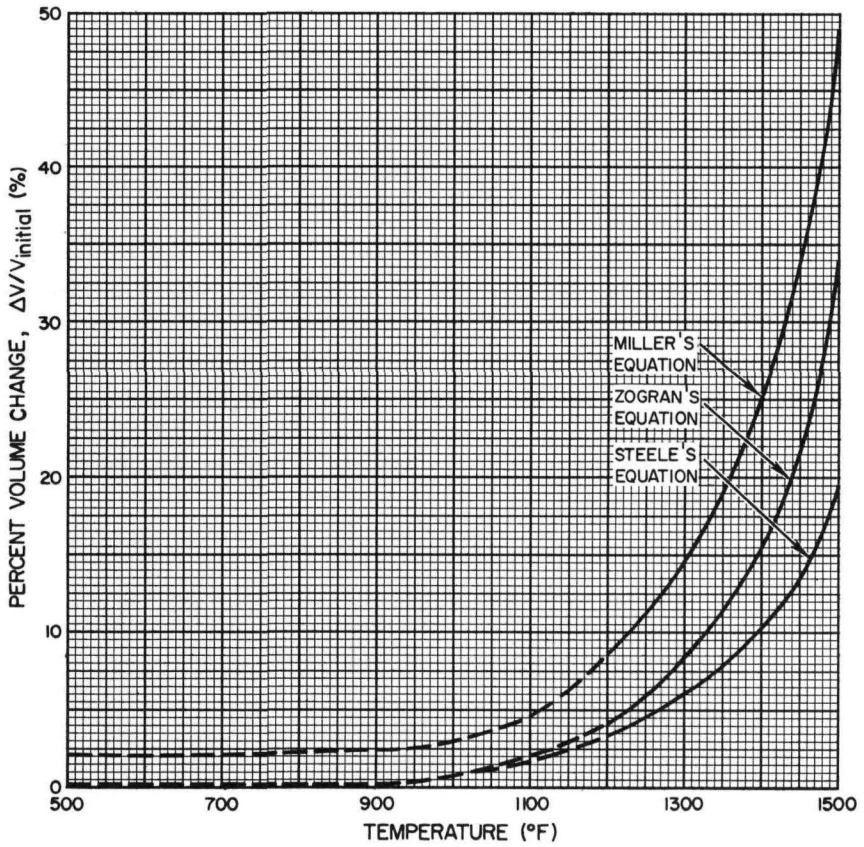

Figure 1.3.3. Comparison of Fuel Swelling Equations Under 2.0 Metal at. % and 10,000 Hr Irradiation Conditions

REFERENCES

1.1 P. T. Gilbert, Jr., "Zirconium Hydride, A Compendium on the Systems Zirconium - Hydrogen and Hafnium - Hydrogen and Related Topics," NAA-SR-1508, October 1956 (Secret-RD)

1.2 G. G. Libowitz, "The Zirconium-Hydrogen Phase Diagram," J. Nuclear Materials, Vol 228 (1962)

1.3 R. L. Beck, "Zirconium-Hydrogen Phase System," ASM Transactions Quarterly, Vol 55, p 542 (September 1962)

1.4 S. S. Sidhu, et al., "Neutron and X-ray Diffraction Studies of Metal Hydrides," ANL 6677, Annual Report for 1962 Metallurgy Division, p 286

1.5 J. Motz, "On the Zirconium-Hydrogen System," Z. Metallkunde, Vol 53, No. 12, p 770 (1962)

1.6 L. D. LaGrange, et al., "A Study of the Zirconium-Hydrogen and Zirconium-Uranium-Hydrogen Systems Between 600 and 800°C," J. Phy. Chem., Vol 63, No. 12, p 2035 (1959)

1.7 D. F. Atkins, "Dissociation Pressures of Hydrided Zirconium-Uranium Alloys," NAA-SR-4245 (Del) February 1962

1.8 H. E. Bigony, R. R. Doig, Jr., and H. H. Krause, Jr., "The Reaction of Hydrogen with Zirconium - 1 and 25 w/o Uranium," BMI 1359, July 1959

1.9 W. L. Korst, "X-ray Studies of δ and ϵ Zirconium Hydrides," NAA-SR-6880, March 1962

1.10 E. A. Gulbrandsen and K. F. Andrew, "Crystal Structure and Thermodynamic Studies on the Zirconium-Hydrogen Alloys," J. Electrochemical Society, Vol 101 p 474 (1954)

1.11 R. L. Beck, "Research and Development of Metal Hydrides," LAR 10, November 1960

1.12 D. S. Parker and C. L. Huffine, "Properties of Hydrided Zirconium," APEX 561, December 1959

1.13 S. M. Toy, "Properties of Zirconium Hydride with Small Alloy Additions," NAA-SR-TDR-6111, February 1961

1.14 P. W. Bickel, "Measurement and Interpretation of Electrical Properties of Zirconium Hydride for Hydrogen-to-Metal Ratios Between 1.5 and 2.0," NAA-SR-4173, January 1960

1.15 R. A. Finch, "Thermal and Electrical Properties of a SNAP-4 Fuel Sample," NAA-SR-MEMO-8134, March 1963 (Confidential RD)

1.16 R. L. Beck, "Thermophysical Properties of Zirconium Hydride," Trans. ASM 55, 556 (1962)

1.17 S. M. Toy and J. B. Vetrano, "Properties of Zirconium Hydride and Zirconium-Uranium Alloy Hydride," NAA-SR-4244, February 1960 (Secret RD)

1.18 R. E. Taylor, "Pulse Heating of Modified Zirconium-Uranium Hydrides," NAA-SR-7736, February 1963

1.19 W. J. Tomasch, "Specific Heats of Delta Phase ZrH and ZrD," Phys. Rev. 123, 510 (1961)

1.20 J. D. Watrous, "Thermal Expansion of Hydrided Zirconium Alloys," NAA-SR-TDR-6046, January 1961

1.21 C. J. Ambrose to D. L. Henry, Personal Communication, Atomics International, A Division of North American Aviation, Canoga Park, California, February 1963

1.22 J. G. Spraul, "Thermal Shock Tests of SNAP Fuel and Their Applicability to SNAP 4," NAA-SR-MEMO-7350, April 1962 (Secret-RD)

1.23 H. E. Flotow and D. W. Osborne, "Heat Capacities and Thermodynamic Functions of ZrH_2 and ZrD_2 from 5 to 350°K and the Hydrogen Vibration Frequency in ZrH_2," J. Chem. Phys. 34, 1418 (1961)

1.24 J. W. Raymond, "Equilibrium Dissociation Pressures of the Delta and Epsilon Phases in the Zirconium-Hydrogen System," NAA-SR-9374, June 1964

1.25 H. E. Johnson, "Hydrogen Dissociation Pressures for Modified SNAP Fuel Rods - Preliminary Report," NAA-SR-MEMO-7765, November 1962 (Confidential-RD)

1.26 H. E. Johnson, "Hydrogen Dissociation Pressures of Modified SNAP Fuels," NAA-SR-9295, March 1964

1.27 G. G. Libowitz, "The Zirconium-Hydrogen System at High Hydrogen Contents," NAA-SR-5015, June 1960

1.28 A. W. Sommer and W. F. Dennison, "Thermal Diffusion of Hydrogen in Nonstoichiometric Zirconium Dihydride," NAA-SR-5066, October 1960

1.29 R. F. Berland, "HYREP - Hydrogen Redistribution Equilibrium Pressure," NAA-SR-MEMO-9193, November 1963

1.30 S. R. deGroot and P. Mazur, "Non-equilibrium Thermodynamics," p 276-278, North-Holland Publishing Co., Amsterdam, 1962

1.31 J. W. Droege, "Thermal Diffusion in a Solid Solution of Hydrogen in Beta Zirconium," BMI-1502, February 1961

1.32 W. M. Albrecht and W. D. Goode, Jr., "The Diffusion of Hydrogen in Zirconium Hydride," BMI 1426, March 1960

1.33 R. W. Dayton and C. R. Tipton, Jr., "Progress Relating to Civilian Applications During November 1959," BMI 1398, December 1959

1.34 V. L. Gelezunas, "The Determination of the Diffusion Coefficient of a Gas-Metal System," APEX-409, September 1957

1.35 R. W. Dayton and C. R. Tipton, Jr., "Progress Relating to Civilian Applications During March 1958," BMI 1259, April 1958

1.36 J. Miller to L. R. Steele, Personal Communication, Atomics International, A Division of North American Aviation, Canoga Park, California, November 1963

1.37 V. L. Gelezunas, "Diffusion Coefficients of ZrH System," Ph.D. Thesis, University of Cincinnati, 1962

1.38 W. Jost, "Diffusion in Solids, Liquids, Gases," p 45, New York Academic Press, 1960

1.39 J. K. Balkwill, "Compatibility of SNAP Fuels and Cladding Materials," NAA-SR-5413, October 1960 (Secret-RD)

1.40 L. B. Lundberg, Unpublished Data, Atomics International, A Division of North American Aviation, Canoga Park, California, November 1963

1.41 D. H. Stone, "Corrosium Tests of Candidate SNAP 4 Fuel Element Material," NAA-SR-TDR-8068, February 1963

1.42 L. B. Lundberg, "Tensile Properties of SNAP 4 Fuel Material at Elevated Temperatures," NAA-SR-MEMO-6957, January 3, 1962

1.43 L. B. Lundberg, Unpublished Data, Atomics International, A Division of North American Aviation, Canoga Park, California, April 1964

1.44 L. B. Lundberg to G. F. Burdi, Personal Communication, Atomics International, A Division of North American Aviation, Canoga Park, California, April 1964

1.45 J. D. Watrous, "Dynamic Modulus of Elasticity for Zr Alloys and Zr Alloy Hydrides," NAA-SR-TDR-5755, October 1960

1.46 C. D. Pears, et al., "The True Stress-Strain Properties of Brittle Materials," TID-17887, October 1962

1.47 J. W. Raymond and S. M. Toy, "Mechanical Strength of Hydrides of Zirconium and Zirconium-Base Alloys," NAA-SR-6732, April 1962 (Secret-RD)

1.48 L. B. Lundberg, "Transverse Rupture Tests on Modified SNAP Fuels" (to be published as NAA-SR-MEMO)

1.49 L. B. Lundberg and J. T. Berling, Unpublished Data, Atomics International, A Division of North American Aviation, Canoga Park, California, September 1963

1.50 J. R. Krohler, Unpublished Data, Atomics International, A Division of North American Aviation, Canoga Park, California, September 1962

1.51 D. S. Parker and C. L. Huffine, "Properties of Hydride Zirconium," APEX 561, December 1959

1.52 L. B. Lundberg, Unpublished Data, Atomics International, A Division of North American Aviation, Canoga Park, California, June 1962

1.53 J. C. Bokros, "Creep Properties of a Zirconium-Hydrogen-Uranium Alloy," J. of N. Materials 3, No. 2, p 216-221 (1961)

1.54 D. J. Huges and R. B. Schwartz, "Neutron Cross Sections," BNL 325 (2nd Edition), July 1958

1.55 J. R. Miller, "NAA 53-1 and 53-2 Irradiation Data," NAA-SR-MEMO-8190, February 4, 1963 (Secret-RD)

1.56 G. W. Greenwood, et al., "The Role of Vacancies and Dislocations in the Nucleation and Growth of Gas Bubbles in Irradiation Fissile Material," J. Nuclear Materials 1, 305-324 (1959)

1.57 L. R. Steele to M. P. Heisler, Internal Letter, "Fuel Swelling," Atomics International, A Division of North American Aviation, Canoga Park, California, 63-IOL-250, July 23, 1963 (Secret-RD)

1.58 P. H. Horton, W. Langweil, and F. H. Welch to L. M. Maki, Internal Letter, "Manned Mission Shield Materials Evaluation Study - SNAP 8 Shield Development Program," Atomics International, A Division of North American Aviation, Canoga Park, California, June 24, 1963 (Confidential-RD)

1.59 Second Annual Report, High-Temperature Materials and Reactor Components Development Programs - Volume II, GEMP-177B, February 1963

1.60 R. Van Houten, "Effect of Certain Processing Variables on Physical Properties of High Hydrogen Density (N_H = 6.0 - 6.16) Zirconium Hydride," April 1961

1.61 J. R. Miller, "Irradiation of Hydrided Zirconium-Uranium Alloy – Experiment NAA 53-1 and NAA 53-2," NAA-SR-9038 (to be published) (Secret-RD)

1.62 P. D. Cohn to R. B. Hinze, Internal Letter, "Use of Modified Fuel in S8ER," Atomics International, A Division of North American Aviation, Canoga Park, California, June 5, 1962 (Secret-RD)

1.63 L. R. Steele to L. Bernath, Internal Letter, "Thermal Diffusion," Atomics International, A Division of North American Aviation, Canoga Park, California, May 29, 1963 (Confidential-RD)

1.64 D. L. Henry, "The Preparation and Properties of the Hydrides of Zirconium, Yttrium, Cerium, and Their Alloys," NAA-SR-3700, July 1959 (Secret-RD)

1.65 C. L. Huffine, "Evaluation of Clad Hydrided Zirconium as Solid Moderator," APEX 335, November 1956 (Secret-RD)

1.66 Aircraft Nuclear Propulsion Department Engineering Progress Report 30 for Period Ending December 1958, APEX 30, January 1959 (Secret-RD)

1.67 R. N. Zogran, "Summary of Available Data on the Swelling of U + Zr + H Fuels Due to Irradiation," NAA-SR-MEMO-9649, March 1964 (Secret-RD)

1.68 T. Paulette, "Post-Irradiation Examination of 53-3," NAA-SR-TDR-9182, February 1964 (Secret-RD)

1.69 J. R. Miller, "Zirconium-Uranium Hydride Dimensional Increases Due to Irradiation," 64-IL-342, Internal Letter, Atomics International, A Division of North American Aviation, Canoga Park, California, April 10, 1964 (Secret-RD)

1.70 R. S. Barnes, "A Theory of Swelling and Gas Release for Reactor Materials," AERE-R-4429, October 1963

1.71 N. H. Katz, "SER Data Report," NAA-SR-MEMO-4722, December 1959 (SRD)

1.72 H. L. Hodges, P. S. Olson, and M. Migliori, "NAA 116-1, -2 Low Temperature Materials Preirradiation Data Compilation," NAA-SR-MEMO-9273, February 1964 (SRD)

1.73 R. K. Edwards, P. Levesque, and D. Cubicciotti, J. Am. Chem. Society, 77, 1307 (1955)

1.74 C. E. Ells and A. D. McQuillan, J. Inst. Metals, 85, 89 (1956)

1.75 T. B. Douglas, J. Am. Chem. Society, 80, 5040 (1958)

2.0 YTTRIUM ALLOY HYDRIDES

2.1 PHYSIOCHEMICAL PROPERTIES

2.1.1 Physical

2.1.1.1 Phase Diagram

The solubility relationships in the yttrium-hydrogen binary system are presented in Figure 2.1.1 as determined at the Denver Research Institute.[2.1] The diagram was established from equilibrium hydriding isotherms, metallography, and x-ray diffraction data on arc-melted yttrium buttons.

The alpha region is single-phased and is characterized by the solid solubility of hydrogen in an expanded, hexagonal, close-packed yttrium structure. A mixture of two crystalline compositions exists between the alpha and the YH_2 boundary, except for the single phase YH_X that has been observed. The YH_3 compound is unstable at temperatures above 586°F, breaking down rather abruptly into hydrogen and more thermally stable YH_2.

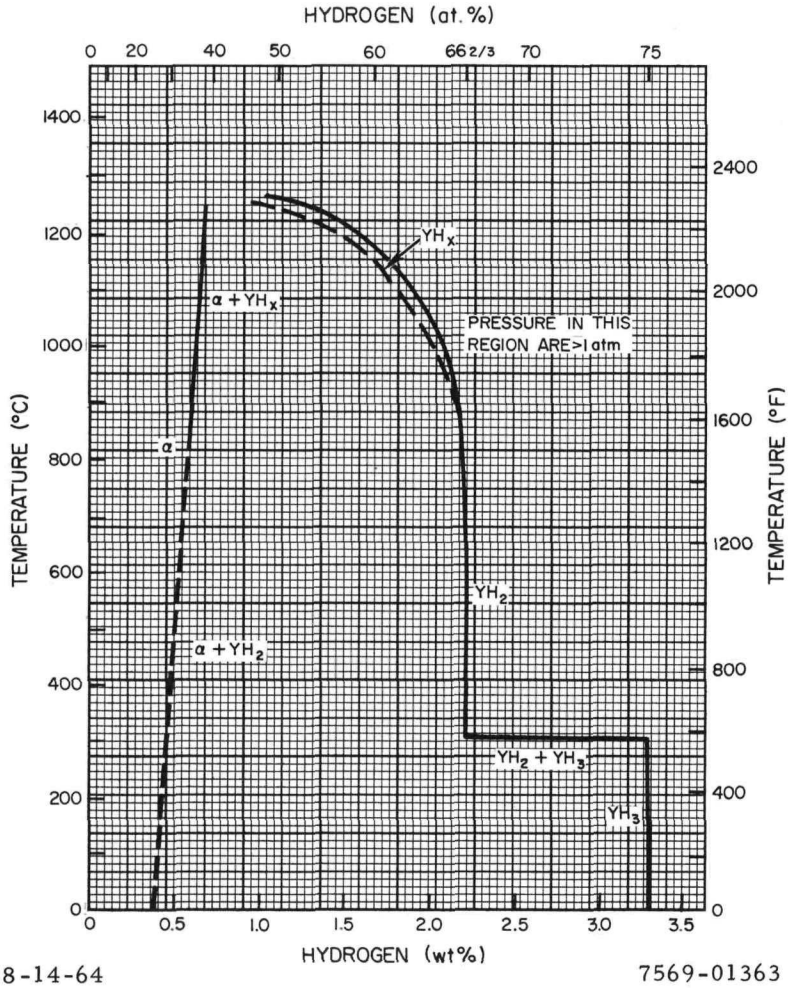

Figure 2.1.1. Phase Diagram of Yttrium-Hydrogen System (Ref 2.1)

2.1.1.2 Crystal Structure

The lattice parameters and structures for the crystalline phases shown in Figure 2.1.1 are given in Table 2.1.1.

TABLE 2.1.1

X-RAY DIFFRACTION DATA ON YTTRIUM, YH_2, and YH_3 COMPOSITIONS

Composition	Crystal Structure	Crystal Type	Lattice Parameters (Å)	Axial Ratio, c_o/a_o	Crystal Density, g/cm^3	Ref.
Y	hcp	Mg	a_o = 3.6474 c_o = 5.7306	1.5711	4.472	2.2
YH_2	fcc	CaF_2	a_o = 5.201		4.293	2.3
Yh_3	hcp		a_o = 3.674 c_o = 6.599	1.796	3.958	2.4

2.1.1.3 Density

In Figure 2.1.2 are shown the densities of both arc-melted yttrium and the alloy 70% yttrium + 30% zirconium* as a function of their hydrogen content. The curve for the first was reported in Ref 2.5 and that for the latter in Ref 2.6. The amount of scatter in the data is not known.

To convert from wt % hydrogen to the atom ratio of hydrogen to metal use the following formulas:

For Y,

$$\frac{H}{M} = 88.21\left(\frac{\text{wt \% H}}{100 - \text{wt \% H}}\right) \qquad \ldots(1)$$

for 70 Y + 30 Zr,

$$\frac{H}{M} = 88.9\left(\frac{\text{wt \% H}}{100 - \text{wt \% H}}\right) \qquad \ldots(2)$$

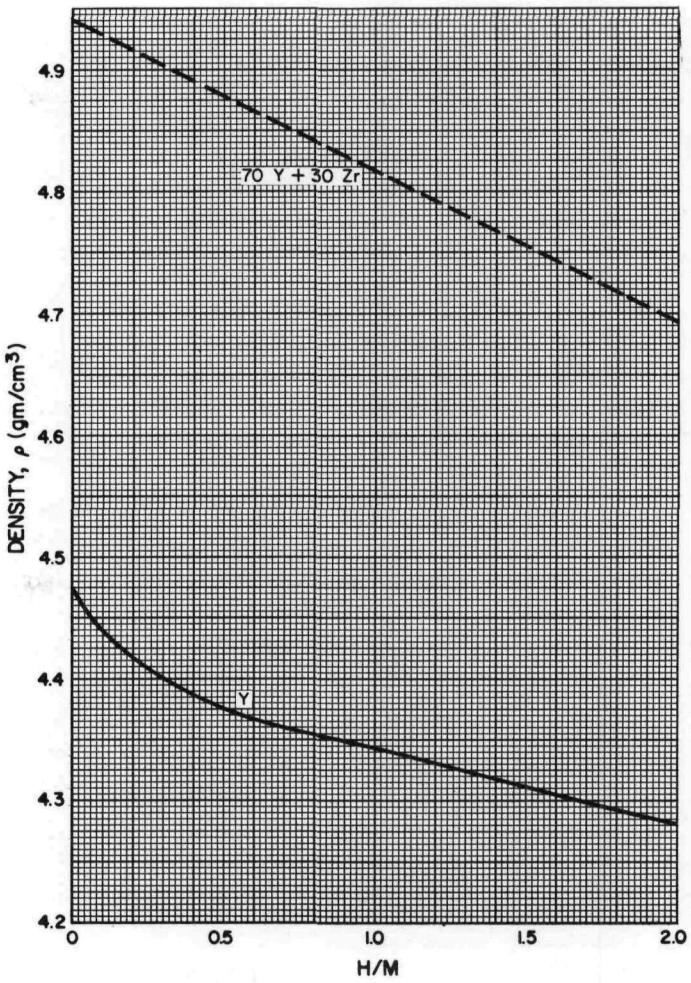

8-14-64 7569-01364

Figure 2.1.2. Densities of Hydrides of Yttrium and 70 Y + 30 Zr Alloy (Ref 2.5 and 2.6)

*All percentages are given by weight unless otherwise specified

2.1.1.4 Hydrogen Density

The concentration of hydrogen in the material, expressed as the number of hydrogen atoms/cm^3 multiplied by 10^{-22}, is called N_H. Figure 2.1.3 shows the dependence of N_H on the atom ratio of hydrogen to metal. These N_H values were calculated from the densities given in Figure 2.1.2.

To convert from the atom ratio of hydrogen to yttrium to the atom ratio of hydrogen to metal use the following formula:

$$\frac{H}{M} = \left[\frac{\frac{wt\ \%\ Y}{88.9}}{\frac{wt\ \%\ Zr}{91.22} + \frac{wt\ \%\ Y}{88.9}}\right]\frac{H}{Y} \qquad \ldots(1)$$

Therefore, for 70 Y + 30 Zr,

$$\frac{H}{M} + 0.705\,\frac{H}{Y} \qquad \ldots(2)$$

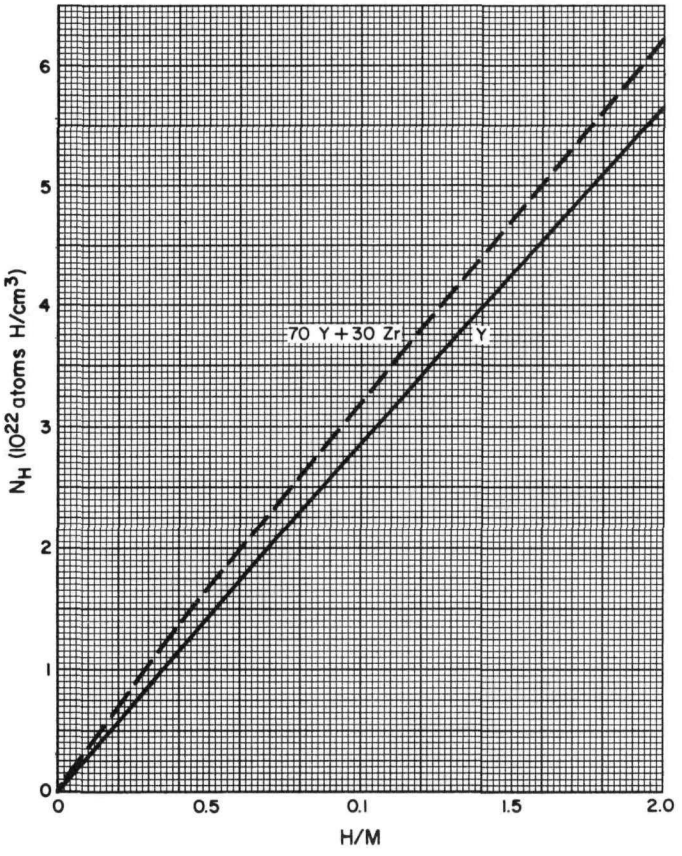

8-14-64 7569-01365

Figure 2.1.3. Hydrogen Density

2.1.2 Electrical

2.1.2.1 Electrical Resistivity

The electrical resistivity of arc-melted yttrium hydride as a function of hydrogen content is shown in Figure 2.1.4. The work was done by Titanium Alloy Manufacturing, Division of Natural Lead, and reported in Ref 2.5.

2.1.2.2 Magnetic Susceptibility

The magnetic susceptibility of arc-melted hydrided yttrium was investigated to determine if this property could be used as a non-destructive test for hydrogen content. The results are given in Figure 2.1.5. The accuracy of the electromagnetic measurements was ±0.05%, and the results were reproducible.

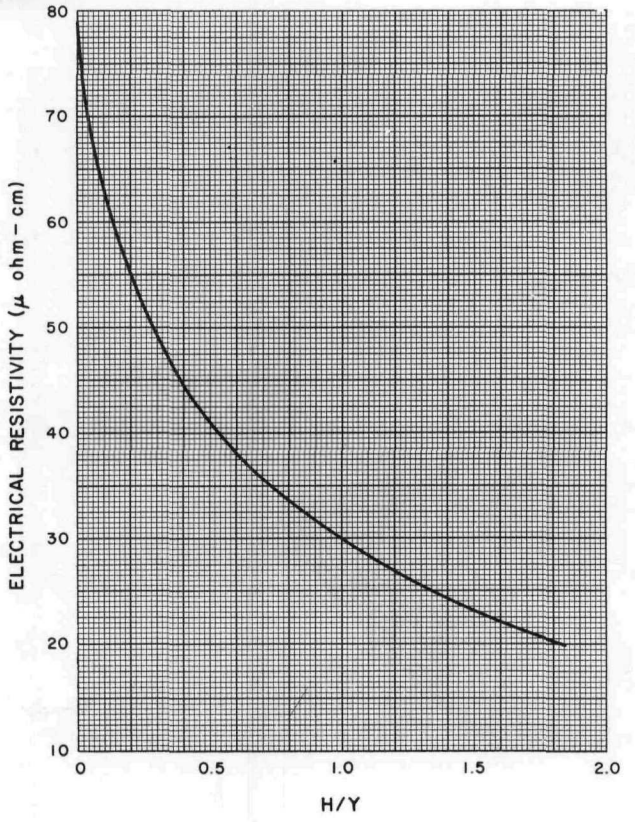

8-14-64 7569-01366

Figure 2.1.4. Electrical Resistivity (Ref 2.5)

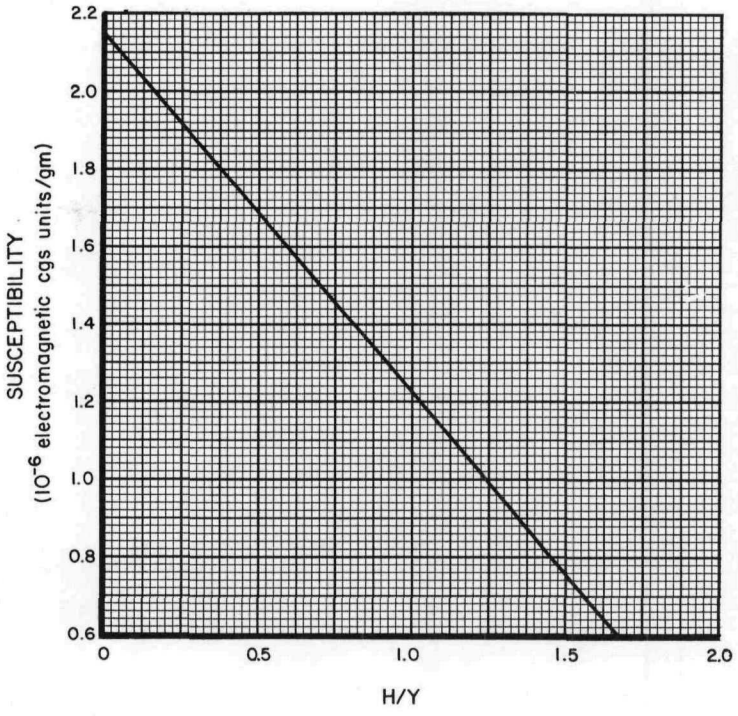

8-12-64 7569-01367

Figure 2.1.5. Magnetic Susceptibility of Hydrided Yttrium (Ref 2.5)

2.1.3 Thermal

2.1.3.1 Thermal Conductivity

The thermal conductivity of hydrided arc-melted yttrium and yttrium alloys decreases with temperature as shown in Figure 2.1.6, which contains all known data. However, the unalloyed yttrium hydride data are inconsistent with electrical resistivity data and are believed to be incorrect.[2.13] A range of thermal conductivity data on zirconium hydride has been included in Figure 2.1.6 for comparison to alloyed and unalloyed yttrium hydride data. It is evident that unalloyed yttrium hydride data should fall above all other data shown in this figure.

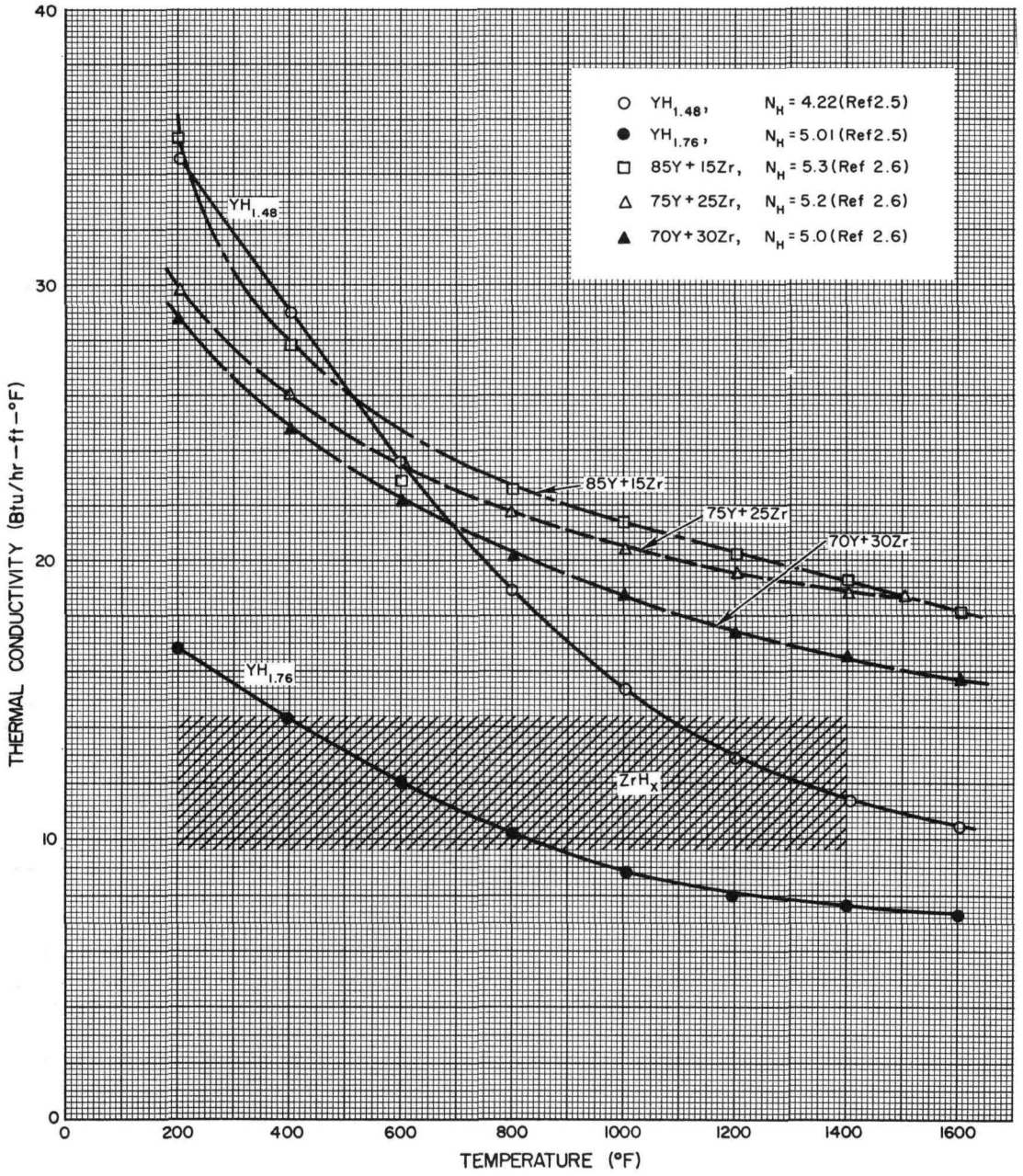

8-14-64 7569-01671

Figure 2.1.6. Thermal Conductivity of Yttrium and Zirconium Hydride Alloys

2.1.3.2 Specific Heat

The specific heats of arc-melted yttrium and alloyed and unalloyed yttrium hydrides as a function of temperature are shown in Figure 2.1.7. The data for the material in the H/Y = 1.7 range indicated a transformation occurred between 1150 and 1250°F. Evidence of transformation in this temperature range has not been manifested in any other way. Brehm[2.13] indicates the shift in slope of the data was caused by an excess loss of hydrogen during the test above 1000°F, and the data should not be used.

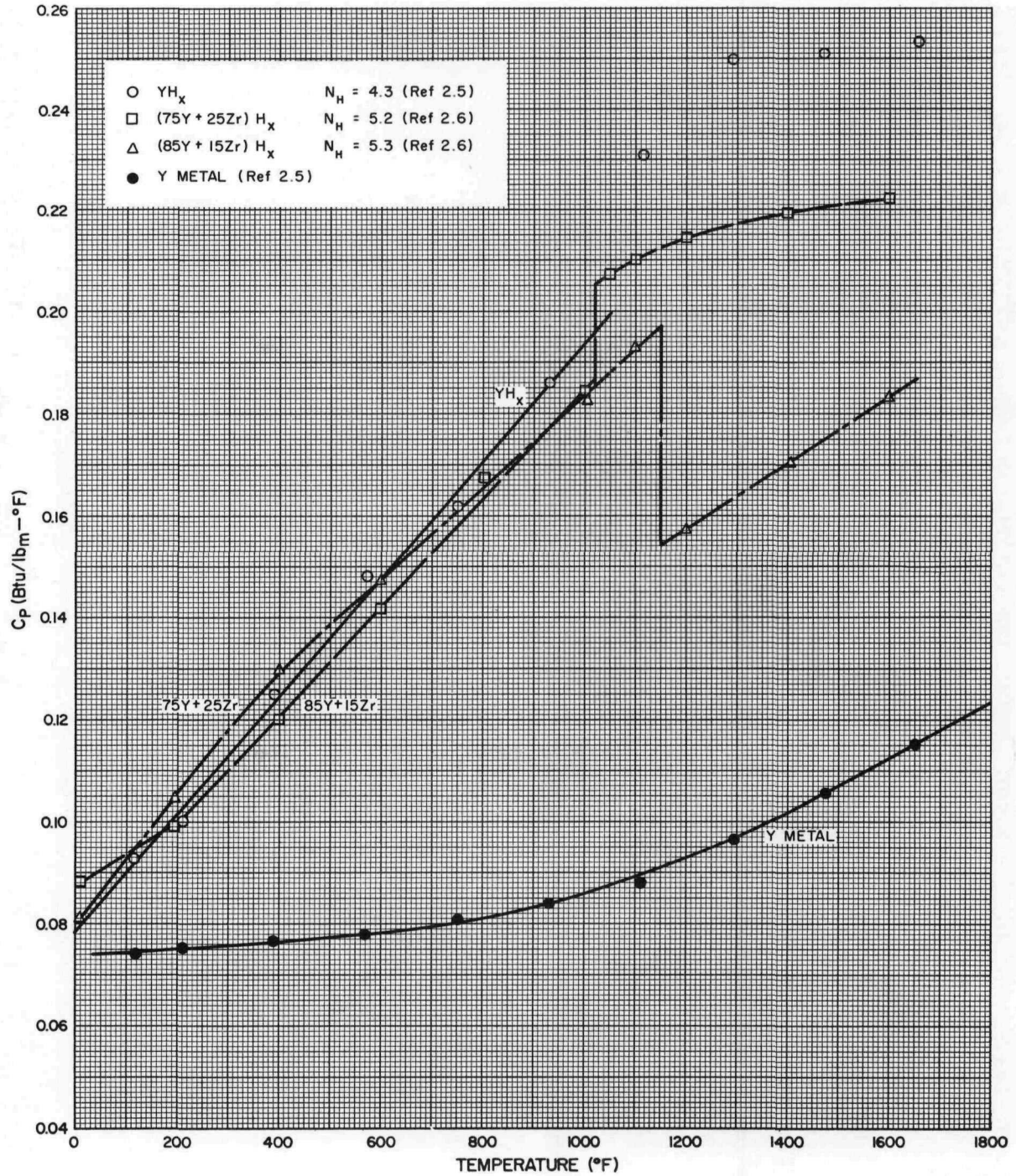

8-14-64 7569-01672

Figure 2.1.7. Instantaneous Specific Heats of Y, YH_x, and $(Y + Zr)H_x$ Alloys

2.1.3.3 Thermal Expansion

The linear thermal expansion of arc-melted yttrium hydride and the 70% yttrium + 30% zirconium alloy hydride is shown in Figure 2.1.8. Data for the solid lines were reported in Ref. 2.5 and 2.9. Data for H/Y = 1.90 were generated by BMI, while the rest were done at ANPD. The alloy data were reported in Ref. 2.6, in which curves for the 85Y+15Zr, 80Y+20Zr, 75Y+25Zr, and 56Y+44Zr alloy hydrides are also given. Scatter in the data was less than 2%.

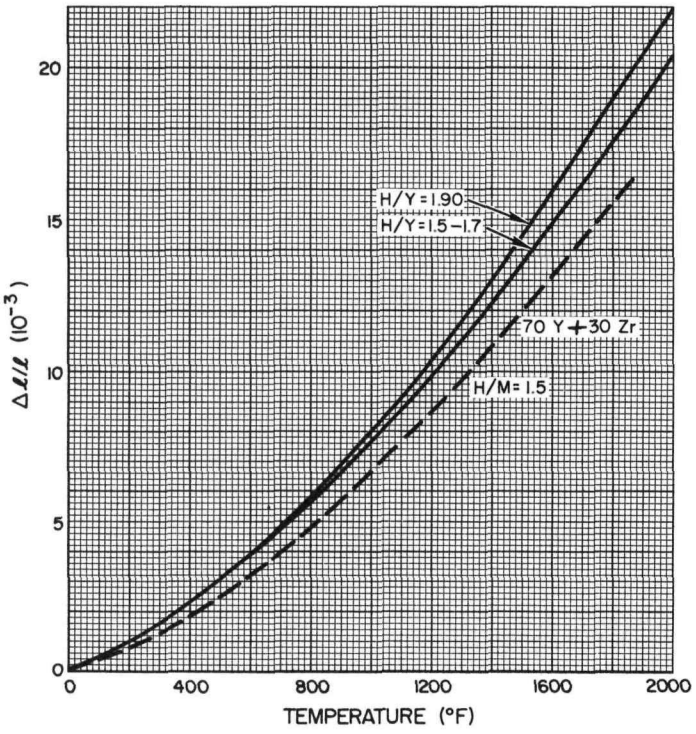

Figure 2.1.8. Thermal Expansion (Ref 2.5, 2.6, and 2.9)

2.1.3.4 Thermal Shock

In one series of tests[2.8] on the thermal shock resistance of arc-melted yttrium hydride and a number of its alloys, samples, 1 in. in diameter and 1-1/2 in. long having a 1/4-in. hole through the center, were temperature cycled in argon from 700 to 2000°F until cracking occurred. The specimens were induction heated at a rate of 500°F per min and cooled by an air blast through a stainless steel tube in the center hole of the specimen. Cooling rates averaged 400°F per min. It was found that specimens of zirconium alloys containing over 25 wt % Zr and chromium alloys containing over 5 wt % Cr could be temperature cycled without significant cracking.

In another series[2.10] specimens of arc-melted yttrium hydride containing less than 2 wt % additions of niobium, molybdenum, chromium, or germanium, 1/4 by 1/4 by 2-1/2 in. long, held at 2000°F in an argon atmosphere, were quenched into water at room temperature in one cycle. An extensive amount of cracking was observed in all the hydrided specimens.

A series of thermal fatigue test[2.10] specimens of the same size and composition as in the previous test were encapsulated individually in quartz tubes containing 1/4 atm of argon and thermal cycled for a total of 100 cycles between approximately 700 and 2000°F, with average heating and cooling times of 2-1/2 and 2-1/4 min, respectively, without any appreciable dwell time. Examination revealed that none of the specimens had formed cracks or fissures.

2.1.4 Chemical

2.1.4.1 Hydrogen Dissociation Pressure

Figure 2.1.9 illustrates the hydrogen dissociation pressure of hydrided arc-melted yttrium as a function of temperature and composition. The principal impurities in the arc-melted yttrium hydrided button specimens were zirconium and oxygen at 0.57 and 0.32%, respectively.[2.12] References 2.7 and 2.9 contain data that are in disagreement with Lundin and Blackledge.[2.12] The most recent data is presented here because of the careful analysis and experiment performed by Lundin and Blackledge. Additional isobar (1 atm) data for hydride yttrium, Cr + 95Y, Cr + 90Y, Zr + 70Y, Zr + 56Y, Sn + 97Y, Ge + 98Y, Ce + 95Y, and Ti + 95Y alloys are presented in Ref 2.8.

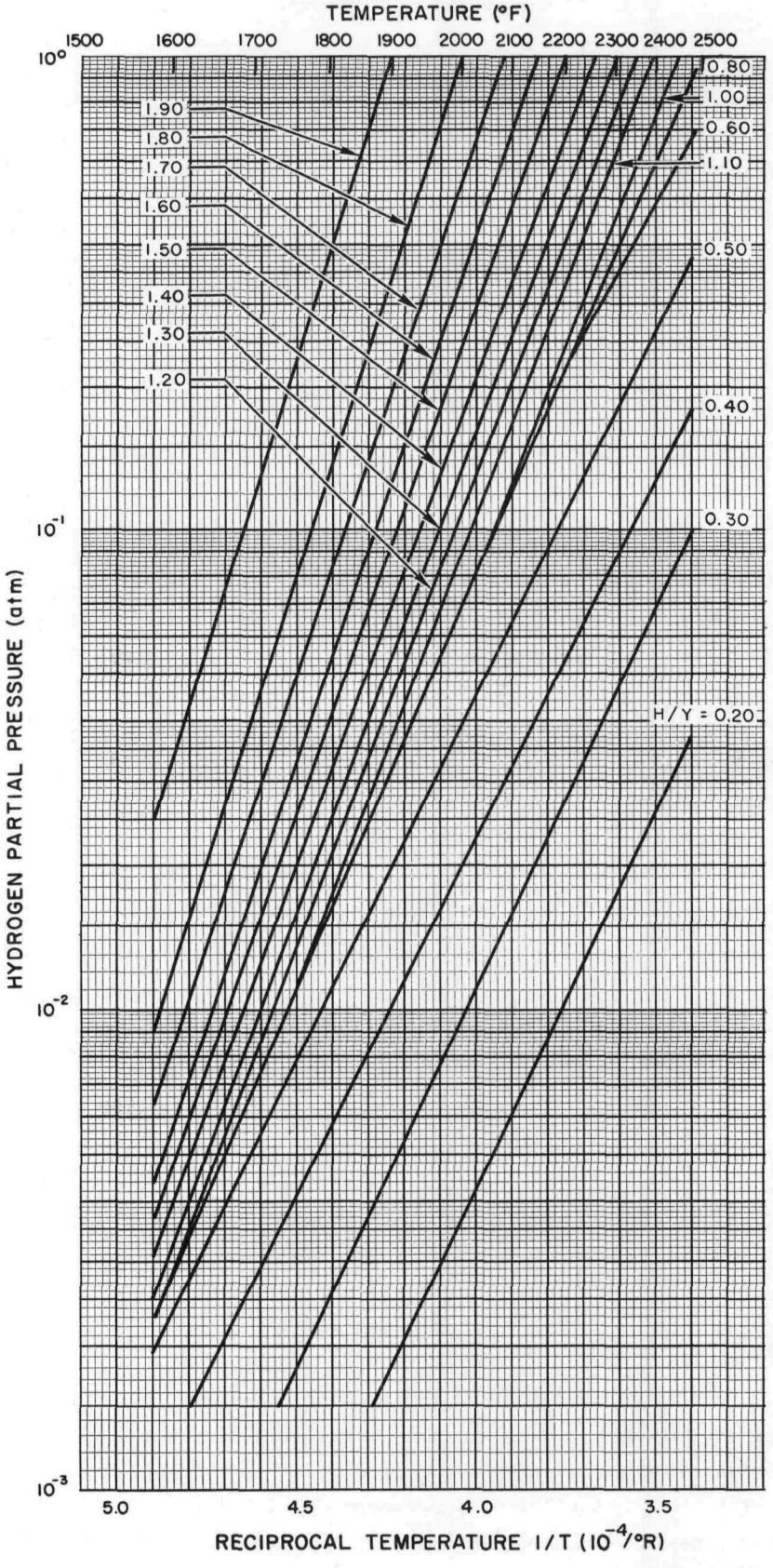

8-14-64

7569-01673

Figure 2.1.9. Hydrogen Dissociation Pressure of YH_x (Ref 2.12)

2.1.4.2 Compatibility

The oxidation resistance[2.8] of arc-melted yttrium and many of its alloys was determined by holding a specimen in air for 2 hr at 1600°F. As a result of these tests the yttrium alloys do not appear to be oxidation-resistant. However, a moderate increase in oxidation resistance can be achieved by the addition of cerium, germanium, titanium, chromium, or possibly silicon. Additions of aluminum, zirconium, lead, or manganese are particularly detrimental to the oxidation of these alloys.

Hydrided yttrium[2.9] is compatible with Fe+Cr+Al alloys to 2100°F and would probably be stable to higher temperatures were it not for the formation of free yttrium that is produced as a result of decomposition of the hydride at such temperatures. Yttrium metal as well as zirconium metal reacts and forms liquid phases with the cladding at temperatures as low as 1700°F.

2.2 MECHANICAL PROPERTIES

2.2.1 Short Time

2.2.1.1 Tensile Properties

Short time tensile properties of arc-melted hydrided yttrium[2.5] are difficult to evaluate as is shown by the data in Figure 2.2.1. Zero percent elongation and reduction in area were observed at temperatures up to 1800°F, with a maximum elongation of 5.5% recorded at 2200°F for the 1.7 H/Y material. The 0.2% offset yield values for the 1.7 H/Y material were about 80 to 170 psi below the ultimate strength at 1600°F.

The modulus of elasticity decreased with temperature from 16 x 10^6 psi at room temperature to 8 x 10^6 psi at 1600°F.

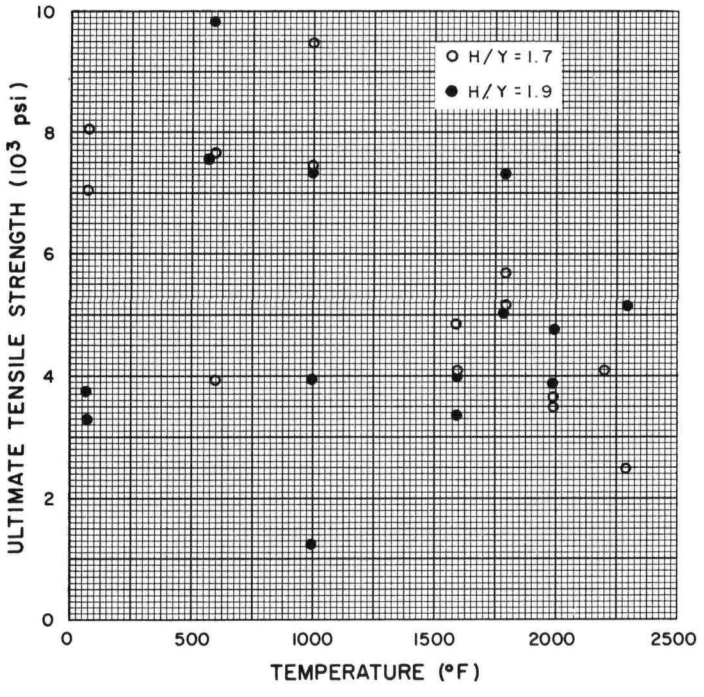

8-14-64 7569-01372

Figure 2.2.1. Ultimate Tensile Strength of Hydrided Yttrium (Ref 2.5)

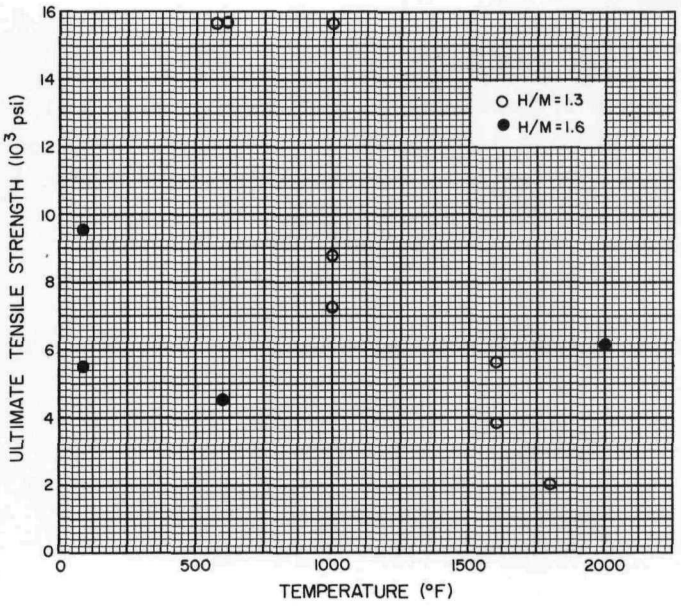

8-14-64 7569-10373

Figure 2.2.2. Ultimate Tensile Strength of Hydrided 70 Y + 30 Zr Alloy (Ref 2.6)

Measured values[2.6] of ultimate tensile strength for the hydrided 70 Y+30 Zr alloy are given in Figure 2.2.2. The data for the H/M = 1.3 material show an almost linear decrease in strength from 600 to 1800°F, but that for the H/M = 1.6 are difficult to evaluate due to the scatter.

No yield was observed below 1800°F. The modulus of elasticity for most of the tests was between 12×10^6 and 17×10^6 psi.

2.2.1.2 Hardness

Hardness data[2.5] are given in Figure 2.2.3 for different hydrogen ratios. The hardness increases with hydrogen content from a value of 100 DPH (diamond pyramid hardness) for the unhydrided arc-melted yttrium. Penetration hardness data made on very brittle material should be taken only as a relative indication and not as a true hardness.

Figure 2.2.4 gives the effect of temperature on hardness of a H/Y = 1.7 material. The data are an average of three impressions on each of two samples at each temperature. The spread between average readings on the two samples ran as high as 10 DPH numbers.

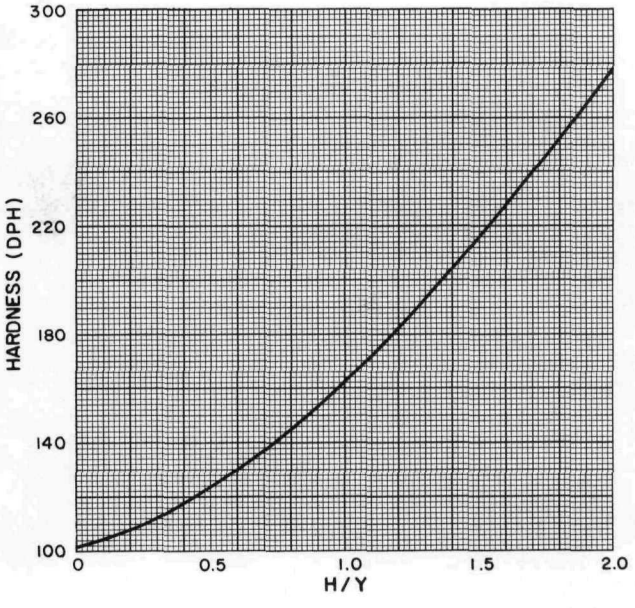

8-14-64 7569-01374

Figure 2.2.3. Hardness vs H/Y at Room Temperature (Ref 2.5)

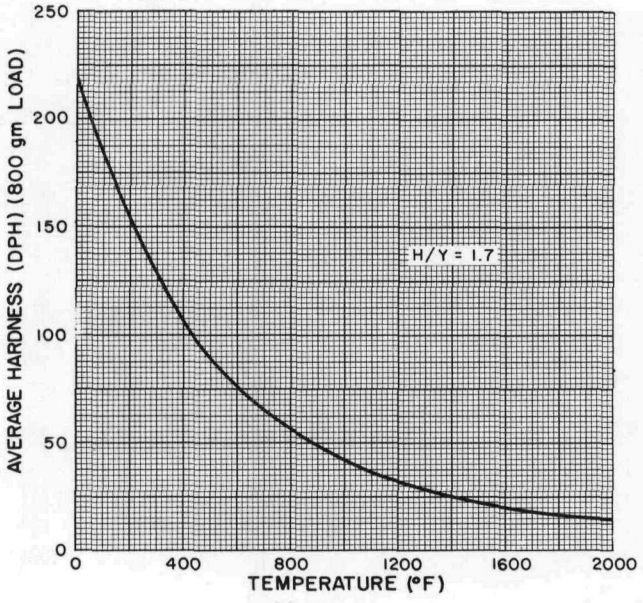

8-14-64 7569-01675

Figure 2.2.4. Effect of Temperature on Hardness (Ref 2.5)

2.2.2 Long Time – Stress-Rupture

Stress rupture data[2.5] for hydrided arc-melted yttrium are shown in Figure 2.2.5. Because of the scatter in the results, correlation was not attempted. For the 7500 psi - 1600°F sample total elongation was 1.6%. For the 2800 psi - 1800°F sample, it was 8.1%. For the 2800 psi - 2000°F sample, it was 11.0%. No change in length was observed for the 6000 psi - 1600°F sample, whereas the length of the 3800 psi - 2000°F sample increased 28%.

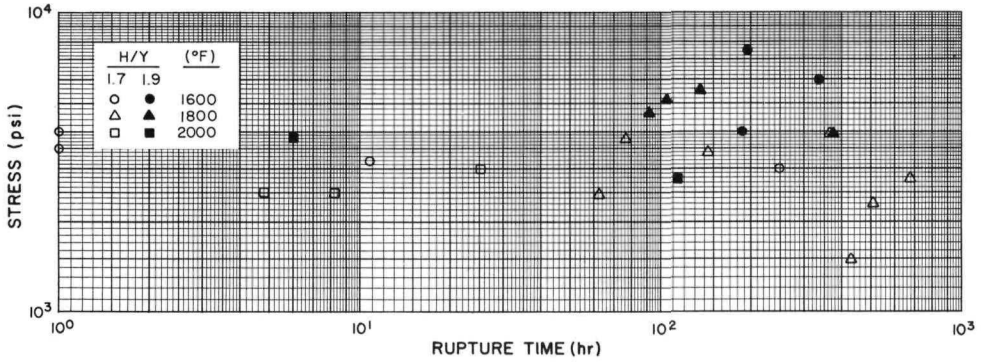

8-14-64 7569-01676

Figure 2.2.5. Stress-Rupture Data for Yttrium Hydride (Ref 2.5)

Stress rupture data[2.6] for the hydrided 70 Y + 30 Zr alloy are given in Figure 2.2.6. The total elongation for the 4000 psi - 1600°F sample was 2.6%, that for the 3000 psi - 1800°F sample was 0.9%, and that for the 2000 psi - 2000°F sample was 3.9%.

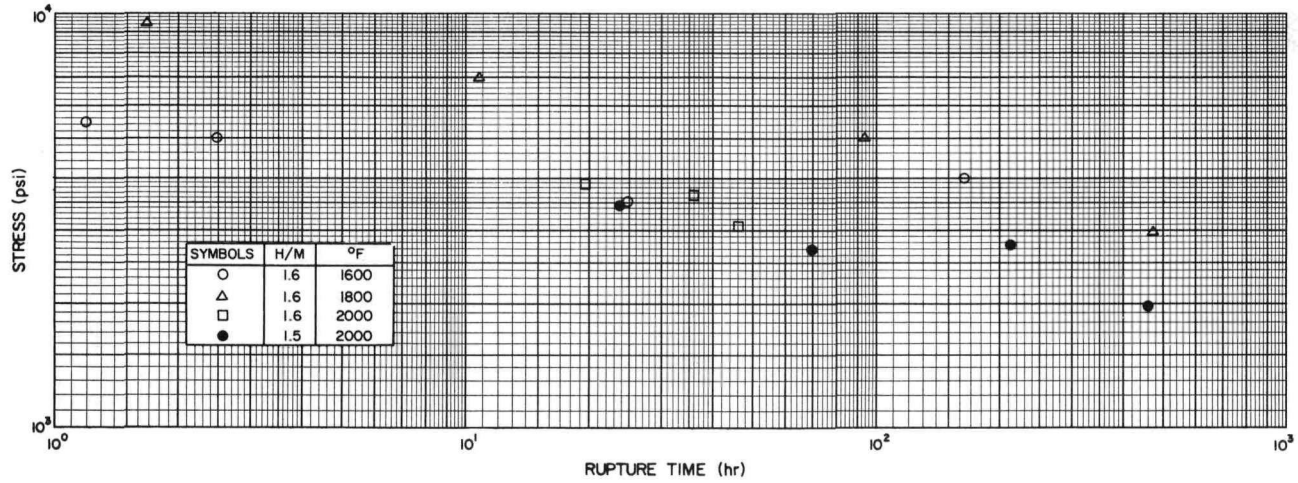

8-14-64 7569-01677

Figure 2.2.6. Stress-Rupture Data for 70 Y + 30 Zr Alloy Hydride (Ref 2.6)

2.3 NUCLEAR – CROSS SECTIONS

In Figure 2.3.1 are shown the macroscopic absorption and scattering cross sections for arc-melted yttrium hydride as a function of H/Y. These curves are based on the microscopic cross sections[2.11] indicated in Figure 2.3.1 and the density given in Figure 2.1.2.

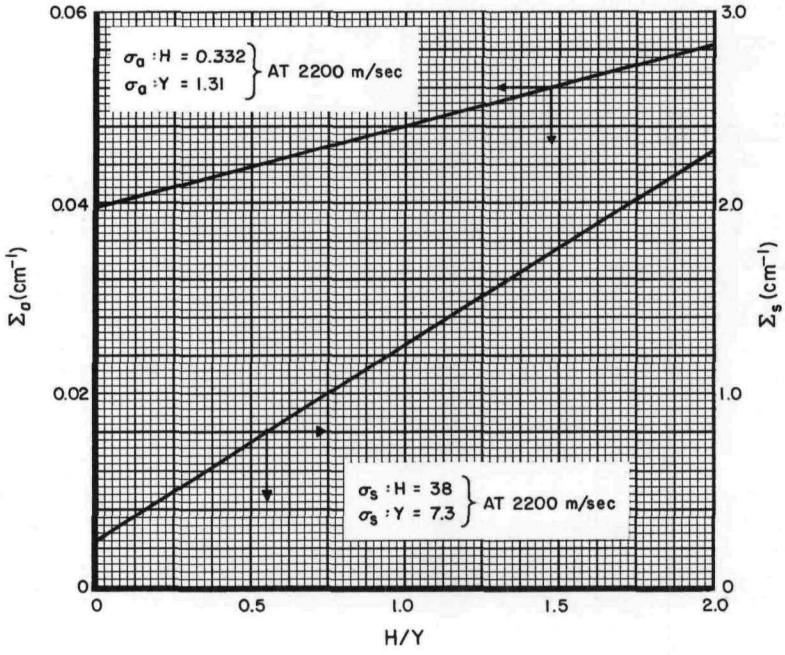

8-12-64 7569-01378

Figure 2.3.1. Neutron Absorption and Scattering Cross-Sections

REFERENCES

2.1 C. E. Lundin and D. T. Klodt, "Fundamental Alloy Development Studies," APEX 334 (August 1, 1957) (Confidential-RD)

2.2 F. H. Spedding and A. H. Daane, "The Preparation and Properties of Rare Earth Metals," Progress in Nuclear Energy, Vol I, Series V (1956)

2.3 C. E. Lundin et al., "Fundamental Alloy Development Studies," APEX 349 (November 15, 1957) (Confidential-RD)

2.4 C. E. Lundin, "Fundamental Alloy Development Studies," APEX 360 (February 20, 1958) (Confidential-RD)

2.5 D. S. Parker, "Properties of Hydrided Yttrium," APEX 558 (May 1960)

2.6 D. S. Parker and C. L. Huffine, "Properties of Hydrided Yttrium-Zirconium Alloys," APEX 562 (December 1959) (Confidential-RD)

2.7 V. P. Calkins et al., "The Technology of Hydrided Yttrium," APEX 545 (June 1958) (Confidential-RD)

2.8 J. M. Williams and C. L. Huffine, "Properties of Hydrided Yttrium Alloys," APEX 551 (October 1959) (Confidential-RD)

2.9 J. A. McGurty et al., "Fabrication and Properties of Hydrided Yttrium," APEX 529 (February 1959) (Confidential-RD)

2.10 S. J. Paprocki et al., "Cladding and Physical Properties of Yttrium Hydride and Yttrium Hydride Alloys," LAR 6, p 217 (February 1960) (Secret-RD)

2.11 D. J. Hughes and R. B. Schwarty, "Neutron Cross Sections," BNL 325 (July 1, 1958)

2.12 C. E. Lundin and J. P. Blackledge, "Pressure-Temperature-Composition Relationships of the Yttrium-Hydrogen System," Journal of the Electrochemical Society, 109, No. 9, (September 1962)

2.13 R. L. Brehm, Unpublished Notes, Atomics International, A Division of North American Aviation, Canoga Park, California (May 1964)

3.0 CLADDING MATERIALS

3.1 ALLOYS AND COMPOSITIONS

Table 3.1.1 lists basic compositions of cladding materials considered usable in SNAP systems. Two general types of nickel base alloys have been developed for high temperature service; solid solution strengthened alloys and precipitation hardened alloys. Solid solution strengthened alloys, exemplified by Hastelloy N and Hastelloy X, are weaker than precipitation hardened alloys, such as Hastelloy R-235 and Rene 41, but maintain strength to higher temperatures and are less affected by a radiation environment. Hastelloy N was jointly developed by ORNL and INCO under the designation INOR-8 for molten salt reactor applications. Hastelloy X has superior oxidation resistance at high temperatures.

Hastelloy R-235 resists overaging to about 1750°F with excellent strength. Rene 41 is used primarily for highly stressed components up to about 1800°F. TD Nickel, a ThO_2 dispersion strengthened pure nickel material, maintains a lower strength until almost reaching the melting point. TZM, a high strength molybdenum alloy, is included for comparison for use in excess of 2000°F.

TABLE 3.1.1
ALLOYS AND COMPOSITION

Alloy	Nominal Composition (wt. %)											Reference
	Cr	Mo	W	Fe	Co	Al	Ti	C	Mn	Si	Other	
Hastelloy N	7	16.5	5*	5*	0.2*	-	0.5*	0.06	0.8*	0.5*	-	3.1
Hastelloy X	22	9	0.6	18.5	1.5	-	-	0.10	1*	1*	-	3.2
Hastelloy R-235	15.5	5.5	-	10	2.5*	2.0	2.5	0.16*	0.25*	0.6*	-	3.3
Rene 41	19	10	-	5*	11	1.5	3	0.12*	0.1*	0.5*	0.006 B	3.4
TD Nickel	-	-	-	-	-	-	-	-	-	-	2 ThO_2	3.5
TZM	-	Bal	-	0.01*	-	-	0.5	0.02	-	0.008	0.002* Ni	3.6

*Indicates maximum allowable amount

3.2 PHYSICOCHEMICAL PROPERTIES

3.2.1 Physical

Table 3.2.1 illustrates the physical properties of the cladding materials considered for SNAP systems. All nickel base alloys have a FCC structure modified by the addition of strengthening elements. Normal strengthening elements are Mo, Cr, and Fe and to a lesser extent Co and W.

Precipitants for strengthening are Ti and Al compounds with Ni and C. TD Nickel utilizes a fine ThO_2 precipitate in the pure nickel matrix for strength. The molybdenum alloy, TZM, uses small amounts of Ti and Zr to strengthen the body centered cubic structure.

TABLE 3.2.1
PHYSICAL PROPERTIES OF CLADDING MATERIALS

Alloy	Structure	Density		Melting Point		Reference
		(lb/in^3)	(gm/cm^3)	(°F)	(°C)	
Hastelloy N	FCC strengthened by Mo, Cr, and Fe	0.317	8.79	2370-2430	1300-1330	3.1
Hastelloy X	FCC strengthened by Cr, Fe, and Mo	0.297	8.23	2350	1288	3.2
Hastelloy R-235	FCC strengthened by Cr, Fe, and Mo with precipitates of Ti and Al compounds	0.296	8.22	2400	1316	3.3
Rene 41	FCC strengthened by Cr, Co, and Mo with precipitates of Ti and Al compounds	0.298	8.25	2385-2450	1310-1345	3.4
TD Nickel	FCC strengthened with THO_2 precipiate	0.322	8.90	2600	1427	3.5
TZM	BCC strengthened by Ti and Zr	0.369	10.22	4730	2610	3.6

3.2.2 Electrical Resistivity

Most nickel base alloys are not used for applications where electrical resistivity must be known as a function of temperature. Manufacturers' literature provides room temperature values, shown in Table 3.2.2, but none at higher temperatures. Values have been determined for TD Nickel and TZM as shown in Figure 3.2.1.

TABLE 3.2.2

ELECTRICAL RESISTIVITY OF ROOM TEMPERATURE PROPERTIES

Alloy	Electrical Resistivity at Room Temperature (μ-ohm-cm)	Reference
Hastelloy N	139	3.1
Hastelloy X	118	3.2
Hastelloy R-235	133	3.3
Rene 41	-	-
TD Nickel	7.6	3.5
TZM	7	3.6

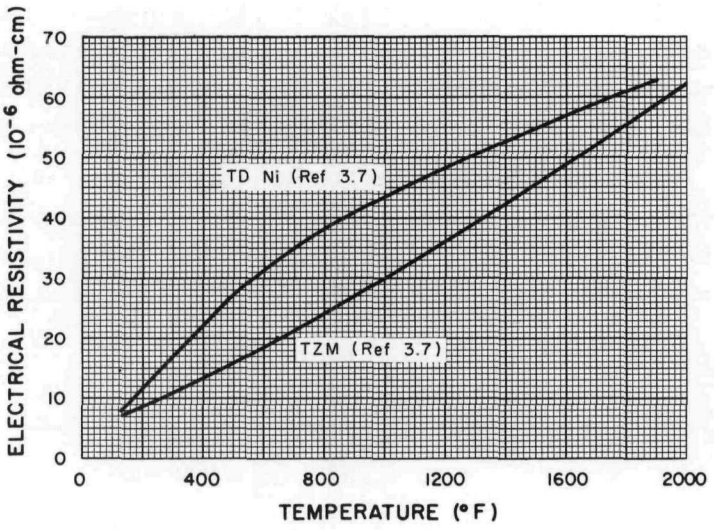

8-14-64 7569-01379

Figure 3.2.1 Elevated Temperature Electrical Resistivity Property of TZM and TD Nickel

3.2.3 Thermal

3.2.3.1 Thermal Conductivity

Vendors have determined thermal conductivities, shown in Table 3.2.3, of their alloys. Methods of determination are unspecified as are accuracies. Elevated temperature values are shown in Figures 3.2.2 and 3.2.3.

TABLE 3.2.3

ROOM TEMPERATURE - THERMAL CONDUCTIVITY

Alloy	Thermal Conductivity at Room Temperature (Btu/hr-ft-°F)	Reference
Hastelloy N	6.0	3.8
Hastelloy X	5.25	3.2
Hastelloy R-235	5.25	3.3
Rene 41	-	-
TD Nickel	47.5	3.9
TZM	82	3.6

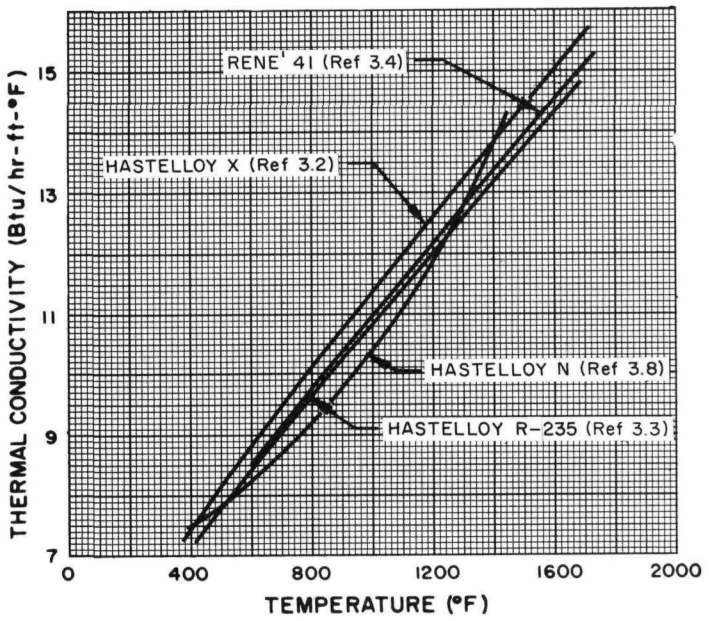

8-14-64 7569-01380

Figure 3.2.2 Elevated Temperature Thermal Conductivity of the Nickel Base Alloys

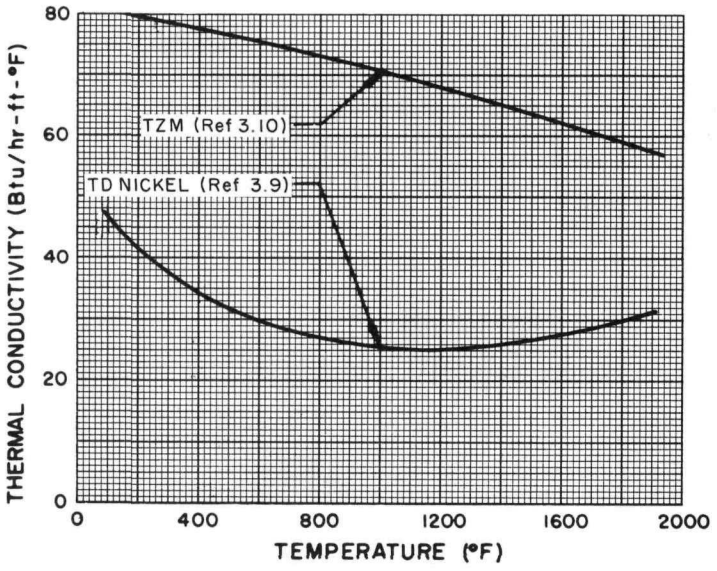

8-14-64 7569-01381

Figure 3.2.3. Elevated Temperature Thermal Conductivity of TZM and TD Nickel

3.2.3.2 Specific Heat

Specific heat values shown in Table 3.2.4 were calculated based on nickel with the addition of the various constituents. Variations of specific heat as function of temperature are shown in Figure 3.2.4. The drop in value for TD nickel is due to the Cure temperature while the increase shown for Hastelloy N is felt to be due to ordering.

TABLE 3.2.4

ROOM TEMPERATURE SPECIFIC HEAT PROPERTY

Alloy	Specific Heat Btu/lb-°F at Room Temperature	Reference
Hastelloy N	0.096	3.8
Hastelloy X	0.105	3.2
Hastelloy R-235	0.1096	3.3
Rene 41	0.108	3.4
TD Nickel	0.106	3.9
TZM	0.066	3.6

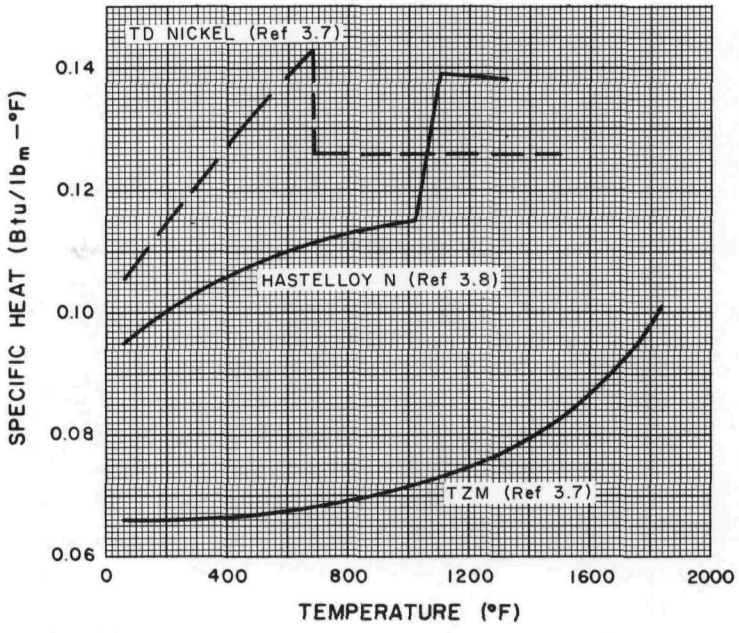

8-14-64 7569-91382

Figure 3.2.4 Elevated Temperature Specific Heat

3.2.3.3 Thermal Expansion

Vendor data was used to show thermal expansion in Figures 3.2.5 and 3.2.6. Variations in the shapes of the curves tend to indicate variations in experimental techniques causing differences in the apparent values shown. In the temperature range of interest, 1200 to 1600°F, maximum and minimum values for all nickel base alloys probably range only ±5% from the mean. The major point to note is the considerably smaller thermal expansion coefficient of TZM when compared to the nickel base alloys.

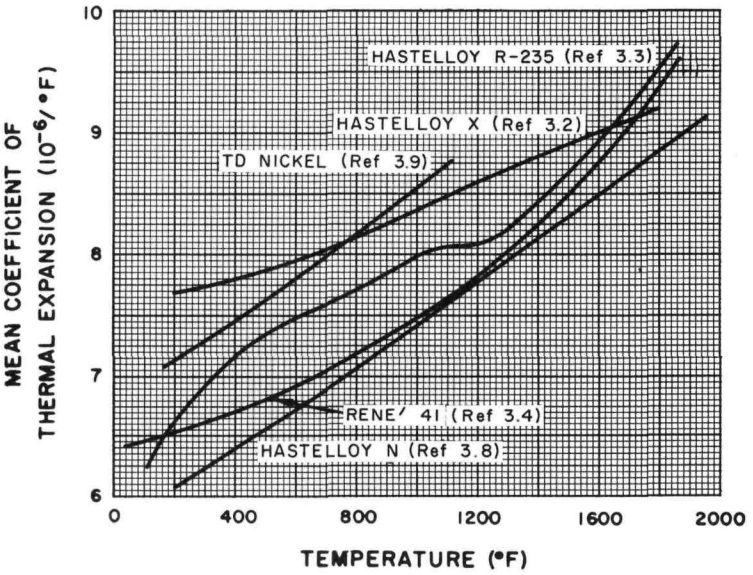

8-14-64 7569-01383

Figure 3.2.5 Mean Coefficient of Thermal Expansion for Nickel Base Alloys (RT to Temperature Indicated)

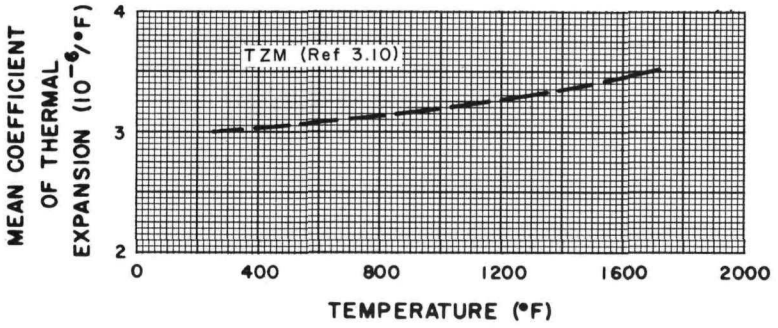

8-14-64 7569-01384

Figure 3.2.6 Mean Coefficient of Thermal Expansion for TZM (RT to Temperature Indicated)

3.2.3.4 Emissivity

Since nickel base alloys* are not generally used for applications where emissivity must be known these values have not been determined. Only values for TD Nickel (and pure nickel) and TZM are listed in Table 3.2.5.

TABLE 3.2.5

ELEVATED EMISSIVITY PROPERTY

Alloy	Emissivity	
	ϵ	T°F
TD Nickel (Ref 3.9)	0.20	1000
	0.65	2000
	0.72	2400
TZM (Ref 3.6)	0.07	1000
	0.27	2000

*Hastelloy N,[3.8] Hastelloy X,[3.2] Hastelloy R-235,[3.3] and Rene 41.[3.4]

3.2.4 Chemical

3.2.4.1 Hydrogen Permeation

The Coating Section contains permeation rates for some common cladding materials. It should be noted that the figure in that section indicates permeation rates for uncoated 10-mil-thick material. If the hydrogen permeation rate of identical uncoated material 5 mil thick is required, the rate would be twice as much as that shown for the 10 mil thick material at the same temperature.

TABLE 3.2.6

CLADDING ALLOYS IN CONTACT WITH ZIRCONIUM HYDRIDE (FUELED AND UNFUELED)[3.17]

Cladding Alloy	Uranium Content In ZrH_x (wt %)	Test Time (hr)	Condition Temperature (°F)	Results
Inconel X*	10	190	1500	Three layer diffusion zone 70 μ wide
Inconel X*	7	360	1600	Diffusion zone 12 μ wide
Hastelloy B†	7	190	1500	Brittle diffusion zone 45 μ wide
Nickel	0	210	1200	No diffusion or reaction
Nickel	7	360	1600	Diffusion zone 225 μ wide on hydride side of original interface
Molybdenum	10	210	1200	No diffusion or reaction
Molybdenum	7	190	1500	No diffusion or reaction
Molybdenum	7	360	1600	Intermittent 20 μ diffusion zone

NOTES: *Inconel X is similar in chemical composition to Hastelloy R-235 except that Inconel X has no Mo
†Hastelloy B is similar in chemical composition to Hastelloy N except the HastelloyB has no Cr

Corrosion of NaK-78 on Hastelloy N, Inconel X, and Molybdenum was determined in closed thermal convection loops using small test coupons. Results are shown in Table 3.2.8.

TABLE 3.2.7

CLADDING ALLOYS IN CONTACT WITH AIR

Alloy	Temperature (°F)	Time (hr)	Weight Change (mg/cm^2)	Reference
Hastelloy N	1600	100	+0.25	3.1
Hastelloy N	1800	100	+0.48	3.1
Hastelloy N	1900	100	+0.52	3.1
Hastelloy N	2000	100	+2.7	3.1
Hastelloy X	2000	100	-2.5	3.2
Hastelloy R-235	2000	100	-13.0	3.2
TD Nickel	2000	100	-10.75	3.9

3.2.4.2 Compatibility

Compatibility tests between potential cladding materials and zirconium uranium hydride fuel were performed on chemically cleaned surfaces held together under static load in a hydrogen atmosphere. Both Ni and Fe form low melting (<1400°F) eutectics with the U causing extensive interactions with the fuel as shown in Table 3.2.6. Molybdenum performs better than the nickel base alloys but still has a diffusion zone at 1600°F which appears to be pressure dependent.

Weight changes in stagnant dry air are shown in Table 3.2.7 at the 100 hr level which was most readily available time for comparison.

TABLE 3.2.8

CLADDING ALLOYS IN CONTACT WITH NaK-78 (Ref 3.18)

Alloy	Temperature (°F)	Time (hr)	Type and Rate of Attack (10^{-3} Inch Depth)
Hastelloy N	1200	1500	Slight evidence of general corrosion
	1200	2500	No apparent attack
	1200	3500	No apparent attack
	1200	4500	1.4 intergranular corrosion
	1400	1500	Slight evidence of intergranular attack
	1400	2500	0.5 general corrosion
	1400	3500	No apparent attack
	1400	4500	Very slight surface attack
Inconel X*	1400	1000	No apparent attack
	1400	2000	Very slight general corrosion
	1400	3000	Very slight pitting, no depth
Molybdenum	1400	1000	No apparent attack
	1400	2000	No apparent attack
	1400	3000	Slight pitting, no depth

*Inconel X is similar in chemical composition to Hastelloy R-235 except that Inconel X has no Mo

3.3 MECHANICAL PROPERTIES

3.3.1 Short Time

3.3.1.1 Tensile Properties

Tensile property measurements are strongly dependent upon test conditions. Best estimates under comparable conditions are tabulated in Table 3.3.1 for room temperature values and figures 3.3.1 through 3.3.4 for elevated temperatures. The solid solution strengthened alloys were tested in an annealed condition while the precipitation strengthened alloys were tested in the aged condition for maximum strength. Rene 41 can be strengthened further for short time applications by aging at 1450°F instead of 1650°F which produces better long term properties. It should be noted that the curves show definite similarity between like alloys but definite disparities between dissimilar alloys. (i.e., solution strengthened vs precipitation strengthened alloys)

TABLE 3.3.1

ROOM TEMPERATURE TENSILE PROPERTIES

Alloy	Heat Treatment Optimum (°F)	Yield Strength for 0.2% Offset (10^3 psi)	Ultimate Tensile Strength (10^3 psi)	Elongation in 2" (%)	Elastic Modulus (10^6 psi)
Hastelloy N[3.1, 3.8]	2150 Air Cool	47	113	53	31.7
Hastelloy X[3.2]	2150 Air Cool	54	113	41	28.6
Hastelloy R-235[3.3]	2200 Air Cool 1600 2 hr.	102 (for 0.02 Offset)	159	27	-
Rene 41[3.4]	2150 Air Cool 1650 4 hr.	97	140	12	31.6
TD Nickel[3.9]	As Received	50	64	22	22
TZM	-	-	-	-	-

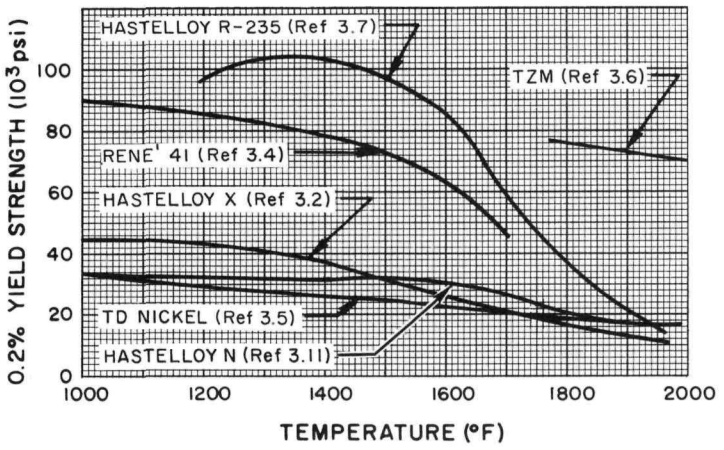

8-14-64 7569-01385

Figure 3.3.1 Elevated Temperature Yield Strength

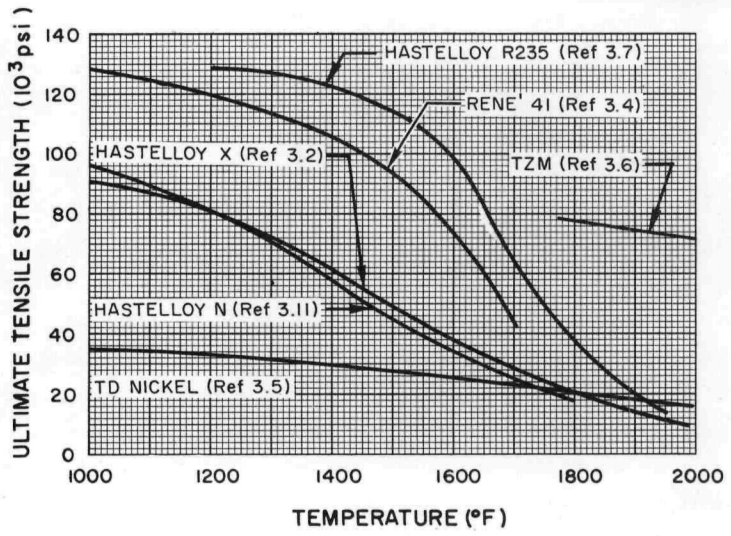

Figure 3.3.2 Elevated Temperature Ultimate Tensile Strength

8-14-64 7569-01386

Figure 3.3.3 Elevated Temperature Elongation

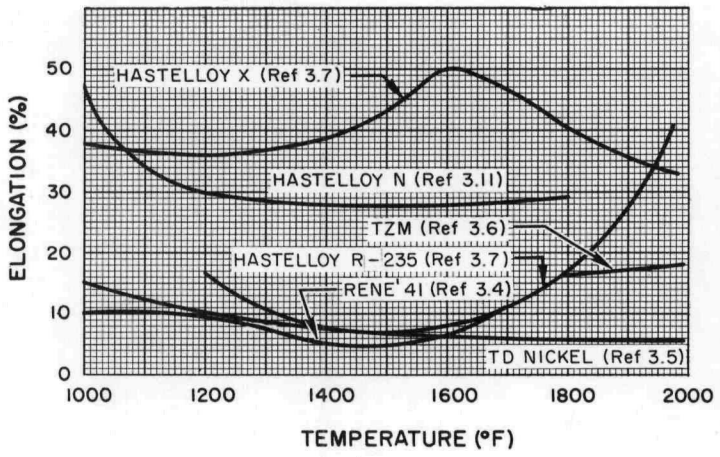

8-14-64 7569-01387

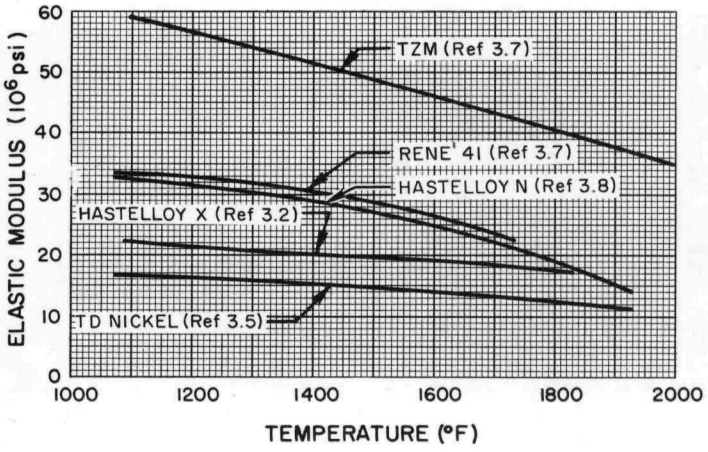

Figure 3.3.4 Elevated Temperature Elastic Modulus

8-14-64 7569-01388

3.3.1.2 Impact Strength

Charpy V-notch impact strength values are listed in Table 3.3.2 and Figure 3.3.5 as determined by individual vendors. The effect of aging of Hastelloy X on its impact strength is also shown.

TABLE 3.3.2

ROOM TEMPERATURE IMPACT STRENGTH PROPERTY

Alloy	Impact Strength (ft-lb)	Reference
Hastelloy N	85	3.8, 3.1
Hastelloy X	-	3.2
Hastelloy R-235	35	3.3
Rene 41	-	3.4
TD Nickel	30	3.9
TZM	140	-

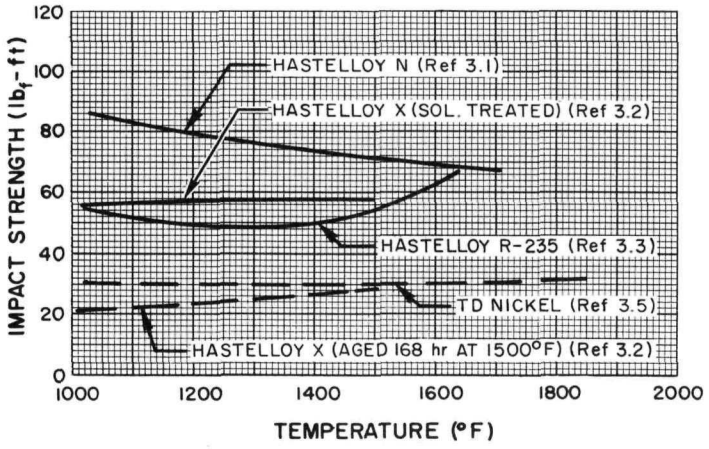

8-14-64 7569-01389

Figure 3.3.5 Elevated Temperature Impact Strength

3.3.2 Long Time

3.3.2.1 Stress-Rupture

Stress-rupture strengths are shown in Figures 3.3.6 and 3.3.7 for 100 and 1000 hr life. Most applications for high temperatures are for relatively short lifetimes which are considerably less than a year. Any extrapolation to a 10,000 hr lifetime would be subject to considerable error due to metallurgical changes which are time dependent. All strengths were determined by vendors except for the Hastelloy N line which was determined on a specific batch by ORNL personnel.

The curves show the definite superiority in strength of the precipitation strengthened alloys. Superiority of TD Nickel at temperatures above 1800°F is also shown. No long term properties are available for TZM other than that shown in Figure 3.3.6.

Optimum heat treatment as shown in Table 3.3.1, which applies for short time properties, also applies for optimum long term properties.

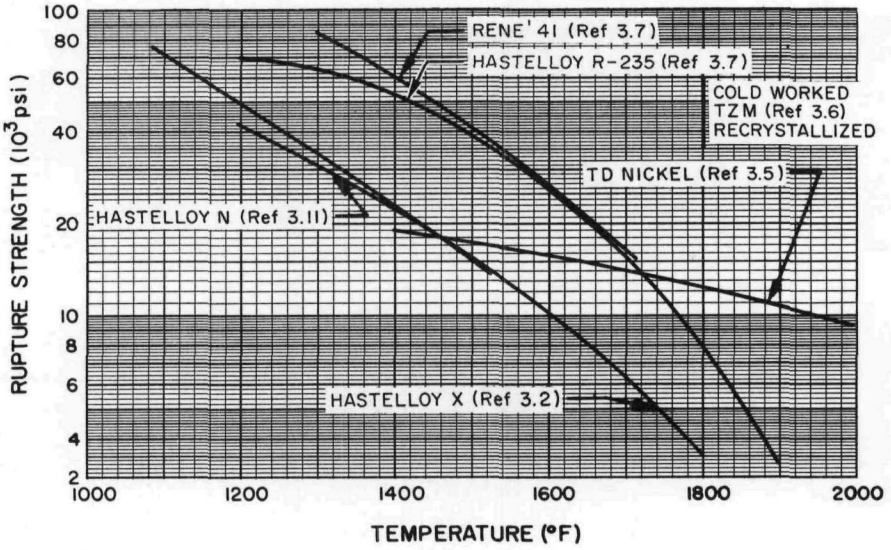

8-14-64 7569-01390

Figure 3.3.6 100-Hour Rupture Strengths

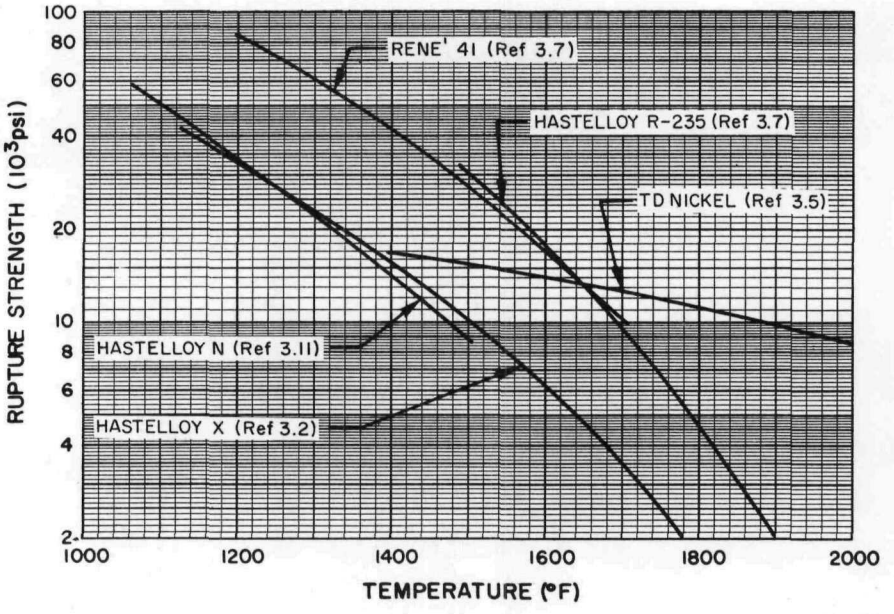

8-14-64 7569-01391

Figure 3.3.7 1000-Hour Rupture Strengths

3.2.2.2 Creep Strength

One percent creep values are shown in Figures 3.3.8 and 3.3.9 for the nickel base alloys for 100 and 1000 hr. Other amounts of creep could be shown but comparative data is not available at other levels. No values have been determined for TD nickel and TZM. Again the precipitation strengthened alloys are definitely stronger than the solution strengthened alloys.

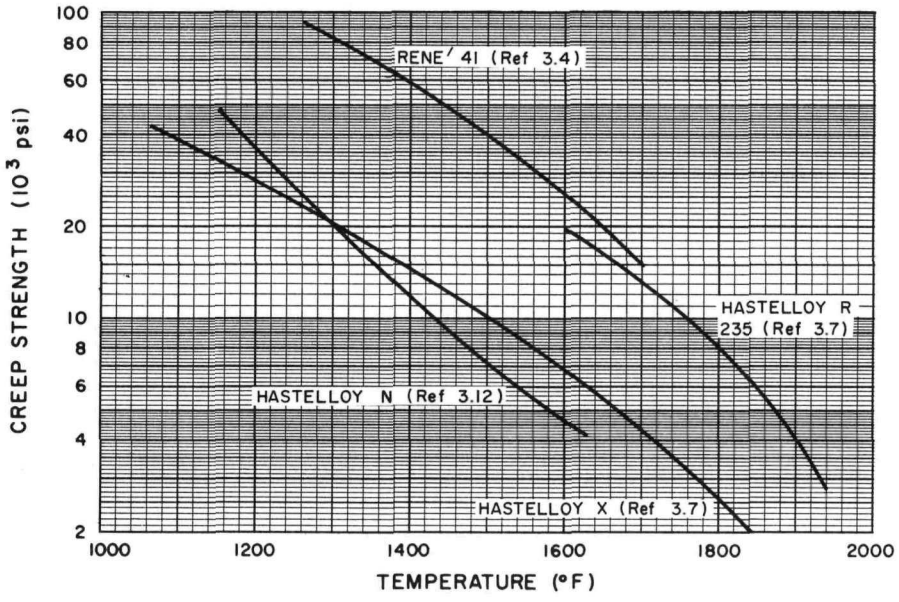

8-14-64 7569-01392

Figure 3.3.8 1% in 100 Hours Creep Strength

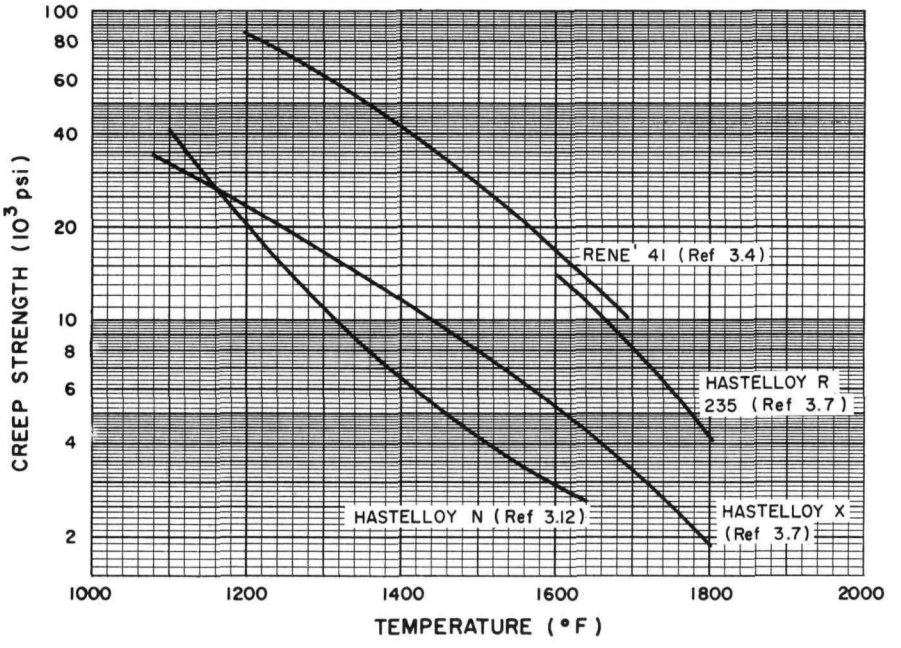

8-14-64 7569-01393

Figure 3.3.9 1% in 1000 Hours Creep Strength

3.3.2.3. Fatigue Strength

Cyclic stress on structural members can cause fatigue failure. Very limited information is available for both Hastelloy X and Hastelloy N but none on other alloys. Comparison between even these materials is difficult due to variations in test techniques.

TABLE 3.3.3

FATIGUE STRENGTH OF HASTELLOY X 3.13

Temperature (°F)	Stress to Cause Failure in 10^6 Cycles (psi)
1400	35,000 to 38,000
1600	18,500
1800	5,300
2000	3,200

TABLE 3.3.4

FATIGUE STRENGTH OF HASTELLOY N 3.14

Material Condition: 2100°F Air Cooled + 1 hr @1600°F Air Cooled

Stress for Failure in 10^6 Cycles

Temperature (°F)	Coarse Grain (ASTM 2)		Fine Grain (ASTM 5)	
	cpm			
	100	3000	100	3000
1100	52	52	-	61
1300	43	45	-	52
1500	-	-	30	36

Stress for Failure in 10^7 Cycles

Temperature (°F)	Coarse Grain (ASTM 2)		Fine Grain (ASTM 5)	
	cpm			
	100	3000	100	3000
1100	46	46	-	-
1300	39	41	-	47
1500	-	-	-	32

3.4 IRRADIATION PROPERTIES

3.4.1 Nuclear — Cross Sections

Macroscopic absorption and scatter cross sections for thermal neutrons were calculated for the six alloys. Rene 41 has the highest absorption cross section due to the presence of 11% Co while TZM, due to being Mo base, was the lowest. TD nickel has the highest scatter cross section because of its high Ni content, while TZM has the lowest value.

TABLE 3.4.1

MACROSCOPIC CROSS SECTIONS

Alloy	Macroscopic Cross Section For Thermal Neutrons (cm^{-1})	
	Absorption	Scatter
Hastelloy N	0.354	1.26
Hastelloy X	0.318	1.02
Hastelloy R-235	0.345	1.14
Rene 41	0.665	0.98
TD Nickel	0.416	1.58
TZM	0.176	0.45

3.4.2 Radiation Behavior

All radiation behavior data available for these nickel base alloys are based upon examination before and after irradiation. Results shown by this type of testing are not necessarily the same as that which occurs under simultaneous stress and radiation. In-pile testing, is underway on selected alloys, but results are not yet available.

Pessel[3.15] reported that at General Electric Company premachined subsize Hastelloy X and Hastelloy R-235 specimens have been tested to determine the effect of irradiation and temperature on the tensile properties of Hastelloy X and Hastelloy R-235 materials in a helium atmosphere; Figures 3.4.1 and 3.4.2 illustrate the results from Pessel. The effect of irradiation and temperature on the tensile properties of Rene 41 material[3.16] is shown in Table 3.4.2. Tables 3.4.3 and 3.4.4 present stress rupture tests[3.16] of Hastelloy X and Rene 41, respectively, illustrating the effect of neutron radiation.

As a matter of comparison some results on Type 347 SS material will also be presented in this section. Figure 3.4.3 presents results reported by Pessel[3.15] on the effect of temperature and irradiation on the tensile properties of Type 347 SS in a helium graphite environment. These results

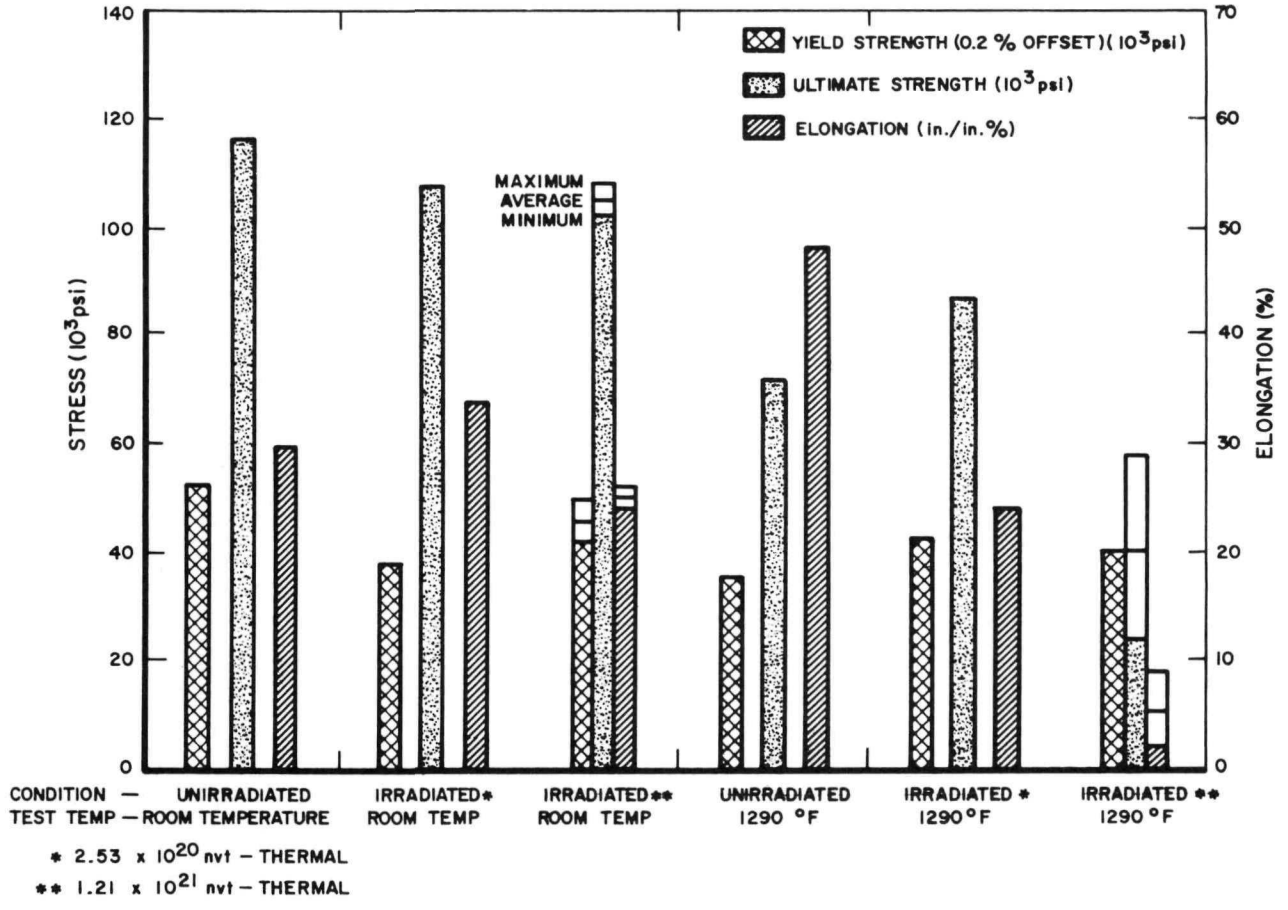

Figure 3.4.1 Effects of Neutron Radiation in Helium Graphite Environment at 1200°F Maximum Upon the Tensile Properties of Hastelloy X at Atmospheric and Elevated Test Temperature (Ref 3.15)

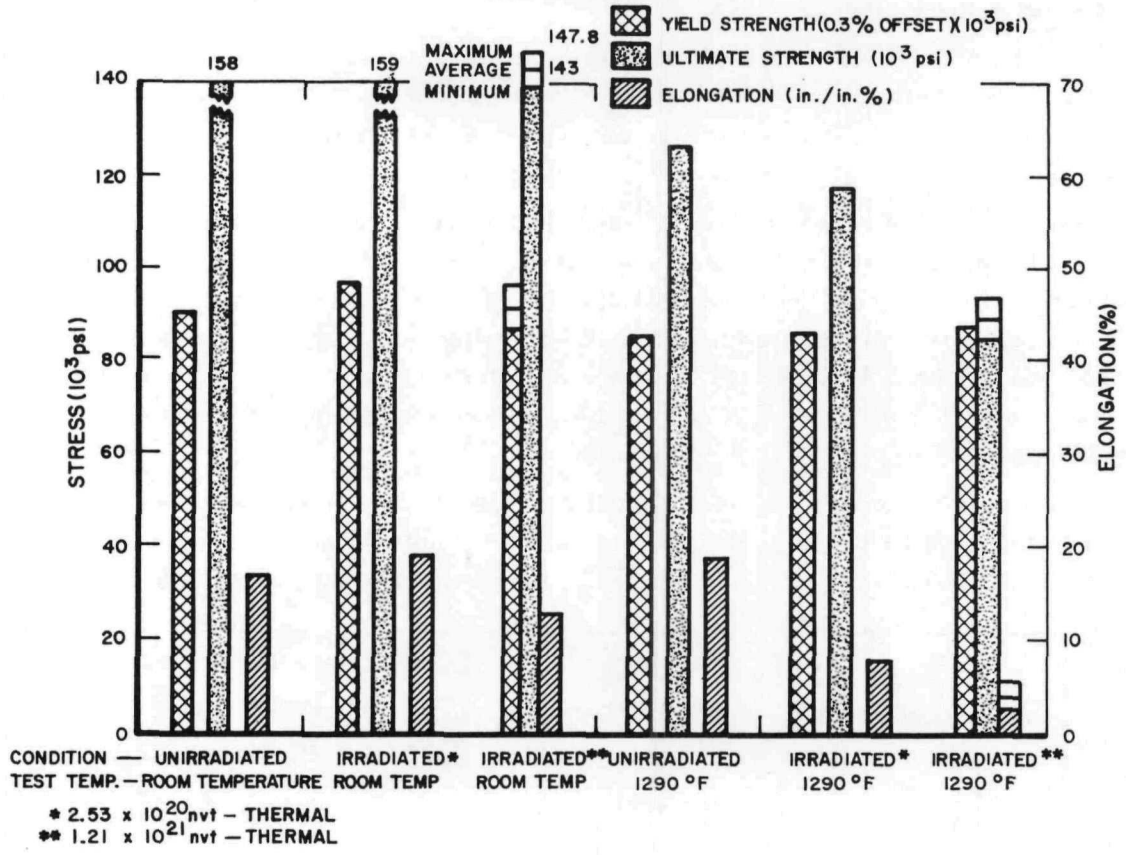

Figure 3.4.2 Effects of Neutron Radiation in Helium Graphite Environment at 1200°F Maximum Upon the Tensile Properties of Hastelloy R-235 at Atmospheric and Elevated Test Temperature (Ref 3.15)

seem to indicate that the tensile properties of Type 347 SS do not change very much due to irradiation at room temperature. Conflicting results were presented by Murr, et al.,[3.19] which are presented in Table 3.4.5, Figure 3.4.4, and Table 3.4.6. The disagreement may occur due to the neutron flux being fast instead of thermal and due to the different environments. The results shown in Table 3.4.5 and Figure 3.4.4 are for subsize specimens under a process water environment. Postirradiation annealing was found to almost completely eliminate the effect of irradiation on the tensile properties. The results shown in Table 3.4.6 are from specimens machined from an on-pile loop after irradiation. The inside surface of the inner loop was under a 2,200 psig steam environment. The annulus formed by the inner and outer loops contained helium gas, and the outside surface of the outer loop was under a process water environment. Metallographic evidence indicated no change in the microstructure of all the specimens as a result of irradiation. This seems to indicate that radiation behavior can not be explained or predicted by merely examining the microstructure.

TABLE 3.4.2

RENE 41 TENSILE TESTS[3.16]

Pre-Irradiation Properties						Post-Irradiation Properties				
						Irradiation Conditions		Test Conditions		
Heat Treatment	Test Temperature (°F)	Pre-Test Treatment	Yield Strength (10^3 psi)	Ultimate Tensile Strength (10^3 psi)	Elongation (%)	Temperature (°F)	10^{19} nvt E>1 Mev	Yield Strength (10^3 psi)	Ultimate Tensile (10^3 psi)	Elongation (%)
A	80	D	102	146	12	1020	7	112	133	7
A	1000	D	95	130	11	1020	7	104	137	18
A	80	E	117	137	3	1245	5	121	139	-
A	80	E	151	199	10	1245	11	142	181	13
A+C	80	-	-	-	-	1245	5	95	160	22
A	1200	E	132	190	13	1245	9	130	166	8
A	1200	E	132	190	13	1245	11	132	175	9
A	1200	E	102	144	12	1245	5	106	138	-
A+C	1200	E+C	87	136	15	1245	5	84	125	10
B	1200	E	131	192	12	1245	6	144	181	5
A	80	F	135	161	2	1600	6	120	142	1
A	1200	F	114	180	4	1600	6	125	165	4
A	1600	F	50	74	25	1580	6	50	56	3
A+C	1600	F+C	70	78	12	1470	6	60	62	4
B	1600	F	41	65	23	1600	6	33	36	3

HEAT TREATMENT CODE

A - 1950°F for 2 Hr, Water Quench; 2150°F for 1/2 Hr, Air Cooled; 1650°F for 4 Hr, Air Cooled.

B - 1950°F for 2 Hr, Water Quench; 1950°F for 1/2 Hr, Air Cooled; 1400°F for 16 Hr, Air Cooled.

C - 1950°F for 2 Hr, Water Quench; 2150°F for 1/2 Hr, Air Cooled; 1650°F for 4 Hr, Air Cooled. (Post Irradiation Heat Treatment Prior to Testing)

D - 1020°F for 100 Hr, Air Cooled.

E - 1200°F for 100 Hr, Air Cooled.

F - 1600°F for 100 Hr, Air Cooled.

TABLE 3.4.3

HASTELLOY X STRESS RUPTURE TESTS[3.16]

Material Condition	Irradiation Conditions		Test Conditions				
	Temperature (°F)	nvt E≥ 1 Mev	Temperature (°F)	100 hr Rupture Strength (10^3 psi)		1000 hr Rupture Strength (10^3 psi)	
				Control	Irradiated	Control	Irradiated
Annealed	1200	8.2×10^{14}	1200	43	42	27	27
(2150°F for 1 hr, Air Cooled)	1200	2.7×10^{16}	1200	43	37	27	27
	1200	5×10^{19}	1200	43	37	27	27
	1200	11×10^{19}	1200	43	42	30	32
	1600	4×10^{19}	1600	9	8	4	5.5
Welded Joints	1200	4×10^{19}	1200	44	35	32	25
	1600	4×10^{19}	1600	8	7.5	3.5	-

TABLE 3.4.4

RENE 41 STRESS RUPTURE TESTS[3.16]

Material Condition	Irradiation Conditions		Test Conditions				
	Temperature (°F)	nvt E≥ 1 Mev	Temperature (°F)	100 hr Rupture Strength (10^3 psi)		1000 hr Rupture Strength (10^3 psi)	
				Control	Irradiated	Control	Irradiated
Aged (2 hr @ 1950°F)	1200	8.3×10^{14}	1200	124	124	101	101
WQ, 1/2 hr @2150°F AC, Aged (4 hr @ 1650°F AC)	1200	2.7×10^{16}	1200	124	113	101	90
	1200	5×10^{19}	1200	107	85	87	67
	1200	11×10^{19}	1200	124	101	101	77
	1600	4×10^{19}	1200	-	104	-	92
	1600	4×10^{19}	1600	23	18	12	13
Not Aged	1600	4×10^{19}	1600	22	11	13	8
Finer Grain Size	1200	11×10^{19}	1200	120	91	96	66
	1600	4×10^{19}	1600	20	11	13	8
Welded Joints	1600	4×10^{19}	1600	25.5	14	15	5.6

TABLE 3.4.5

EFFECT OF IRRADIATION, TEMPERATURE AND ANNEALING ON THE TENSILE PROPERTIES OF TYPE 347 SS SUBSIZE SPECIMENS (Ref 3.19)

Total Integrated Fast Flux (>1 Mev), nvt	Capsule	Condition	0.2 Per Cent Offset Yield Strength, 1000 psi	Ultimate Tensile Strength, 1000 psi	Uniform Elongation, per cent	Total Elongation, per cent in 1.1 in.	Reduction of area, per cent
Tested at 75 F							
0	-	Unirradiated	34.5	87.7	>40.0	61.8	75.0
0	-	Unirradiated	36.0	90.0	>40.0	62.6	73.5
0	-	Unirradiated	34.5	89.5	>40.0	66.3	72.0
0(a)	-	Unirradiated	38.3	92.5	-	63.4	75.0
0(a)	-	Unirradiated	38.7	92.8	-	64.7	76.0
0(a)	-	Unirradiated	39.3	92.4	-	64.7	75.6
7.6×10^{21}(b)	BMI 24-18	As irradiated	104.0	112.0	25.8	34.5	68.5
5.5×10^{21}(c)	BMI 24-18	As irradiated	88.7	111.5	24.7	32.7	70.0
1.1×10^{22}(c)	BMI 24-6	As irradiated	103.5	112.5	24.3	30.9	70.0
9.2×10^{21}(b)	BMI 24-6	As irradiated	109.0	113.0	25.4	30.9	78.0
1.1×10^{22}(c)	BMI 24-18	Irradiated and annealed at 1800 F 1 hr	33.0	87.1	52.1	55.5	75.0
2.6×10^{21}(b)	BMI 24-6	Irradiated and annealed at 1800 F 1 hr	33.8	87.5	57.5	61.0	77.0
Tested at 600 F							
0(a)	-	Unirradiated	26.9	63.8	-	36.4	71.0
0(a)	-	Unirradiated	28.5	66.5	-	34.9	71.6
0(a)	-	Unirradiated	28.0	65.9	-	34.9	69.4
7.2×10^{21}(b)	BMI 24-18	As irradiated	81.8	83.0	10.7	14.5	61.0
5.5×10^{21}(c)	BMI 24-18	As irradiated	80.0	84.0	13.2	16.4	60.0
1.1×10^{22}(c)	BMI 24-6	As irradiated	86.8	89.0	10.1	13.3	60.7
8.7×10^{21}(b)	BMI 24-6	As irradiated	85.3	87.5	9.0	11.9	60.7
1.0×10^{22}(b)	BMI 24-6	Irradiated and annealed at 1800 F 1 hr	28.2	64.3	27.7	30.0	68.0
5.5×10^{21}(c)	BMI 24-18	Irradiated and annealed at 1800 F 1 hr	27.4	65.0	28.7	31.7	68.0

(a) Tests made by Knolls Atomic Power Laboratory.
(b) Values based on $Fe^{54} \rightarrow Mn^{54}$ reaction.
(c) Values based on cycle-to-cycle determination of $Ni^{58} \rightarrow Co^{58}$ reaction.

TABLE 3.4.6

EFFECT OF IRRADIATION ON TENSILE SPECIMENS MACHINED FROM SECTIONS OF THE J-10 IN-PILE LOOP (Ref 3.19)

Specimen	Approximate Peak Irradiation Test Temperature, F	Fast-Neutron (> 1 Mev) Exposure[a]		Temperature of Test, F	0.2 Per Cent Offset Yield Strength, 10^3 psi	Ultimate Tensile Strength 10^3 psi	Total Elongation, per cent, in 2 in.	Reduction of Area, per cent
		10^{14} nv	10^{21} nvt					
Inner Loop, Initial Tests								
ST-3-L	510	1.0	1.9	75	132.0	132.0	4.25	53.5
ST-2-I	625	2.0	3.9	75	145.0	145.0	6.50	54.5
ST-2-H	735	3.7	7.1	75	149.0	149.0	10.30	58.2
ST-2-L	540	1.1	2.1	750	103.0	103.0	4.50	42.7
SB-2-1	740	2.7	5.1	750	115.0	115.0	1.50	40.8
SB-2-H	760	3.6	6.9	750	120.0	120.0	2.50	50.5
Control[b]	-	-	-	70	52.5-60.7	91.3-93	53-61	68-72
Handbook data[c]	-	-	-	750	40-50	70-80	45-50	-
Inner Loop, Duplicate Tests								
ST-7-L	540	0.87	1.7	75	130.0	134.0	6.5	59.1
ST-7-I	675	2.9	5.57	75	139.5	144.8	10.6	59.8
ST-7-H[d]	735	1.7	3.26	75	143.0	147.0	9.4	61.5
SB-7-L	700	1.2	2.3	750	115.3	115.3	4.2	64.0
SB-7-1	760	1.9	3.65	750	123.0	123.5	4.2	45.5
SB-7-H	760	3.4	6.5	750	125.4	125.8	4.1	40.5
Outer Loop								
LT-4-L	120	0.91	1.8	75	100.0	103.5	31.5	54.0
LT-4-I	120	1.8	3.5	75	95.2	101.3	26.0	57.0
LB-3-H	120	3.4	6.5	75	102.5	108.0	25.0	60.5
LT-3-L	120	3.1	2.0	750	62.5	66.7	13.3	54.0
LT-3-I	120	2.4	4.5	750	65.4	69.3	11.4	54.6
LT-3-H[e]	120	2.7	5.1	600	71.8	73.3	12.5	48.3
Control 1[f]	-	-	-	75	46.8	99.7	50.4	61.8
Control 2[f]	-	-	-	750	36.5	67.6	26.2	62.9

(a) Exposures based on manganese-54.
(b) From McInnes Company reports on samples cut from as-machined J-10 pressure tube.
(c) Metals Handbook, Vol. 1, Eighth Edition, p 503.
(d) Less than 1 mg of sample was submitted for analysis; therefore, the analysis may be inaccurate due to small weighing errors. On the basis of the location of the specimen, a value of $\sim 7 \times 10^{21}$ nvt would be expected.
(e) Only 1.5 mg of sample was analyzed. Small weighing errors could have caused significant errors in analysis. It is believed that the actual value would duplicate LB-3-1 since the specimen came from adjacent position.
(f) Samples cut from portion of J-10 pressure tube above reactor core.

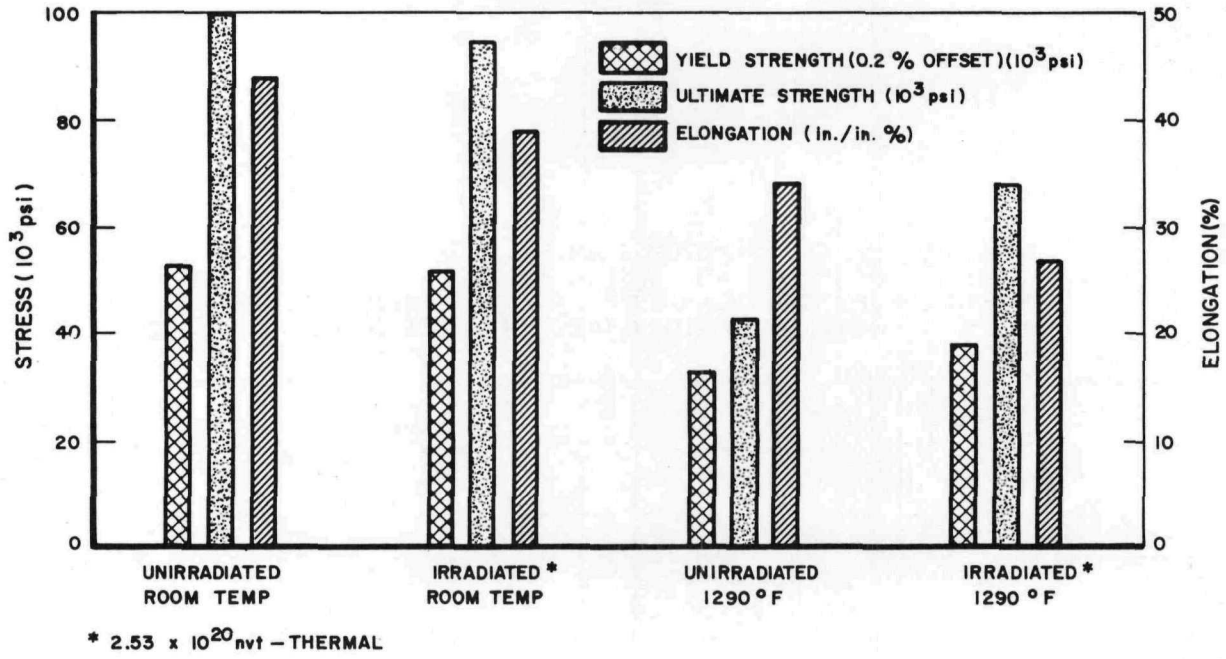

8-10-64 7569-01681

Figure 3.4.3. Effects of Neutron Radiation in Helium Graphite Environment at 1200°F Maximum Upon the Tensile Properties of Type 347 SS at Atmospheric and Elevated Test Temperature (Ref 3.15)

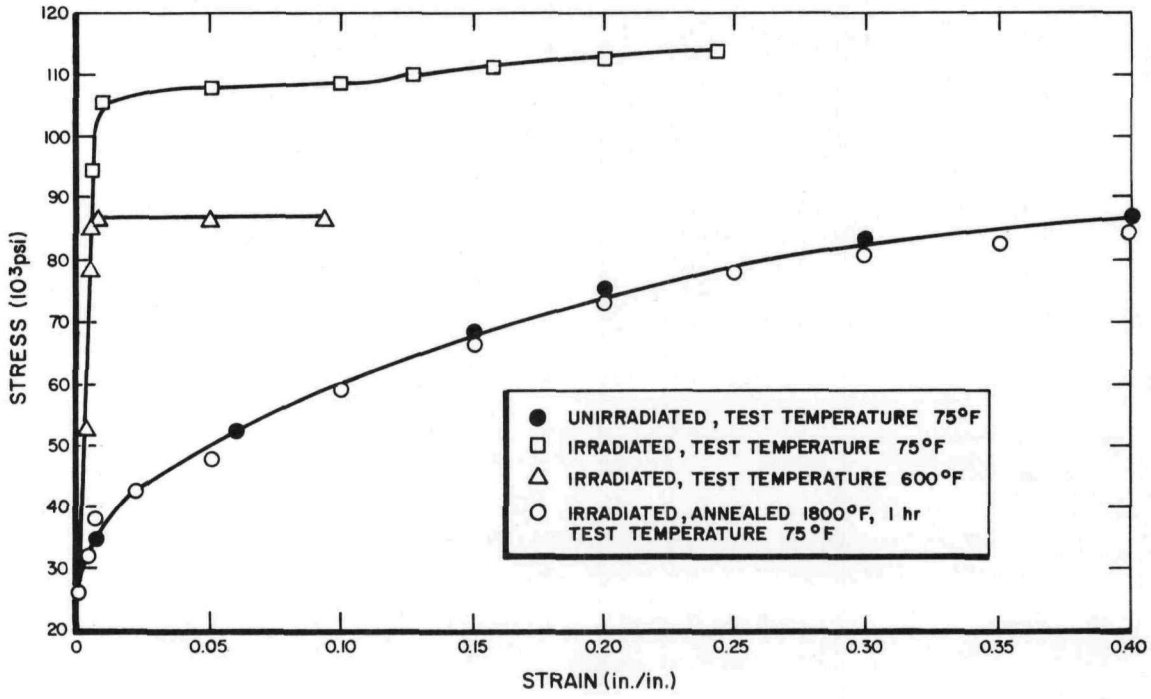

10-22-64 7569-01683A

Figure 3.4.4. Effect of Irradiation to 1.1 x 10^{22} nvt Fast on the Stress-Strain Property of Type 347 SS (Ref 3.19)

REFERENCES

3.1. Haynes Stellite Company, Hastelloy Alloy N, Kokomo, Indiana, April, 1962

3.2. Haynes Stellite Company, Hastelloy Alloy X, Kokomo, Indiana, August, 1961

3.3. Haynes Stellite Company, Hastelloy R-235, Kokomo, Indiana, September, 1962

3.4. Union Carbide Stellite Company, Haynes Alloy No. R-41, Kokomo, Indiana, April, 1963

3.5. F. J. Anders, Jr., G. B. Alexander, and W. S. Wartel, "A Dispersion Strengthened Nickel Alloy," Metal Progress, 82, p 88, December, 1962

3.6. Climax Molybdenum Company of Michigan, Developmental Data Climalt TZM, Detroit, Michigan, January, 1962

3.7. Metals Handbook, Volume I, Properties and Selection of Materials, Metals Park, Ohio, American Society for Metals, 1961

3.8. ASME Code Case 1315, "Nickel-Molybdenum-Chromium-Iron Alloy as Material for ASME Boiler and Pressure Vessel Construction," July 15, 1961

3.9. R. E. Stuart and C. D. Starr, "New Design Data on TD Nickel," Materials in Design Engineering 58, p 81, August, 1963

3.10. Climax Molybdenum Company, Molybdenum Metal, New York, 1960

3.11. Supplied by A. Taboada, Oak Ridge National Laboratories, Oak Ridge, Tennessee in a letter to L. B. Lundberg, Atomics International, a division of North American Aviation, Inc., Canoga Park, California, February 15, 1963

3.12. R. W. Swindeman, "The Mechanical Properties of INOR 8", ORNL 2780, January 27, 1961

3.13. Army Gas-Cooled Reactor Systems Program Monthly Progress Report for November, 1960, IDO 28566 December 30, 1960

3.14. R. G. Carlson, "Fatigue Studies of Hastelloy N," BMI 1354 June 26, 1959

3.15. Proceedings of the Nuclear Superheat Meeting - No. 7, September 12-14, 1962, Sioux Falls, South Dakota, TID 7658, October 1962

3.16. High Temperature Materials Program Progress Report Number 19, Part A, GEMP 19A January 25, 1963

3.17. J. K. Balkwill, "Compatibility of SNAP Fuel and Cladding Materials," NAA-SR-5413, October 1960 (Secret-RD)

3.18. M. A. Perlow, "SNAP 2 Primary Coolant Development," NAA-SR-6439, July 15, 1961

3.19. W. E. Murr, F. R. Shober, R. Lieberman, and R. F. Dickerson, "Effects of Large Neutron Doses and Elevated Temperature on Type 347 Stainless," BMI 1609, January 1963

4.0 COATINGS

4.1 COMPOSITION AND TECHNIQUES

4.1.1 Solaramic 14-35A

This coating is a proprietary coating made from technical grade oxides, nitrates, and carbonates. The basic frit consists of the following oxides: SiO_2, BaO, TiO_2, ZrO_2, Li_2O, Na_2O, K_2O, ZnO, MnO, MgO, CaO, and SrO.[4.1] Table 4.1.1 lists the method of producing the coating with mill addition weights given in grams.

TABLE 4.1.1

SOLARAMIC 14-35A PRODUCTION

Mill Additions (grams)		Application Technique	Time at Temperature
Frit	– 100	For spraying or dipping use a coating with specific gravity of 1.74 gm/cc	15 minutes at 1800°F for each coat
Ferro Black Label clay	– 6		
Cr_2O_3	– 2		
Bentonite	– 0.25		
KNO_3	– 0.12		
Distilled H_2O	– 58		

4.1.2 AI8763D

This coating was developed by Atomics International, a Division of North American Aviation, and has all hydrogen reducible oxides eliminated. Consequently, this coating has a higher temperature stability and lower permeation rate than the Solaramic. Table 4.1.2 lists the ingredients and method of producing this coating.[4.2]

TABLE 4.1.2

AI8763D INGREDIENTS AND PRODUCTION

Raw Batch Material (grams)	Basic Frit Oxide (% by wt)	Mill Additions (grams)		Application Technique	Time at Temperature
SiO_2 – 688	SiO_2 – 47.2	Frit	– 100	For spraying or dipping use a coating with a specific gravity of 1.74 gm/cc	15 to 20 minutes at 1950°F for each coat
$BaCo_3$ – 625	BaO – 31.6	Ferro Green Label clay	– 6		
TiO_2 – 152	TiO_2 – 9.9	Cr_2O_3	– 2		
$LiCO_3$ – 86	Li_2O – 2.3	Bentonite	– 0.25		
Zircon – 115	ZrO_2 – 5.0	KNO_3	– 0.12		
$CaCO_3$ – 42	SiO_2 –	Distilled H_2O	– 58		
MnO_2 – 17	CaO – 1.5				
$SrCO_3$ – 23	MnO_2 – 1.1				
MgO – 5	SrO – 1.1				
	MgO – 0.3				

4.1.3 SCB1

This coating is a four component glass coating. Table 4.1.3 lists the ingredients and method of producing this coating.[4.3]

TABLE 4.1.3

SCB1 INGREDIENTS AND PRODUCTION

Raw Batch Material (grams)	Basic Frit Oxide (% by wt)	Mill Additions (grams)	Application Technique	Time at Temperature
SiO_2 – 46.7 BaO_2 – 36.1 TiO_2 – 13.1 Al_2O_3 – 7.5	SiO_2 – 46.7 BaO – 32.7 TiO_2 – 13.1 Al_2O_3 – 7.5	Frit – 100 Ferro Black – 3 Label clay Bentonite – 0.25 Distilled H_2O – 70	For spraying or dipping use a coating with a specific gravity of 1.66 to 1.69 gm/cc	5 minutes at 2100°F for each coat.

4.1.4 Al_2O_3

This coating is a vapor deposited polycrystalline oxide. $AlCl_3$ gas is reacted with H_2O (introduced as CO, CO_2, and H_2) at the hot metal surface producing Al_2O_3.[4.4] The reaction is:

$$2AlCl_3 + 3H_2 + 3CO_2 \longrightarrow Al_2O_3 + 6HCl + 3CO\uparrow$$

Temperatures are between 2100 and 2400°F.

4.1.5 SiC

This vapor deposited polycrystalline coating is proprietory to Texas Instruments Corporation. Vapor deposition is performed at temperatures between 2000 and 2500°F.

4.2 PHYSICOCHEMICAL PROPERTIES

4.2.1 Physical

4.2.1.1 Structure

S14-35A, AI8763D, and SCB1 structures consist of a complex system of silicate crystals in silicate glass.

Al_2O_3 and SiC have a polycrystalline structure. The crystalline structure of vapor deposited polycrystalline materials depends on its thermal and environmental history. For instance, vapor deposited Al_2O_3 can be in one of several crystallographic forms, highly oriented, and very fine grained. The structure and properties can vary accordingly on this experimental coating, because the deposition parameters are not definite.

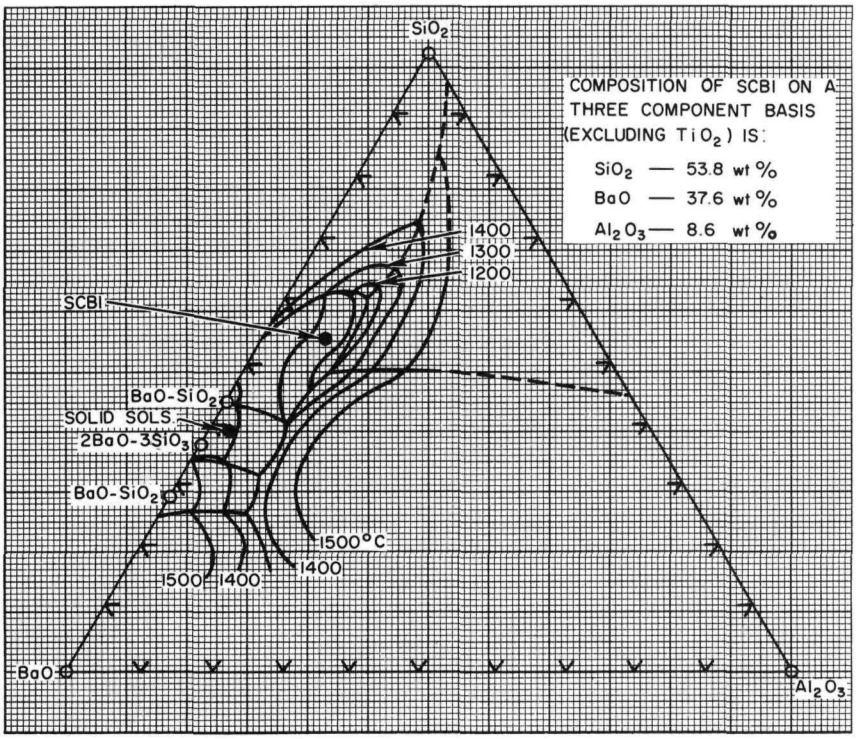

8-14-64 7569-01684

Figure 4.2.1. Equilibrium Diagram of $BaO-Al_2O_3-SiO_2$ System (Reference 4.5)

TABLE 4.2.1

COATING DENSITIES

Coating	Theoretical (gm/cc)	Actual (gm/cc)
S14-35A	3.1 (Reference 4.1)	2.8
AI8763D	3.1 (Reference 4.2)	2.8
SCB1	3.2 (Reference 4.3)	2.9
Al_2O_3	4.0 (Reference 4.6)	-
SiC	3.2 (Reference 4.6)	-

TABLE 4.2.2

THERMAL CONDUCTIVITIES OF COATINGS[4.7]

Coating	Thermal Conductivity (gm-cal/sec-cm-°C)
S14-35A	-
AI8763D	-
SCB1	-
Al_2O_3	0.069 at 100°C 0.021 at 600°C 0.031 at 1200°C
SiC	0.49 at 600°C

4.2.1.2 Phase Diagram

The phase diagram for S14-35A and AI8763D is too complex to illustrate, while no diagram is available for SiC. SCB1 can be studied by looking at a $SiO_2 + BaO + Al_2O_3$ diagram, which is presented in Figure 4.2.1.

The Al_2O_3 coating is stoichiometric Al_2O_3; therefore, no phase diagram need be presented.

4.2.1.3 Density

The density of the various coatings is listed in Table 4.2.1. The actual density listed is an estimated density of the as-fired (unaged) coating.

4.2.2 Electrical

No data on the electrical resistivity of the five coatings considered in this handbook are available. However, it is known that the electrical resistivity of Al_2O_3 is very sensitive to impurities.[4.17]

4.2.3 Thermal

4.2.3.1 Thermal Conductivity

Table 4.2.2 lists the thermal conductivities of Al_2O_3 and SiC. No data are available for S14-35A, AI8763D, and SCB1 coatings.

4.2.3.2 Specific Heat

The specific heat of the Al_2O_3 and SiC coatings are listed in Table 4.2.3. No data are available for the other three coatings shown in this table.

TABLE 4.2.3

SPECIFIC HEATS OF COATINGS[4.7]

Coating	Specific Heat (cal/gm-°C)
S14-35A	-
AI8763D	-
SCB1	-
Al_2O_3	0.21 at 20°C 0.25 at 500°C 0.28 at 1000°C
SiC	0.143 at 0°C

4.2.3.3 Thermal Expansion

Table 4.2.4 lists the coefficient of thermal expansion as a function of temperature for five coatings. Figures 4.2.2, 4.2.3, and 4.2.4 illustrate the thermal expansion behavior of unaged S14-35A, unaged AI8763D, and unaged SCB1, respectively, as a function of temperature. The sudden drop-off at the end of the curves represents points where the softening temperatures have been reached.

Figures 4.2.5 and 4.2.6 show data indicating the aging effect on the coefficient of thermal expansion of S14-35A and AI8763D membranes, respectively, at 600°C. A best-fit curve is shown drawn through the data points from quenched specimens to indicate the radical behavior of coatings.

TABLE 4.2.4

COEFFICIENT OF LINEAR THERMAL EXPANSION OF COATINGS FROM ROOM TEMPERATURE (20°C)

Coating	Temperature (°C)	Average Coefficient (10^{-6} cm/cm-°C)
S14-35A[4.8]	100	5.9
	200	6.3
	300	6.6
	400	6.9
	500	7.2
	600	7.8
AI8763D[4.8]	100	7.7
	200	10.3
	300	9.9
	400	9.5
	500	9.4
	600	9.6
SCB1[4.3]	700	5.8
Al_2O_3[4.7]	500	7.0*
	100	9.0*
SiC[4.7]	600 (recrystalized)	4.9
	1500	4.7

*Sensitive to crystallite orientation

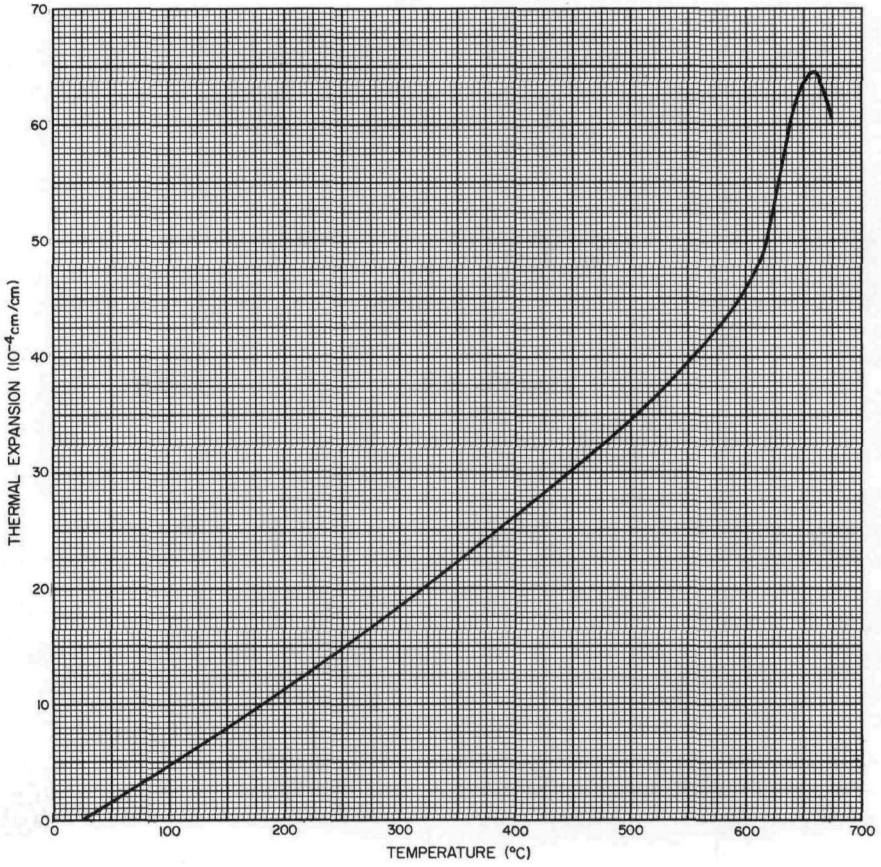

8-14-64 7569-01685

Figure 4.2.2. Thermal Expansion of Unaged Solaramic S14-35A (Reference 4.8)

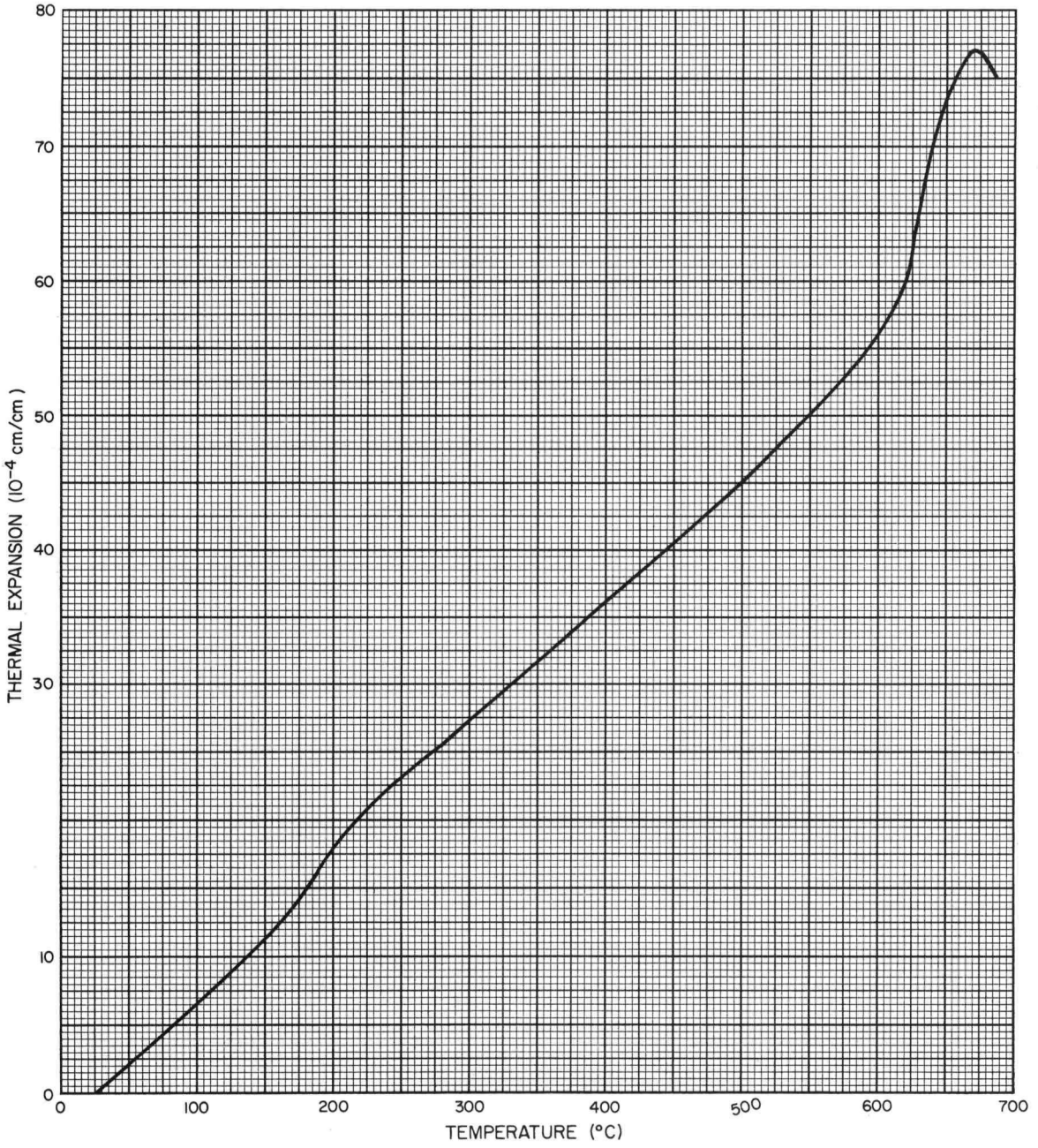

Figure 4.2.3. Thermal Expansion of Unaged AI8763D (Reference 4.8)

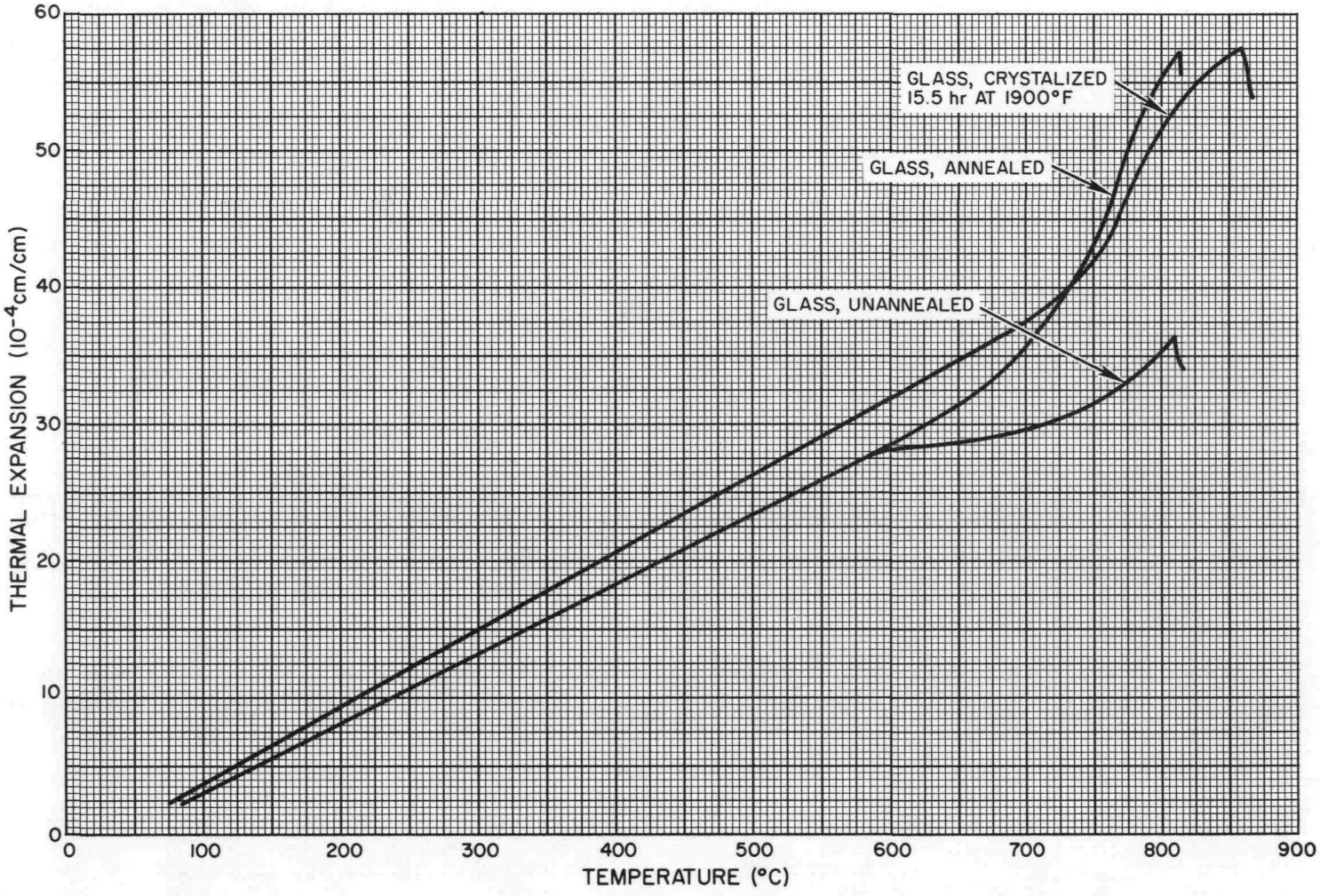

Figure 4.2.4. Thermal Expansion of Unaged SCB1 (Reference 4.3)

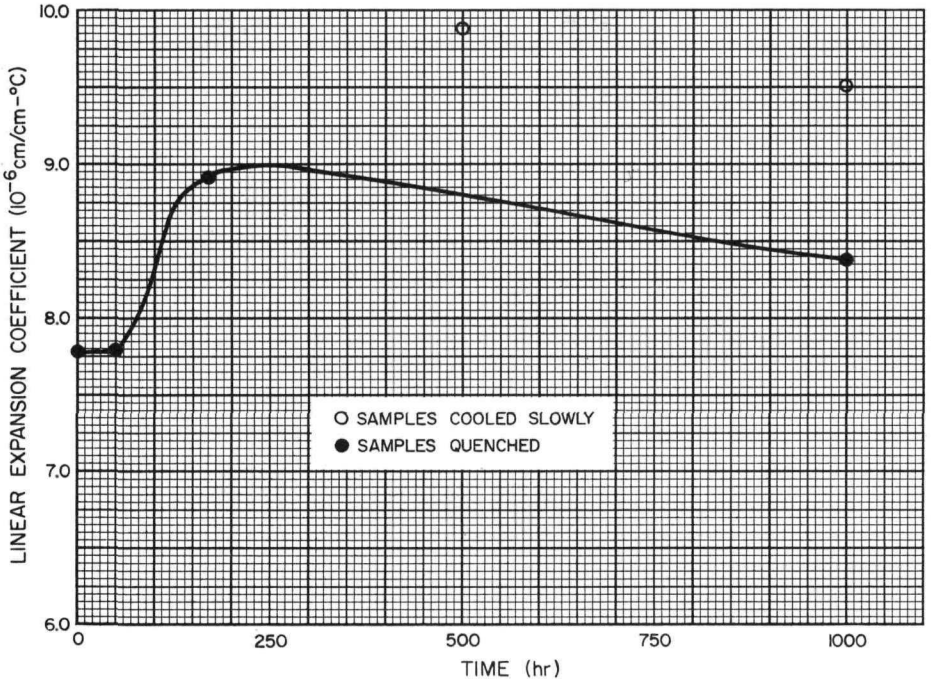

8-14-64 7569-01688

Figure 4.2.5. The Effect of Aging* on the Thermal Expansion of Solaramic S14-35A From 20 to 600°C (Reference 4.8)

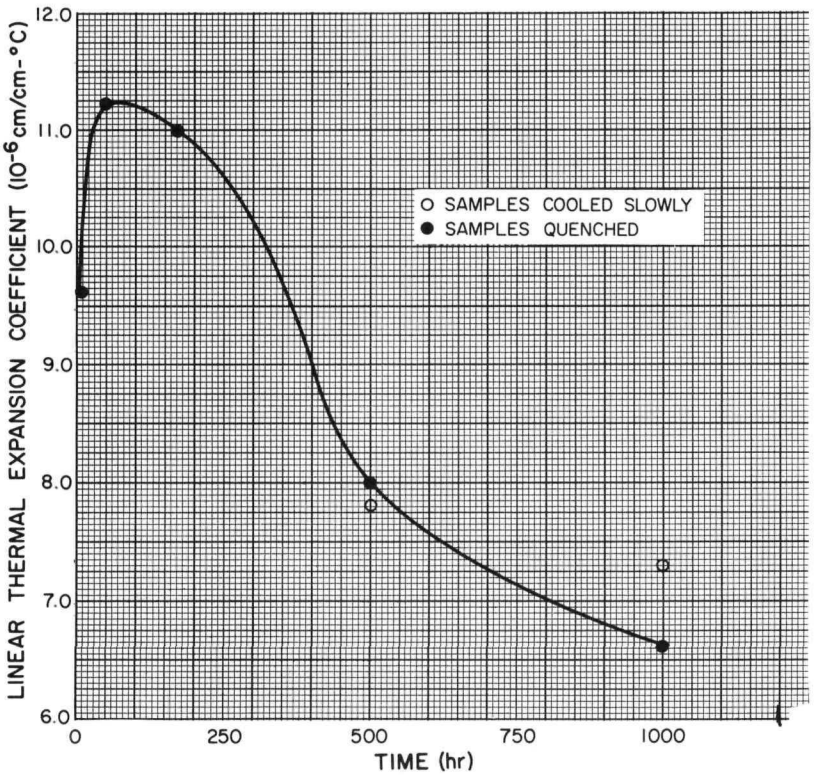

8-14-64 7569-01689

Figure 4.2.6. The Effect of Aging* on the Thermal Expansion of AI8763D From 20 to 600°C (Reference 4.8)

*Aging was in 1 atm hydrogen at 1500°F

4.2.3.4 Softening Temperature

Table 4.2.5 lists the data that are available on the softening temperature property of the five coatings.

TABLE 4.2.5

SOFTENING TEMPERATURE OF COATINGS

Coating	Softening Temperature (°F)		Reference
	Unaged	Aged	
S14-35A	1220	>1292	4.8
AI8763D	1229	>1292	4.8
SCB1	1490	1670	4.3
Al_2O_3	3659	3659	4.5
SiC	>4892	>4892	4.5

4.2.3.5 Shock Resistance

S14-35A, AI8763D, and SCB1 coatings have excellent shock resistance; however, the resistance may deteriorate slightly with time, temperature, and hydrogen environment.[4.8] Al_2O_3 and SiC coatings seem to have good resistance to shock.

4.2.4 Chemical

4.2.4.1 Hydrogen Permeation

Figures 4.2.7, 4.2.8, and 4.2.9 illustrate the effect of time, temperature, and pressure, respectively, on the hydrogen permeation rate of S14-35A coated membranes.[4.9] These same variables for AI8763D coated membranes are illustrated in Figures 4.2.10, 4.2.11, and 4.2.12, respectively.[4.10] Additional data for AI8763D at 1500°F is presented in Figure 4.2.13.[4.8]

Time has very little effect on the hydrogen permeation rate of SCB1 coating. Results[4.8] indicate that for uncrystallized membranes at 1500°F and 1 atm H_2, the permeation rate changes from 1.31×10^{-3} to 1.46×10^{-3} cc (STP)/hr-cm^2 after 633 hr at temperature. Figure 4.1.14 illustrates the effect of temperature, pressure, and crystallization on SCB1 coated Hastelloy N tubes (membranes). Figure 4.1.15 is a cross plot of Figure 4.1.14 illustrating more clearly the effect of pressure on the permeation rate. A change in the activation energy for diffusion was observed at about 1400°F (see Figure 4.1.14), which is within the glass softening range. This phenomenon may have been overlooked in previous investigations on AI8763D and Solaramic S14-35A coatings, since softening occurs at a much lower temperature (1100 to 1200°F); additionally, hydrogen permeation rates at these low temperatures are very small which may result in the possibility of a change not being detected in the activation energy.[4.18]

No data are available on the Al_2O_3 and SiC coatings.

4.2.4.2 Degradation

S14-35A coating is unstable above 1200°F, because K_2O, Na_2O, and ZnO are reduced by hydrogen.[4.8] The reaction products, metal and metal vapors, plus other gaseous impurities cause an increase in porosity that is time and temperature dependent.

AI8763D coating is chemically stable, but its porosity increases with time and temperature starting at about 1400°F due to gaseous impurities.[4.8]

SCB1 coating is chemically stable, and it is relatively free of impurities. It can be used to 1900°F for short periods. Its porosity does not change appreciably at 1500°F.

No data are available for Al_2O_3 and SiC.

4.2.4.3 Adherence

No adherence data will be presented here, because without a complete analysis and discussionof the data, the results would be misleading. However, a complete report is being prepared at Atomics International, a Division of North American Aviation, Canoga Park, California, which will include adherence data.[4.3]

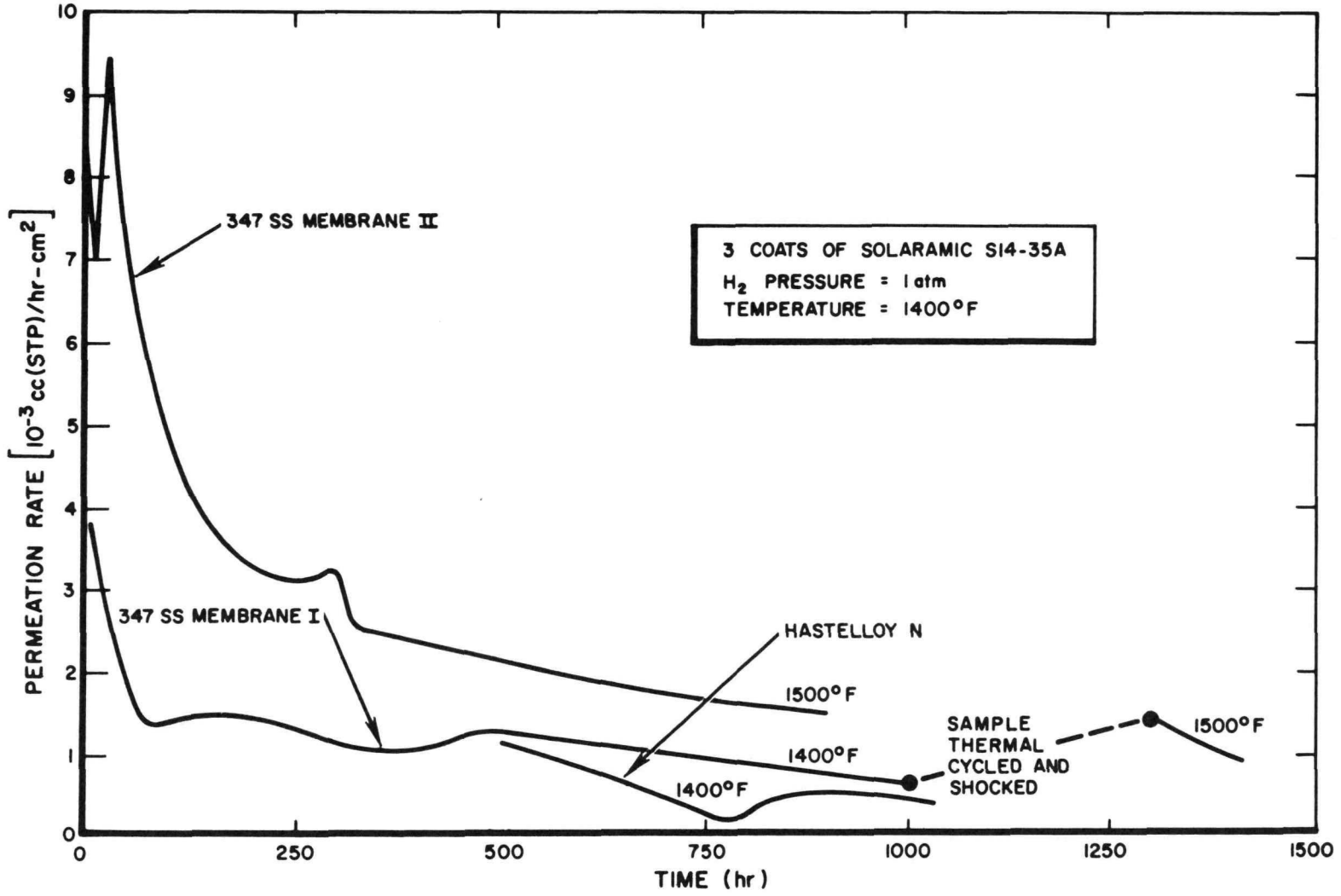

8-14-64

7569-01690

Figure 4.2.7. Permeation Rate Through Solaramic Coated 347 SS (Membranes I and II) and Hastelloy N (Reference 4.9)

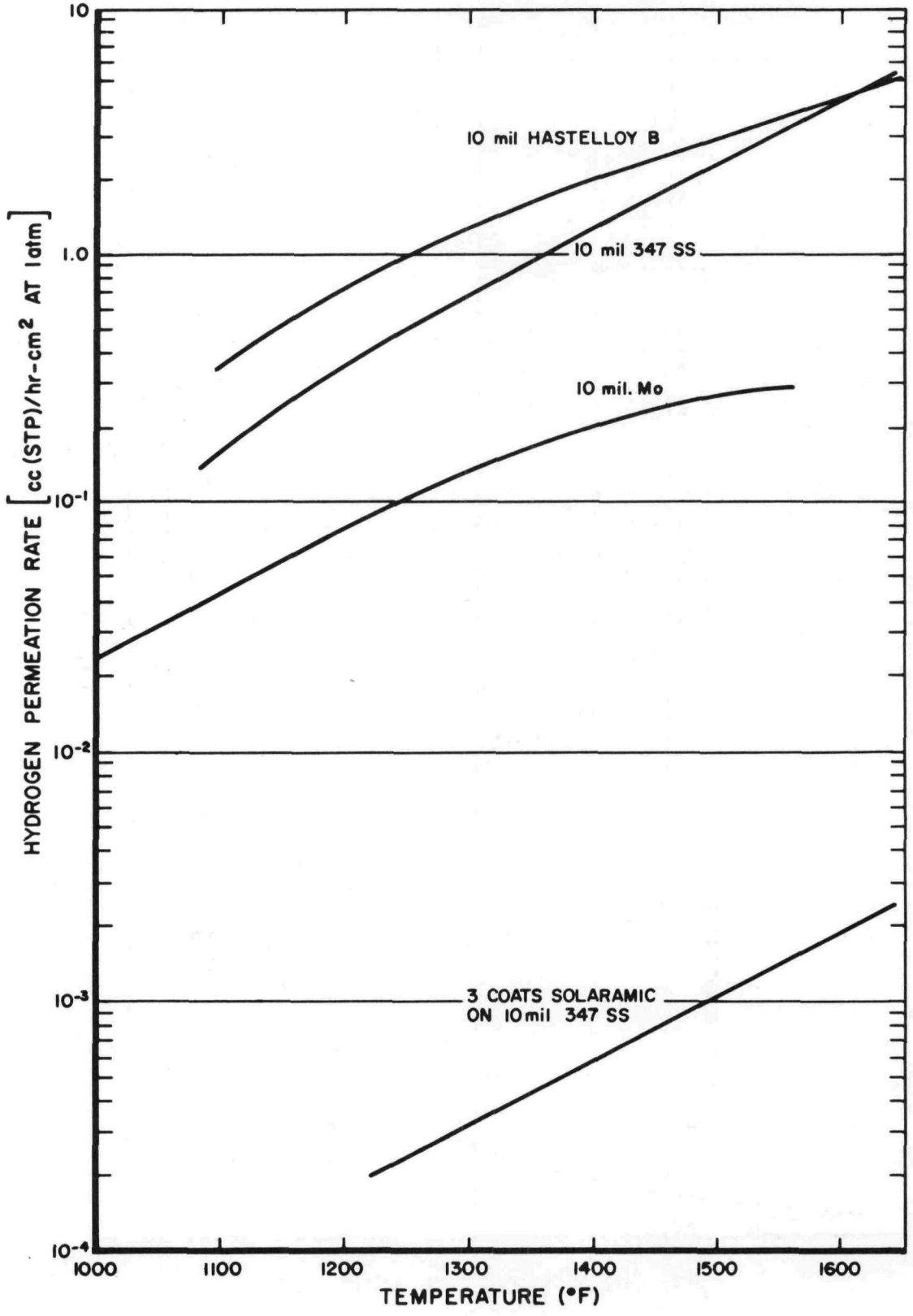

8-14-64

7569-01691

Figure 4.2.8. Comparison of Hydrogen Permeation Rates Through Solaramic and Metals (Reference 4.9)

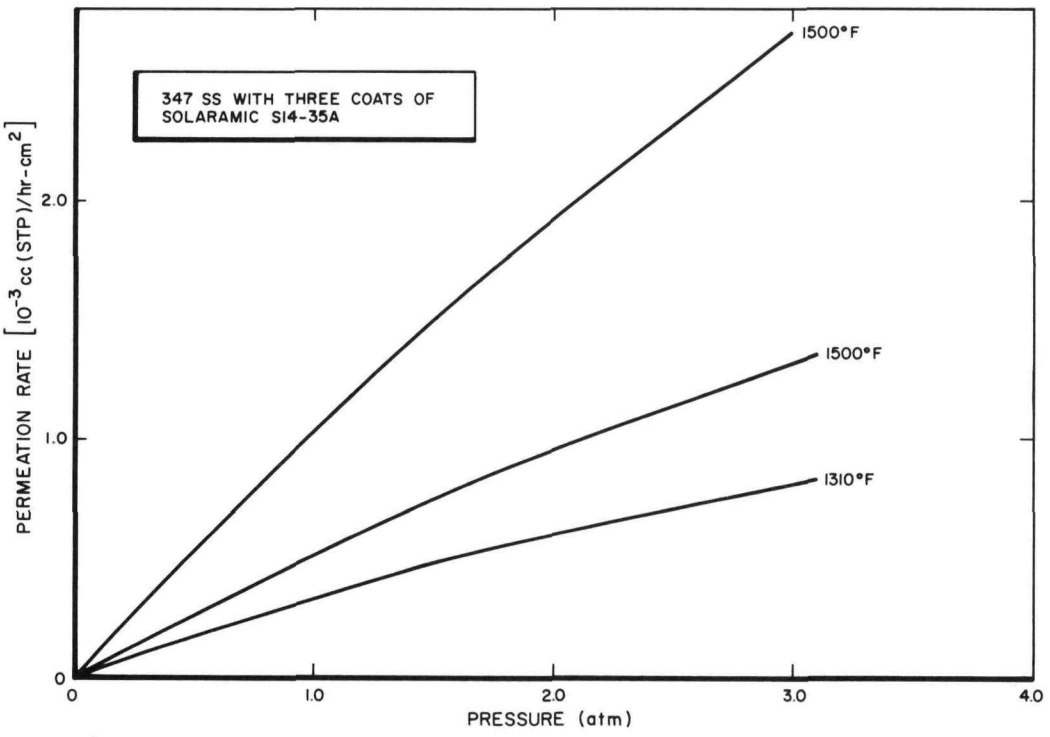

8-14-64 7569-01692

Figure 4.2.9. Pressure Dependence of Permeation Rate (Reference 4.9)

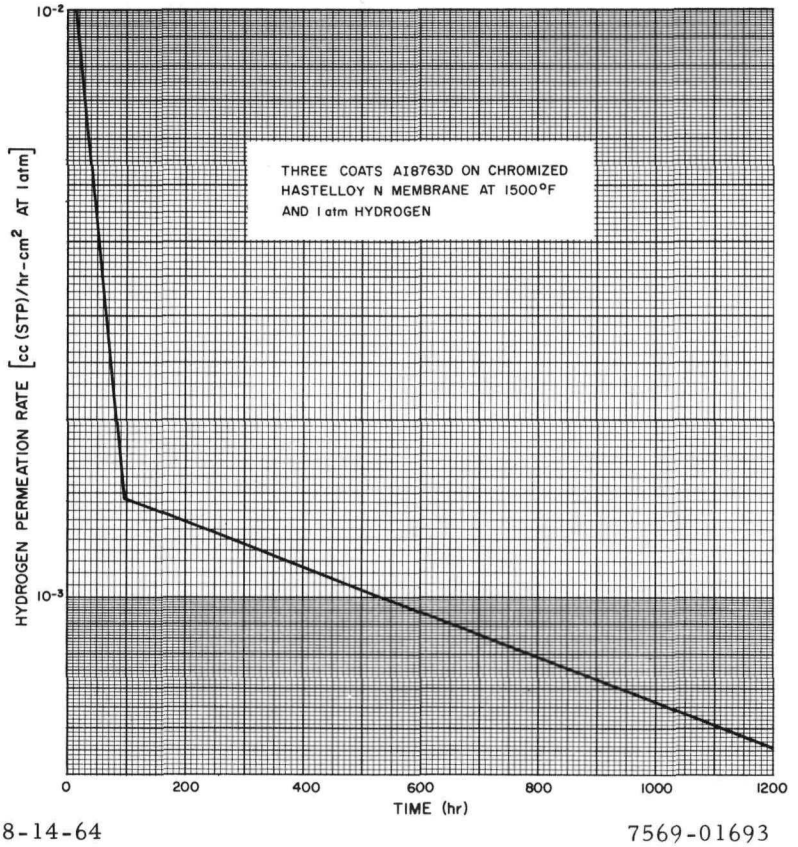

8-14-64 7569-01693

Figure 4.2.10. Hydrogen Permeation Rates Through AI8763D vs Time (Reference 4.10)

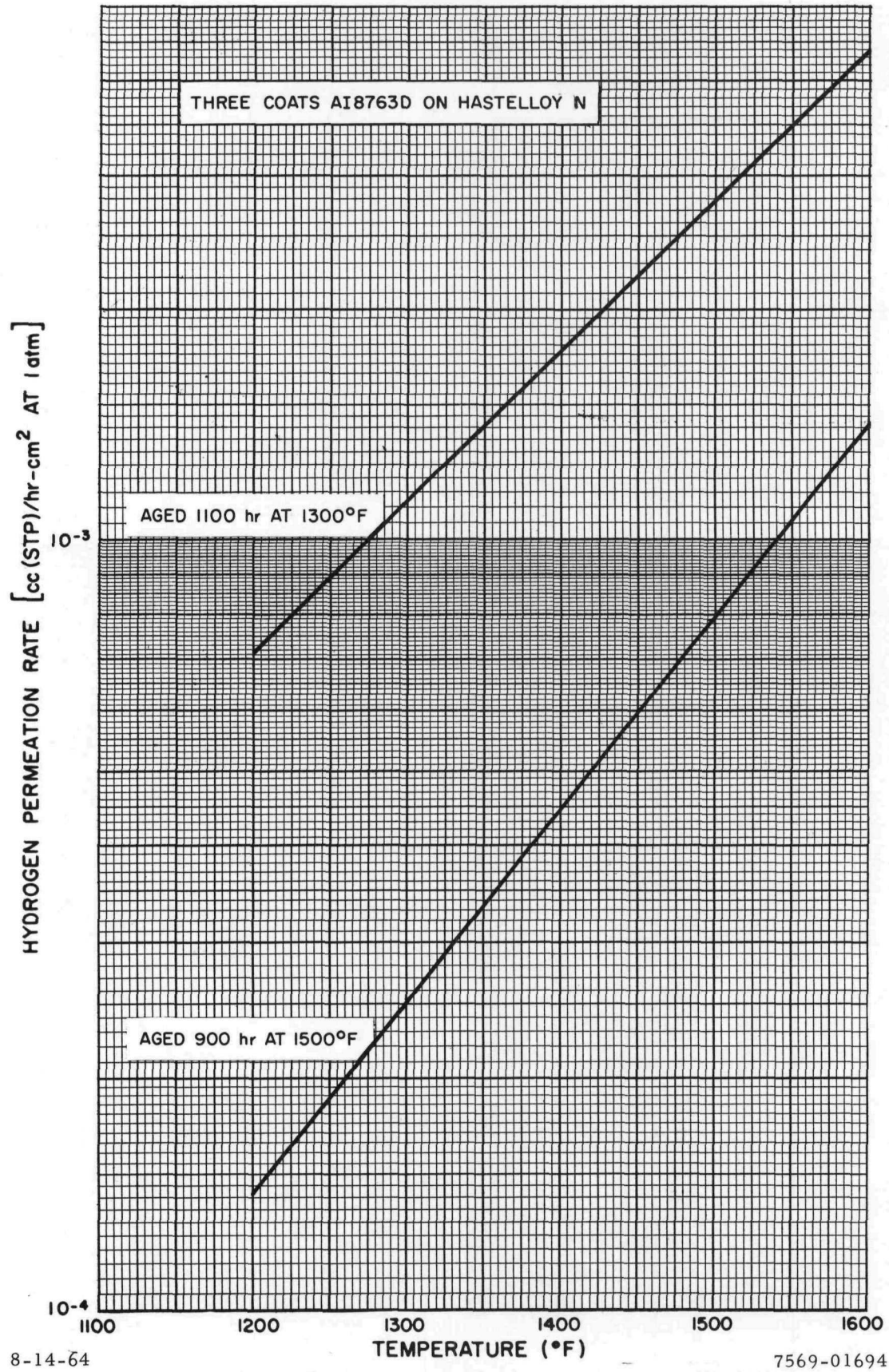

Figure 4.2.11. Hydrogen Permeation Rates Through AI8763D vs Temperature (Reference 4.10)

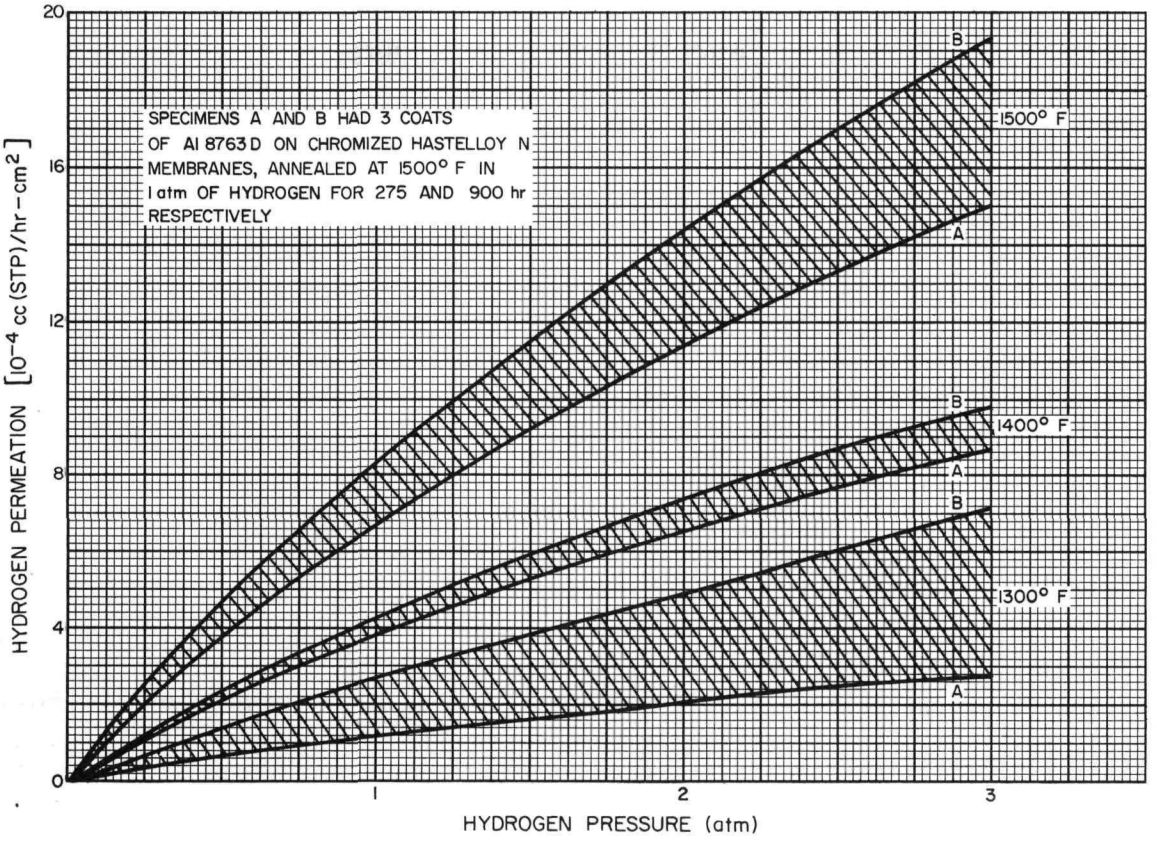

8-14-64 7569-01695

Figure 4.2.12. Hydrogen Permeation Rates Through AI8763D vs Pressure (Reference 4.10)

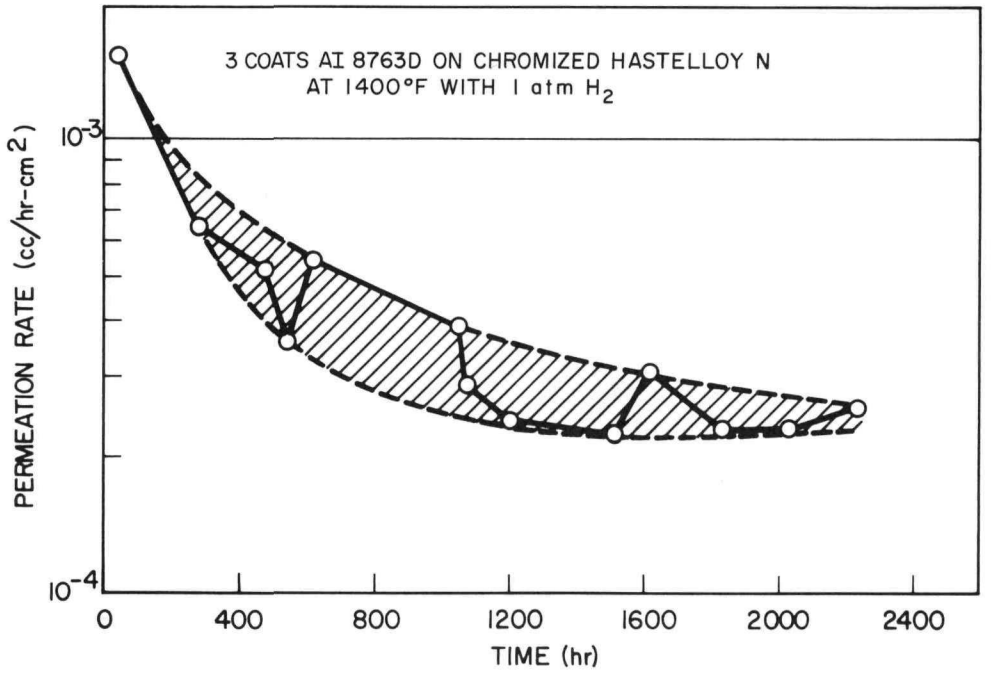

1-7-64 7568-0807

Figure 4.2.13. Permeation vs Time at 1500°F for AI-8763D Hydrogen Coated Tube (Reference 4.18)

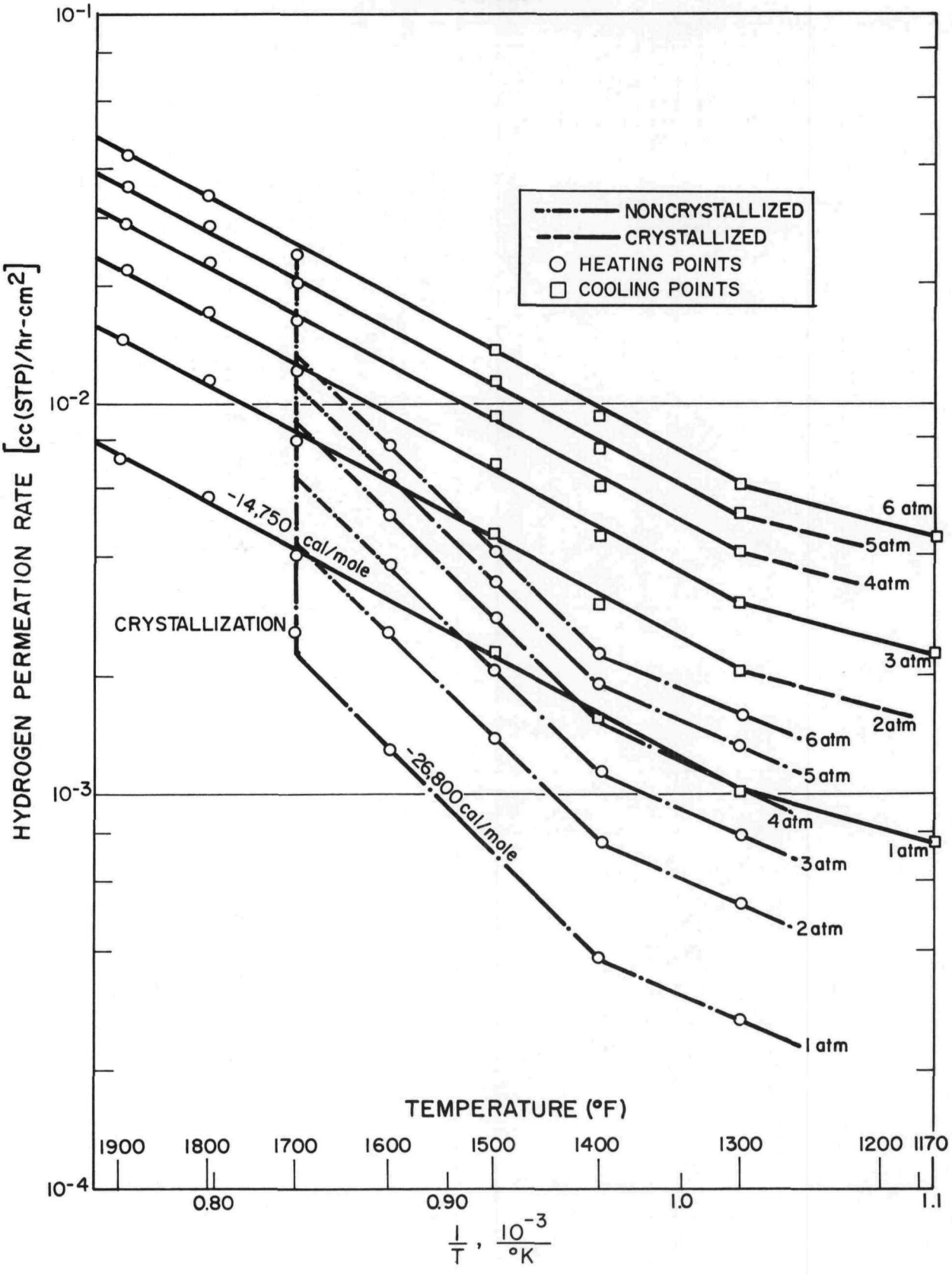

8-25-64

7568-0805A

Figure 4.2.14. Hydrogen Permeation Rate vs Temperature for SCB1 Coated Tube RD-40 (Reference 4.18)

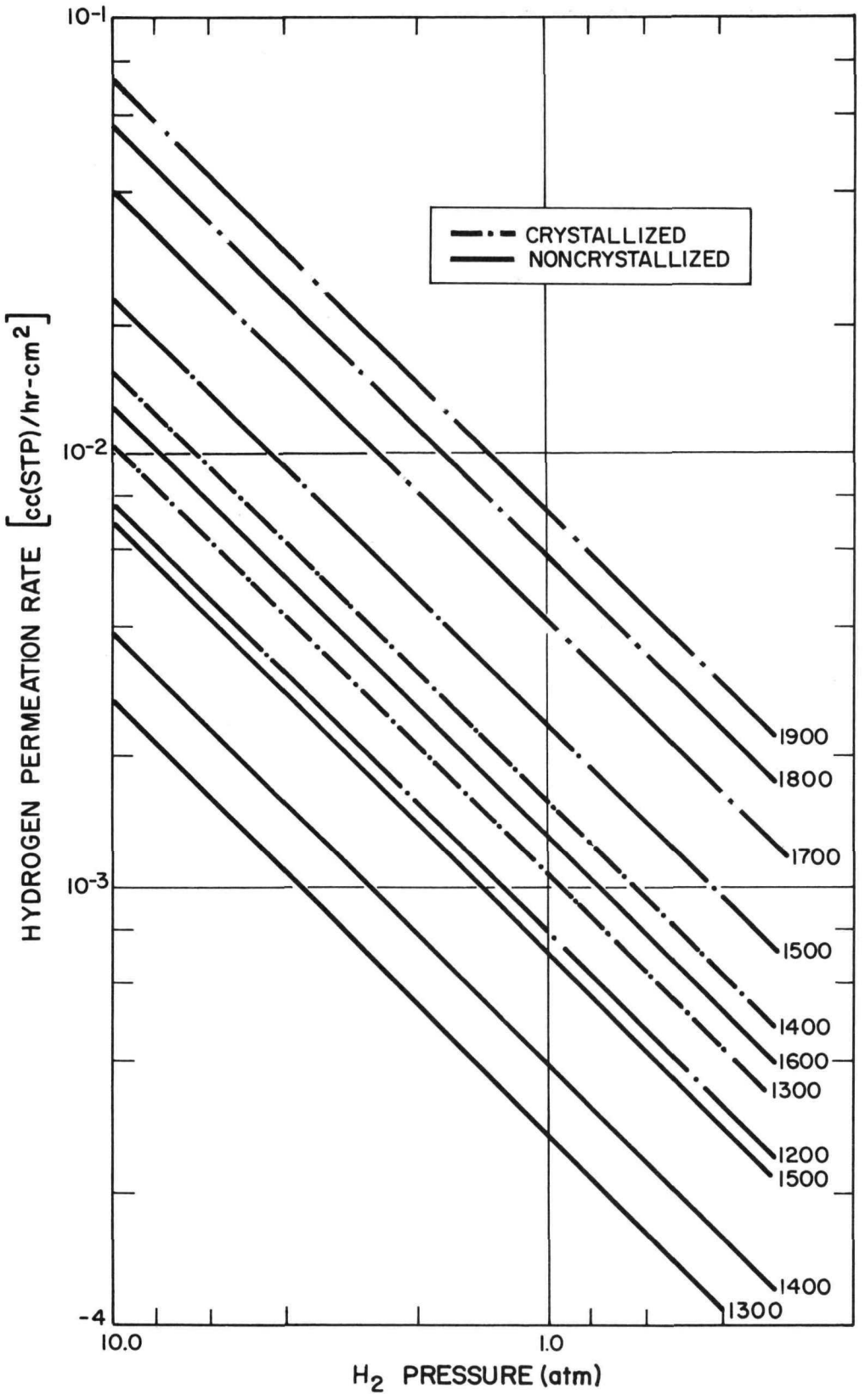

Figure 4.2.15. Hydrogen Permeation Rates vs Pressure for SCB1 Coated Tube RD-40 (Reference 4.18)

4.2.4.4 Compatibility

Table 4.2.6 lists some compatibility data on the S14-35A coating. AI8763D coating was also tested with unmodified Zr + 10U hydride (H/Zr ≅ 1.6) in a hydrogen atmosphere for 340 hr at 1450°F; results indicated no reaction occurred. No data are available on the SCB1, Al_2O_3, and SiC coatings.

TABLE 4.2.6

S14-35A COATING COMPATIBILITY WITH SOME MATERIALS IN A HYDROGEN ATMOSPHERE[4.11, 4.12]

Material	Time at Temperature (hr)	Remarks
Unmodified Zr + 10U Hydride (H/Zr ≅ 1.6)	513 at 1450°F	No reaction
Be	1000 at 1300°F	No reaction*
BeO	1000 at 1300°F	No reaction
Al_2O_3	1000 at 1300°F	No reaction
ZrO_2	1000 at 1300°F	No reaction
ThO_2	1000 at 1300°F	No reaction
Cr plated Be	1000 at 1300°F	No reaction

*A reaction can occur if there exists a pressure contact between the material and coating.

4.3 MECHANICAL PROPERTIES – HARDNESS

AI8763D coating, as-fired, has a diamond point hardness (DPH) between 700 and 724 under 100 and 200 gram loadings, respectively.[4.13] SiC coating has a 2500 knoop hardness under a 500 gram loading.[4.13] No data are available on the other coatings.

4.4 IRRADIATION PROPERTIES

4.4.1 Nuclear

4.4.1.1 Absorption Cross Section

Table 4.4.1 lists the macroscopic absorption cross section of various coatings. The values were calculated neglecting the following ingredients: mill additions, including Sm_2O_3 were ignored; oxygen and carbon contents were neglected because of their relatively low cross section; and impurities having a high cross section, such as boron, were neglected (less than 50 ppm of boron are found in S14-35A and AI8763D by emission spectrographic analysis). Densities and weight percents used in the calculations were obtained from Sections 4.2.1.3 and 4.1, respectively.

TABLE 4.4.1

MACROSCOPIC NUCLEAR ABSORPTION CROSS SECTIONS FOR COATINGS AT THERMAL ENERGY

Coating	Thermal Cross Section (cm^{-1})
S14-35A	Proprietary
AI8763D	0.11
SCB1	0.016
Al_2O_3	0.0058
SiC	0.0053

No data are presented here on the scattering cross sections, because a complicated scattering phenomena occurs when the nucleus is bounded to a molecular structure, as in a compound. The chemical bonds between the struck nucleus and the rest of the molecule give it an increased rigidity; consequently, the neutron responds as though it had collided with a much larger mass than that of the target nucleus. Scattering cross sections for the various containings cannot be calculated by neglecting the oxygen content, because its cross section represents a substantial amount of the total cross section. However, the total scattering cross section of a coating is quite small as compared to the other components of a fuel element and is ignored in nuclear calculations.

4.4.1.2 Poisoning

Results with S14-35A, AI8763D, and SCB1 coatings indicate that Sm_2O_3 additions up to 4% by weight have no apparent effect on the properties (other than nuclear properties) of these coatings.[4.2, 4.3, 4.8] No results are available for Al_2O_3 and SiC coatings.

4.4.2 Radiation Behavior

Table 4.4.2 lists results as of June 1, 1964, on the irradiation capsule experiments being performed by Atomics International to determine the hydrogen permeation coating barrier behavior under fast neutron radiation.

TABLE 4.4.2

EFFECT OF IRRADIATION ON HYDROGEN PERMEATION COATINGS

Hydrogen Barrier	Reactor Experiment	Temperature Range (°F)	Accumulated Time (hr)	Radiation Dose (nvt) (E_m > 1 Mev)	Comments
S14-35A on SS (Reference 4.14)	NAA 53-1	800-850	2000	10^{19}	Visual examination revealed the following results: coating was in excellent condition, and there was the usual dark film covering the coating.
	NAA 53-2	800-1000	3876	2×10^{19}	Same as above; however, the coating was evidently damaged, because it suddenly failed as a hydrogen barrier during post-irradiation testing.
AI8763D on chromized Hastelloy N (Reference 4.15 and 4.19)	NAA 53-3	900-1000	1446	1.4×10^{19} upper 1.2×10^{19} lower	Reduction in permeation rate by a factor of two while hydrogen content decreased by a factor of 100 leads to the conclusion that the coating lost some of its effectiveness as a barrier during irradiation. Adhesion of the coating to the fuel in the lower capsule occurred.
	NAA 68-1	1000-1200	~3700	1×10^{21}	No gross change to the coating.
SCB on chromized Hastelloy N (Reference 4.16)	NAA 77-1	1200-1500	4333	2.58×10^{21}	No detrimental effect on hydrogen permeation rates occurred in this in-pile permeation experiment.
	NAA 77-2	1300	1413	4.48×10^{20}	Same as above. This experiment is still progressing and thus far, the integral fission fragment per inch is 6.4×10^{17}.
	NAA 77-3	1500	1413	4.48×10^{20}	Same as above except the integral fission fragment per inch is 6.75×10^{17}.
	NAA 77-4	1700	0	0	Irradiation has just begun.

REFERENCES

4.1 R. W. Webb, Personal Communication, Atomics International, a Division of North American Aviation, Canoga Park, December 1963 (Secret)

4.2 R. W. Webb, "SNAP 8 Experimental Reactor (S8ER) Hydrogen Barrier Coating Development," NAA-SR-9618, June 1964 (Secret-RD)

4.3 H. W. Carpenter, "Development of Crystallized Hydrogen Barriers for SNAP 8 Reactors," Atomics International, a Division of North American Aviation, Canoga Park (to be published) (Secret-RD)

4.4 C. J. Ambrose, Personal Communication, Atomics International, a Division of North American Aviation, Canoga Park, December 1963 (Secret-RD)

4.5 R. H. Thomas, Journal of American Ceramic Society, 33 (2) 43 (1950)

4.6 Handbook of Chemistry and Physics, Chemical Rubber Publishing Company, 1957

4.7 J. M. Ward, "Refractories for Nuclear Energy," The Refractories Institute Bulletin, No. 94, February 1956

4.8 H. W. Carpenter, "Environmental Testing of SNAP 8 Hydrogen Barriers," Atomics International, a Division of North American Aviation, Canoga Park (to be published) (Secret-RD)

4.9 H. Rosenberg, Editor, "SNAP 8 Reactor Preliminary Design Summary," NAA-SR-6207, June 1961 (Secret-RD)

4.10 C. J. Engberg, "Hydrogen Permeation of SNAP Hydrogen Barrier Material," Atomics International, a Division of North American Aviation, Canoga Park (to be published) (Secret-RD)

4.11 L. B. Lundberg, "SNAP Fuel and Core Materials Compatibility Screening Test," NAA-SR-9007 (to be published) (Secret-RD)

4.12 J. K. Balkwill, "Compatibility of SNAP Fuel and Clad Materials," NAA-SR-5413, October 1960 (Secret-RD)

4.13 H. Taketani, Personal Communication, Atomics International, a Division of North American Aviation, Canoga Park, November 1963

4.14 J. R. Miller, Personal Communication, Atomics International, a Division of North American Aviation, Canoga Park, December 1963

4.15 D. A. Polak, Personal Communication, Atomics International, a Division of North American Aviation, Canoga Park, December 1963

4.16 R. C. Courtwright and C. J. Engberg, Personal Communication, Atomics International, a Division of North American Aviation, Canoga Park, California, June 1964

4.17 J. Cohen, Bulletin American Ceram. Soc. 38, 441-446, 1959

4.18 C. E. Johnson, "SNAP 8 Progress Report, October 1963 through January 1964," NAA-SR-9392, March 1964 (Secret RD)

4.19 J. R. Miller and D. A. Polak, "Irradiation of Hydrided Zr-U Alloy – NAA 53 Experiments" (to be published) (Secret-RD)

5.0 FUEL ELEMENTS

5.1 INTRODUCTION

The object of a fuel element is to generate heat efficiently and reliably. Fuel element development programs are being conducted at Atomics International for the sole purpose of accomplishing this objective.

The fuel element consists of a massively hydrided zirconium uranium alloy encapsulated in a metal tube. A glass hydrogen barrier is placed on the internal surface of the cladding to slow down loss of hydrogen due to permeation through the metal. End pieces are welded to the tube and ceramic seals are used to prevent hydrogen loss through these closures.

Several modifications to the fuel elements have been incorporated since the fuel element development programs were initiated. One of these modifications was the addition of as much as 0.4 wt % carbon to the basic zirconium uranium alloy which greatly increased the yield of useable hydrided fuel rods. Without carbon the fuel consisted of large columnar grains which resulted in an inability of the fuel to withstand hydriding without cracking. With the addition of carbon in amounts as small as 0.10%, the grain structure remains fine during hydriding and the frequency of cracking was greatly reduced, thus increasing the percentage of acceptable fuel elements.

Another modification was the replacement of the fuel element axial reflectors with additional fuel material. Initially, beryllium was used as the material for the fuel element end reflectors; however, the compatibility of Be with neighboring materials was very poor. BeO was found to be compatible with these materials, henceforth, Be was replaced by BeO material. After the design of S2DR fuel elements it was determined that if the BeO fuel element end reflectors were replaced by increasing the length of the fuel material in the fuel element, a significant increase in reactivity could be achieved with a minimum of weight increase and actual savings in complexity. Thus, current fuel elements do not contain end reflectors.

During its lifetime, the fuel element increases in volume due to fission product formation, both solid and gaseous. This growth is accommodated radially by original assembly gaps, but an axial gap must also be provided to accommodate this expected growth. A spacer device was designed for incorporation at one end of the S8DRM-1 fuel element to provide an axial gap during testing but to collapse under the axial pressure of the fuel material during irradiation. The first series of devices failed during shock and vibration tests but was retained in the S8DRM-1 design due to time considerations. It was removed from the S8DS-1 fuel elements which will not undergo launch or test vibration and shock. Further effort is underway for possible use of a new spacer device, if it proves necessary, for future reactors.

The fourth modification is the replacement of the two piece end closure used in past fuel element designs, including the S8ER fuel element, by a one piece cup plug. The one piece closure provides a cheaper, stronger, and more reliable seal against hydrogen leakage.

Significant progress has occurred in the technology of preventing loss of hydrogen from the fuel element. The glass barrier composition has evolved from a commercially available material, through an improved modification of this composition, to the present coating (SCB-1) which was chemically tailored for the SNAP application. Accompanying these changes in coating material was considerable effort to improve the coating technique and to improve the end closure technology which has progressed through evolution to the present methods.

The following sections briefly describe designed and fabricated fuel elements along with test procedures and results at Atomics International. Many tests are still being conducted so that updating of this section will be vital.

5.2 CONFIGURATION AND MATERIALS

5.2.1 Reactors

Reactors	Purpose	Fuel Element Status
S2ER	Test reactor core under design temperature and power conditions	Fabricated, operated, dismantled
S2DR	Mate reactor to SNAP 2 power conversion system	Fabricated, operated (without power conversion system) and dismantled
S10A	Demonstrate SNAP 10A system 90-day ground operation and orbital capability	Fabricated and operational (see Figure 5.2.1)
SNAPTRAN	Determine effect of reactor transients	Cores I-IV fabricated
S2FS	Ground demonstration of SNAP 2 flight system	Designed
S8ER	Demonstrate SNAP 8 reactor capability	Fabricated and operational (see Figure 5.2.1
S8DRM-1	Nonnuclear flight system mockup	Fabricated
S8DS-1	Demonstrate ground operation of SNAP 8 system	Designed
S8FS, S8FR-1 and -2	Ground operation	Conceptual design
S8FR-3, -4, and -5	Orbital operation	Conceptual design

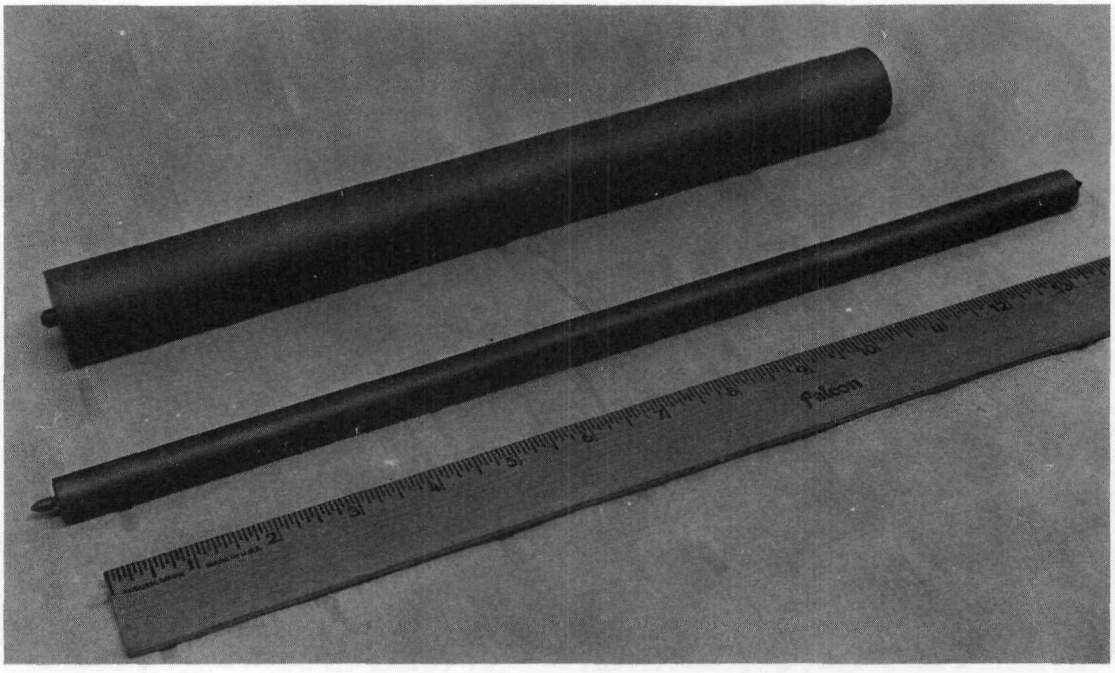

5-28-62 7550-51571

Figure 5.2.1. Comparison of S10FS-1 and S8ER Fuel Elements

5.2.2 S2ER DESCRIPTION[5.1]

Fuel Element	
Assembly drawing	7512-971801
Number required	61*
Length	
Between end flats	14.000″
Overall	14.750″
Internal axial gap	0.020″
Diameter	
Overall	1.000″
Hydrogen permeation rate (cc/hr-element)	at 1200°F
Average	0.26
Range	0.08 to 0.82
Design limit	-
Fuel	
Configuration	
Length	10.000″
Diameter	0.975″
Composition	
Uranium	
Enrichment	93.15 % U^{235}
Average (wt %)	6.86
Range	6.68 to 7.03
Carbon (wt %)†	-
Average	-
Range	~0.02 to 0.05
Hydrogen N_H	
Average	6.07
Range	5.80 to 6.30
Zirconium	Balance
Cladding	
Material	Type 347 SS§
Inside diameter	0.980″
Outside diameter	1.000″
Wall thickness	0.010″
Hot End	
Closure type	Blended tapered plug
Pin diameter	0.245″
Cold End	
Closure type	Blended tapered plug
Pin diameter	0.248″
Internal Reflector	
Material	Be
Length	1.500″
Diameter	0.975″
Coating	
Material	
Standard	Solaramic S14-35A
Poison	-
Thickness	
Average	0.0025″
Range	0.0017 to 0.0043″
Sm_2O_3 Content (mg/tube)	
Average	-
Range	-

*Including four thermocoupled elements and two thermocoupled and pressure probed elements.
†Residual
§Three elements were clad in Hastelloy B.

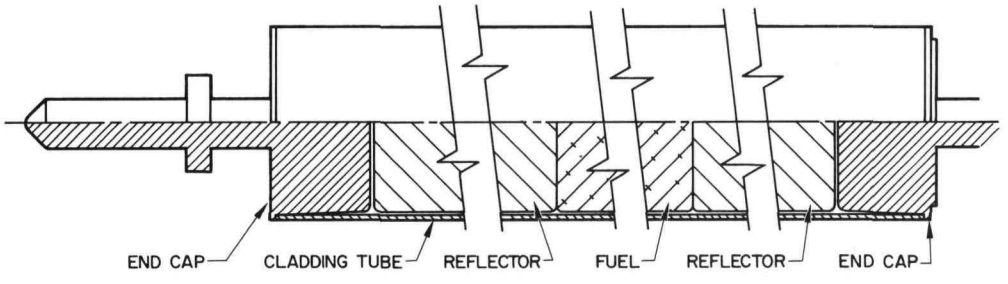

8-10-64 7569-01696

Figure 5.2.2. S2ER Fuel Element

5.2.3 S2DR Description[5.2]

Fuel Element	
Assembly drawing	7512-22151
Number required	37*
Length	
Between end flats	13.225″
Overall	13.975″
Internal axial gap	0.000
Diameter	
Overall	1.250″
Hydrogen permeation rate (cc/hr-element)	at 1200°F
Average	0.80*
Range	0.29 to 1.74*
Design limit	-
Fuel	
Configuration	
Length	10.000″
Diameter	1.2120″
Composition	
Uranium	
Enrichment	93.15% U^{235}
Average (wt %)	10.14
Range	9.8 to 10.4
Carbon (wt %)†	
Average	-
Range	~0.02 to 0.05
Hydrogen N_H	
Average	6.45
Range	6.23 to 6.64
Zirconium	Balance

Cladding	
Material	Hastelloy N
Inside diameter	1.220″
Outside diameter	1.250″
Wall thickness	0.014§
Hot End	
Closure type	Welded H cap
Pin diameter	0.180″
Cold End	
Closure type	Blended A cap
Pin diameter	0.180″
Internal Reflector	
Material	BeO
Length	1.500″
Diameter	1.211″
Coating	
Material	
Standard	Solaramic S14-35A
Poison	Solaramic S14-35-SM2
Thickness	
Average	0.0030″
Range	0.0018 to 0.0040″
Sm_2O_3 content (mg/tube)	
Average	88
Range	82 to 93

*Including three instrumented elements
†Residual
§Four cladding tubes averaged 0.0110 instead of the nominal 0.014

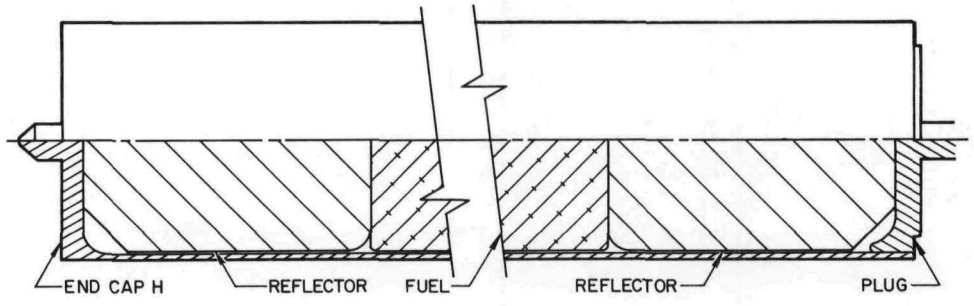

8-7-64 7569-01697

Figure 5.2.3. S2DR Fuel Element

5.2.4 S10A Description[5.3]

Fuel Element	
Assembly drawings	7573-18002
Number required	37
Length	
Between end flats	12.450"
Overall	12.815"
Internal axial gap	0.003"
Diameter	
Overall	1.250"
Hydrogen permeation rate (cc/hr-element)	at 1200°F
Average	-
Range	-
Design limit	0.5
Fuel	
Configuration	
Length	12.250"
Diameter	1.210"
Composition	
Uranium	
Enrichment	93.15% U^{235}
Average (wt %)	10.15
Range	±0.3
Carbon (wt %)	
Average	0.15
Range	±0.05
Hydrogen N_H	
Average	6.35
Range	±0.10
Zirconium	Balance
Cladding	
Material	Hastelloy N
Inside diameter	1.220"
Outside diameter	1.250"
Wall thickness	0.015"
Hot End	
Closure type	Welded cap
Pin diameter	0.243"
Cold End	
Closure type	Blended grooved cup plus welded plug
Pin diameter	0.181"
Internal Reflector	
Material	None
Length	-
Diameter	-
Coating	
Material	
Standard	Solaramic S14-35A
Poison	Solaramic S14-35 + Sm_2O_3
Thickness	
Average	0.0025
Range	0.001 to 0.004
Sm_2O_3 content (mg/tube)	
Average	98
Range	88 to 108

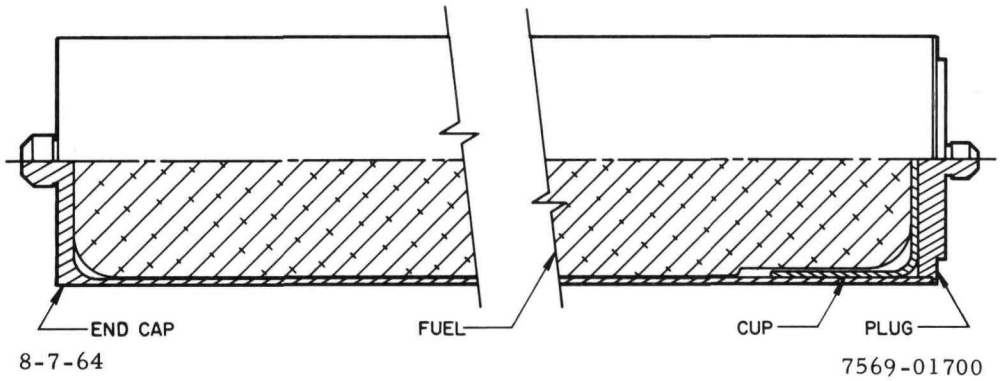

Figure 5.2.4. S10A Fuel Element

5.2.5 SNAPTRAN Description – Cores I and II

Fuel Element	
Assembly drawing	7580-18035 and 7611-18001
Number required	37
Length	
Between end flats	12.450″
Overall	13.262″
Internal axial gap	0.003″
Diameter	
Overall	1.250″
Hydrogen permeation rate (cc/hr-element)	at 1200°F
Average	
Core I	1.01*
Core II	0.24
Range	
Core I	0.06 to 2.60*
Core II	0.03 to 0.47
Design limit	0.50
Fuel	
Configuration	
Length	12.250″
Diameter	1.210″
Composition	
Uranium	
Enrichment	93% U^{235}
Average (wt %)	
Core I	10.04*
Core II	10.03
Range	
Core I	9.92 to 10.14*
Core II	9.87 to 10.15
Carbon (wt %)	
Average	
Core I	0.41*
Core II	0.41
Range	
Core I	0.34 to 0.51*
Core II	0.33 to 0.51
Hydrogen N_H	
Average	
Core I	6.53*
Core II	6.50
Hydrogen N_H (Continued)	
Range	
Core I	6.44 to 6.63*
Core II	6.38 to 6.63
Zirconium	Balance
Cladding	
Material	Hastelloy N
Inside diameter	1.220″
Outside diameter	1.250″
Wall thickness	0.015″
Hot End	
Closure type	Welded cap
Pin diameter	0.181″
Cold End	
Closure type	Blended grooved cup plus welded plug
Pin diameter	0.640″
Internal Reflector	
Material	None
Length	-
Diameter	-
Coating	
Material	
Standard	Solaramic S14-35A
Poison	Solaramic S14-35-Sm_2
Thickness	
Average	0.025″
Range	0.001 to 0.004″
Sm_2O_3 content (mg/tube)	
Average	
Core I	100
Core II	99
Range	
Core I	88
Core II	85 to 124

*Core I consisted of 23 converted reject S10FS1 high carbon high leak rate elements for which the data is tabulated. Data for the other 14 elements are: hydrogen permeation rate – average 0.05, range 0.02 to 0.11; uranium – average 10.18, range 10.10 to 10.39; carbon – average 0.15, range 0.14 to 0.19; hydrogen N_H – average 6.51, range 6.38 to 6.60.

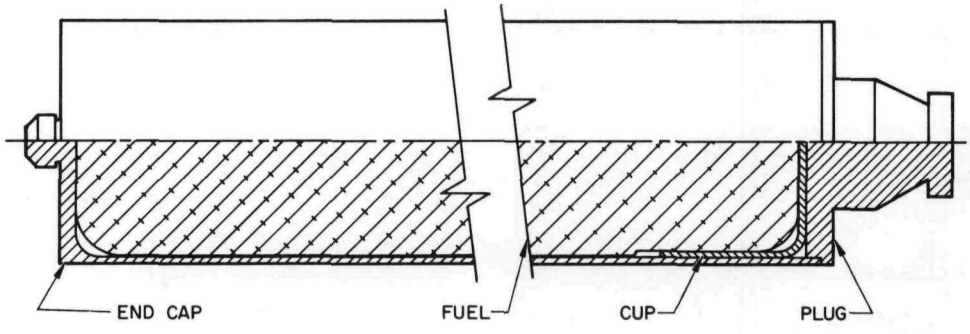

8-10-64 7569-01699

Figure 5.2.5. SNAPTRAN Fuel Element

5.2.6 S2FS Description[5.3]

Fuel Element	
Assembly drawing	7622-18001
Number required	37
Length	
Between end flats	12.450"
Overall	12.815"
Internal axial gap	0.003"
Diameter	
Overall	1.250"
Hydrogen permeation rate (cc/hr-element)	at 1200°F
Average	-
Range	-
Design limit	0.5
Fuel	
Configuration	
Length	12.250"
Diameter	1.210"
Composition	
Uranium	
Enrichment	93.15% U^{235}
Average (wt %)	10.15
Range	±0.30
Carbon (wt %)	
Average	0.15
Range	±0.05
Hydrogen N_H	
Average	6.35
Range	±0.10
Zirconium	Balance

Cladding	
Material	Hastelloy N
Inside diameter	1.220"
Outside diameter	1.250"
Wall thickness	0.015"
Hot End	
Closure type	Welded cap
Pin diameter	0.243"
Cold End	
Closure type	Blended cup plus welded plug
Pin diameter	0.181"
Internal Reflector	
Material	None
Length	-
Diameter	-
Coating	
Material	
Standard	AI8763D
Poison	AI8763D + Sm_2O_3
Thickness	
Average	0.0025"
Range	0.001 to 0.004"
Sm_2O_3 content (mg/tube)	
Average	98
Range	88 to 108

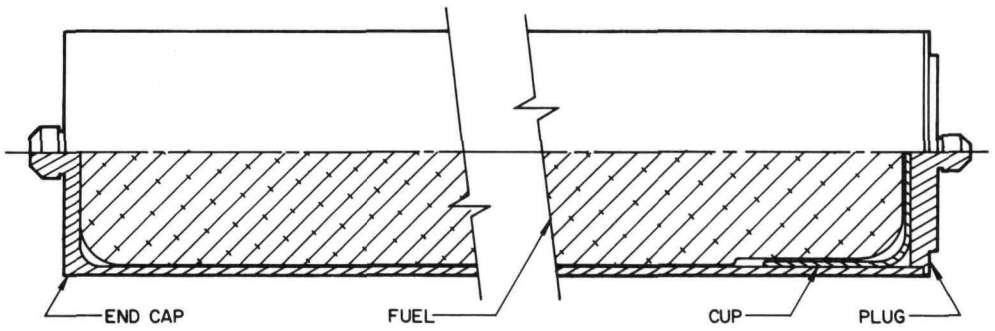

8-7-64 7569-01701

Figure 5.2.6. S2FS Fuel Element

5.2.7 S8ER Description[5.18]

Fuel Element	
Assembly drawing	7570-18011
Number required	211
Length	
Between end flats	14.470"
Overall	15.090"
Internal axial gap	0.025"
Diameter	
Overall	0.560"
Hydrogen permeation rate (cc/hr-element)	at 1400°F
Average	0.54
Range	0 to 1.6
Design limit	1.6
Fuel	
Configuration	
Length	14.000"
Diameter	0.5325"
Composition	
Uranium	
Enrichment	93.16% U^{235}
Average (wt %)	10.00
Range	9.72 to 10.29
Carbon (wt %)	
Average	*
Range	0.02 to 0.6*
Hydrogen N_H	
Average	5.96
Range	5.66 to 6.25†
Zirconium	Balance

Cladding	
Material	Hastelloy N
Inside diameter	0.540"
Outside diameter	0.560"
Wall thickness	0.010"
Hot End	
Closure type	Welded cap
Pin diameter	0.140"
Cold End	
Closure type	Blended grooved cup plus welded plug
Pin diameter	0.140"
Internal Reflector	
Material	None
Length	-
Diameter	-
Coating	
Material	
Standard	AI8763D
Poison	AI8763D + Sm_2O_3
Thickness	
Average	0.0023"
Range	0.0007 to 0.0041*
Sm_2O_3 content (mg/tube)	
Average	45
Range	30 to 60*

*Tolerance limits where 95% of population will be contained at the 95% confidence level
†Individual fuel rods manufactured to three carbon levels, i.e., none intentionally added, 0.15% and 0.5%. Manufactured according to Reference 5.4.

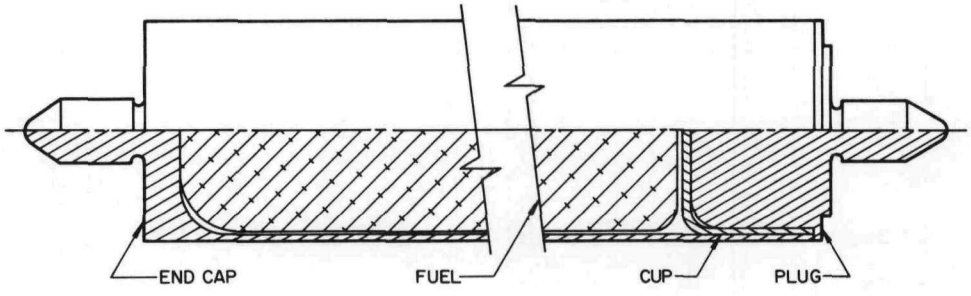

8-7-64 7569-01702

Figure 5.2.7. S8ER Fuel Element

5.2.8 S8DRM-1 Description[5.5]

Fuel Element	
Assembly drawing	7568-18022
Number required	40*
Length	
Between end plate	14.630"
Overall	15.658"
Internal axial gap	0.003†
Diameter	
Overall	0.560"
Hydrogen permeation rate (cc/hr-element)	at 1400°F
Average	0.75
Range	-
Design limit	1.50
Fuel	
Configuration	
Length	14.000§
Diameter	0.5275"
Composition	
Uranium	
Enrichment	Natural U
Average (wt %)	10.0
Range	±0.3
Carbon (wt %)	
Average	0.20
Range	± 0.05
Hydrogen N_H	
Average	6.0
Range	±0.2
Zirconium	Balance
Cladding	
Material	Hastelloy N
Inside diameter	0.540"
Outside diameter	0.560"
Wall thickness	0.010"
Hot End	
Closure type	Welded cap
Pin diameter	0.245"
Cold End	
Closure type	Blended grooveless cup – plug
Pin diameter	0.2483"
Internal Reflector	
Material	None**
Length	-
Diameter	-
Coating	
Material	
Standard	AI8763D
Poison	None
Thickness	
Average	0.003"
Range	0.001 to 0.004"
Sm_2O_3 content (mg/tube)	
Average	-
Range	-

*Remainder of 211 core positions to be filled with dummy stainless steel elements.
†Axial gap 0.065 for elements without spacer assembly
§Fuel length 14.343 for elements without spacer assembly
**Steel internal spacer provides for axial fuel swelling while maintaining fuel in position. Manufactured according to Reference 5.5.

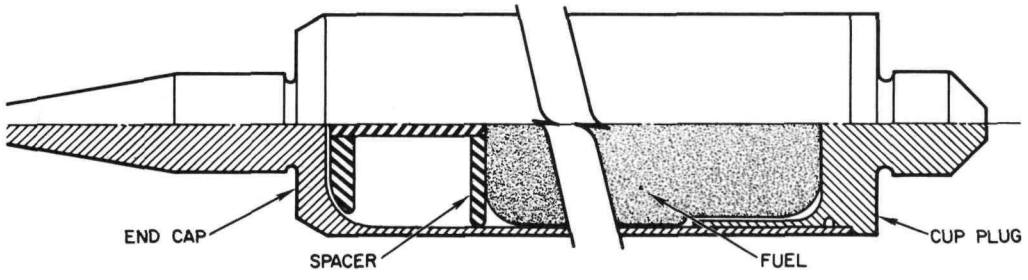

8-14-64 7569-01703

Figure 5.2.8. S8DRM-1 Fuel Element

5.2.9 S8DS-1 Description[5.6]

Fuel Element	
Assembly drawing	7568-18034
Number required	211
Length	
Between end flats	17.145"
Overall	18.173"
Internal axial gap	0.003"
Diameter	
Overall	0.560"
Hydrogen permeation rate (cc/hr-element)	at 1400°F
Average	0.40
Range	-
Design limit	0.95
Fuel Configuration	
Length	16.825"
Diameter	0.5300"
Composition	
Uranium	
Enrichment	93.15% U^{235}
Average (st %)	10.5
Range	± 0.3
Carbon (wt %)	
Average	0.15
Range	±0.05
Hydrogen N_H	
Average	6.05 ± 0.05
Range	5.8 to 6.15
Zirconium	Balance

Cladding	
Material	Hastelloy N
Inside diameter	0.540"
Outside diameter	0.560"
Wall thickness	0.010"
Hot End	
Closure type	Welded cap
Pin diameter	0.245"
Cold End	
Closure Type	Blended groove-less cup – plug
Pin diameter	0.2483"
Internal Reflector	
Material	None*
Length	-
Diameter	-
Coating	
Material	
Standard	SCB
Poison	SCB + Sm_2O_3
Thickness	
Average	0.0020"
Range	0.001 to 0.003"
Sm_2O_3 content (mg/tube)	
Average	57.6
Range	±14.1

*Steel internal spacer provides for axial fuel swelling while maintaining fuel in position.

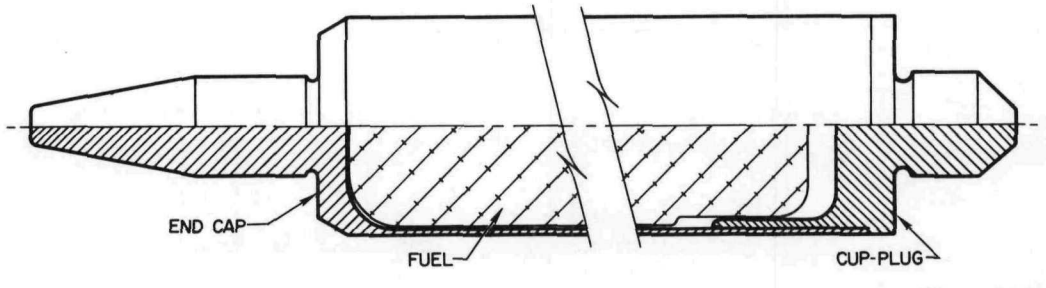

8-11-64 7569-01704

Figure 5.2.9. S8DS-1 Fuel Element

5.3 FABRICATION

5.3.1 SNAP 10A/2 Fuel Element[5.7, 5.8]

5.3.1.1 Fuel Fabrication

5.3.1.1.1 Melting and Forming

1) Compact 1-1/2 by 1-1/2 by 10 in. bars using zirconium sponge, uranium chop stock, and powdered zirconium carbide in the correct proportions.
2) Butt weld either two or three compacts end to end with an electrode connector on one end.
3) Using consumable electrode technique vacuum arc melt two of the two compact electrodes into one 3-in. ingot and a three compact electrode into another 3-in. ingot.
4) Machine surfaces of ingots and butt weld the two 3 in. ingots into one electrode with a connector at one end.
5) Using consumable electrode technique vacuum arc melt into a 4 in. melt pot and machine this ingot for first extrusion.
6) Coat billet with a special glass used as an extrusion lubricant and extrude at approximately 1000°F to a rod 1.125 in. diameter.
7) The extrusion rod is cut into four pieces and cleaned after which these rods are bundled and welded to a connector.
8) Using consumable electrode technique arc melt under vacuum into a 4 in. melt pot and machine for final extrusion.
9) Coat billet with a special glass lubricant and extrude at a temperature ~650°F to a rod 1.250 in. diameter.
10) Cut to length, machine to size for hydriding, and inspect.

5.3.1.1.2 Hydriding

1) Load three machined fuel rods with zirconium end plugs and zirconium turnings into ceramic tubes and insert into a furnace retort.
2) Evacuate retort, leak check and heat to 1650°F under a vacuum of ~5 x 10^{-5} TORR.
3) Add hydrogen at a rate to achieve an H/Zr = 1.0 in not less than 4 hr, then to H/Zr = 1.5 in approximately 12 additional hr.
4) Cool to 1250°F at 20°F per hour maintaining retort pressure of 1200 mm Hg.
5) When calculated amount of hydrogen has been added, shut off hydrogen and furnace power and allow furnace to cool.
6) Remove rods from furnace retort, weigh rods and calculate weight gain, then machine to the required configuration.
7) Verify hydrogen content by statistical chemical sampling techniques.

5.3.1.2 Cladding Components

5.3.1.2.1 Procurement

Components are purchased from vendors using Atomics International, A Division of North American Aviation, Canoga Park, Calif., supplied Hastelloy N material.

5.3.1.2.2 Tube Assembly

1) Butt weld end cap to tube using tungsten inert gas process.

2) Chromize all surfaces, vacuum outgas, and straighten.

3) Sandblast interior of tubes and clean.

4) Using a flow coating process coat the interior of the SNAP 10A assemblies with Solaramic S14-35A and SNAP 2 assemblies with AI8763D material.

5) Dry assemblies and fire at 1850°F for SNAP 10A and 1900°F for SNAP 2.

6) Repeat operation two more times using basic coating material plus Sm_2O_3 addition.

7) If tube inside diameter is still too large, apply an additional coating of the basic material.

8) Inspect and cut tubes to the required length for assembly.

5.3.1.2.3 End Cups

1) Chromize all surfaces, and vacuum outgas.

2) Spray coat all surfaces with the same basic material as used on the tube assemblies, dry it, and fire.

3) Repeat the coating process until required dimensions are met.

5.3.1.3 Final Assembly

1) Insert fuel rod into tube assembly and place in assembly fixture.

2) Shrink fit end cup into tube under 15 mm He pressure using induction heating to expand the tube.

3) Blend ceramic seal by heating to 1700°F for SNAP 10A and 1750°F for SNAP 2.

4) Helium leak check seal.

5) Final machine end plug to fit tube assembly.

6) Weld end plug to fit tube assembly using tungsten inert gas process and helium leak check.

7) Final machine to required dimensions.

8) Liquid hone, rinse, and dry.

5.3.1.4 Acceptance Testing

1) Inspect all dimensions for conformance to the applicable drawings.

2) Determine isothermal hydrogen permeation rate at 1200°F for SNAP 10A or 1300°F for SNAP 2.

3) Perform acceptance vibration and shock program according to the applicable specification.

4) Redetermine isothermal hydrogen permeation rate.

5.3.2 SNAP 8 Fuel Elements (S8DS-1 Type) 5.8, 5.9, 5.10

5.3.2.1 Fuel Fabrication

5.3.2.1.1 Melting and Forming

1) Compact 1-1/2 by 1-1/2 by 10 in. bars using zirconium sponge, uranium chop stock, and powdered zirconium carbide in the correct proportions.

2) Butt weld either two or three compacts end to end with an electrode connector at one end.

3) Using consumable electrode technique arc melt under vacuum two of the two compact electrodes into one 3 in. ingot and a three compact electrode into another 3 in. ingot.

4) Machine surfaces of ingots and butt weld the two 3 in. ingots into one electrode with a connector at one end.

5) Using consumable electrode technique arc melt under vacuum into a 4 in. melt pot and machine for first extrusion.

6) Coat billets with a special glass used as an extrusion lubricant and extrude at approximately 1000°F to a rod 1.125 in. diameter.

7) After cutting and cleaning weld a connector to the end of each rod.

8) Using consumable electrode technique arc melt under vacuum into a 2 in. melt pot and machine for final extrusion.

9) Coat billets with a special glass lubricant and extrude at a temperature ~650°F to rods 0.632 in. diameter.

10) Cut and machine rods to size for hydriding.

5.3.2.1.2 Hydriding

1) Load eight fuel rods into ceramic tubes and insert into a furnace retort.

2) Evacuate retort, leak check, and heat to 1650°F under a vacuum of ~5 x 10^{-5} TORR.

3) Add hydrogen at a rate to achieve an H/Zr = 1.0 in not less than 4 hr, then to H/Zr = 1.5 in approximately 12 additional hr.

4) Cool to 1400°F at 20°F/hr while allowing retort pressure to decrease from 1200 to 1000 mm pressure.

5) When calculated amount of hydrogen has been added, shut off hydrogen and furnace power, and allow to furnace cool.

6) Remove rods from retort, determine hydrogen content by a weight gain technique, and machine to the required configuration.

7) Verify hydrogen content by statistical chemical sampling techniques.

5.3.2.2 Cladding Components

5.3.2.2.1 Procurement

Components, excepting the spacer assembly, are fabricated from Hastelloy N.

5.3.2.2.2 Tube Assembly

1) Butt weld end cap to tube using tungsten inert gas process.
2) Chromize all surfaces, vacuum outgas and straighten.
3) Sandblast interior of tubes and clean.
4) Using a flow coating technique coat the interior of the assemblies using AI SCB material.
5) Dry assemblies and fire at ~2100°F.
6) Repeat coating operation two more times using the basic coating material plus an addition of Sm_2O_3.
7) Recoat using basic material until dimensions are met.
8) Inspect and cut tubes to length for assembly.

5.3.2.2.3 Cup-Plugs

1) Chromize all surfaces and vacuum outgas.
2) Spray coat required surfaces with the same basic material as used on the tube assemblies, dry it, and fire.
3) Repeat until required dimensions are met.

5.3.2.2.4 Spacer Assembly

1) Machine components to drawing requirements.
2) Weld assembly using electron beam welding method.
3) Coat flat surface to be in contact with fuel to prevent reaction with fuel. Coating material is AI8763D.

5.3.2.3 Final Assembly

1) Insert spacer assembly into tube assembly.
2) Insert fuel rod into tube assembly and trim tube to length.
3) Shrink fit cup-plug into tube assembly under a vacuum using induction heating to heat the tube.
4) Liquid hone to produce oxide-free surface.
5) Electron beam weld cup-plug to tube assembly.
6) Final machine to required dimensions.
7) Blend ceramic seal by heating to ~1950°F followed by controlled cooling.

5.3.2.4 Acceptance Testing

1) Determine isothermal hydrogen permeation rate at 1400°F.
2) Inspect all dimensions for conformance to applicable drawing.

5.4 PERFORMANCE TESTING

5.4.1 Qualification Testing

5.4.1.1 General Description

Qualification testing shall be done to establish performance characteristics and reliability of normal fuel elements under single exposure to anticipated environmental conditions. The design hydrogen permeation rate specified in the fuel element specification must be met after completion of all qualification tests for an element to be fully qualified.

5.4.1.2 SNAP 10A Fuel Element Sequence[5.11]

Permeation Test
1100°F

3 Thermal Cycles: Heat at ≤300°F/hr from <400 to 1100°F,
Dwell at 1100°F for 10 hr, Cool at ≤300°F/hr to <400°F)

Permeation Test
1100°F

Vibration and Shock

	Axis	Magnitude	Frequency - cps
Vibration:	Longitudinal,	1/8 in. 0 to Peak	5 to 20
	Lateral and	5 g	20 to 400
	Normal	7.5 g	400 to 3000

	Axis	Magnitude	No. of Shocks	Duration
Shock:	Longitudinal	20 g	2 each direction	6 ± 1 msec
	Lateral and Normal	10 g	2 each direction	6 ± 1 msec

Permeation Test
1100°F

5 Ramp Heat Cycles: Heat at 150°F/min from 600 to 1150°F
Cool at 50 to 600°F

Permeation Test
1100°F

Thermal Endurance
1100°F for 1 yr

Permeation Test
1100°F

Destructive Analysis
Dimensions, Metallography, and Hydrogen Analysis

RESULTS: Sixty-six SNAP 10A fuel elements have completed qualification inputs with the exception of thermal endurance. The data collected to date shows that none of the qualification inputs have significantly harmed the hydrogen barrier of any of the elements. The problem of outgassing and aging has not been sufficiently solved in order to accurately measure and theoretically predict (within ±20%) hydrogen leak rates.[5.19]

5.4.1.3 SNAP 2 Fuel Element Sequence

Permeation Test
1200°F

3 Thermal Cycles: Heat at ≤300°F/hr from <400 to 1200°F,
Dwell at 1200°F for 10 hr, cool at ≤300°F/hr to <400°F

Permeation Test
1200°F

Vibration and Shock

	Axis	Magnitude	Frequency - cps
Vibration:	Longitudinal,	1/8 in. 0 to Peak	5 to 20
	Lateral and	5 g	20 to 400
	Normal	7.5 g	400 to 3000

	Axis	Magnitude	No. of Shocks	Duration
Shock:	Longitudinal,	20 g	2 each direction	6 ± 1 msec
	Lateral and Normal	10 g	2 each direction	6 ± 1 msec

Permeation Test
1200°F

5 Ramp Heat Cycles: Heat at 150°F/min from 600 to 1250°F
Cool at 50 to 600°F

Permeation Test
1200°F

Thermal Endurance
1200°F for 1 yr

Permeation Test
1200°F

Destructive Analysis:
Dimensions, Metallography, and Hydrogen Analysis

RESULTS: Tests not completed.

5.4.1.4 SNAP 8ER Fuel Element Sequence[5.12]

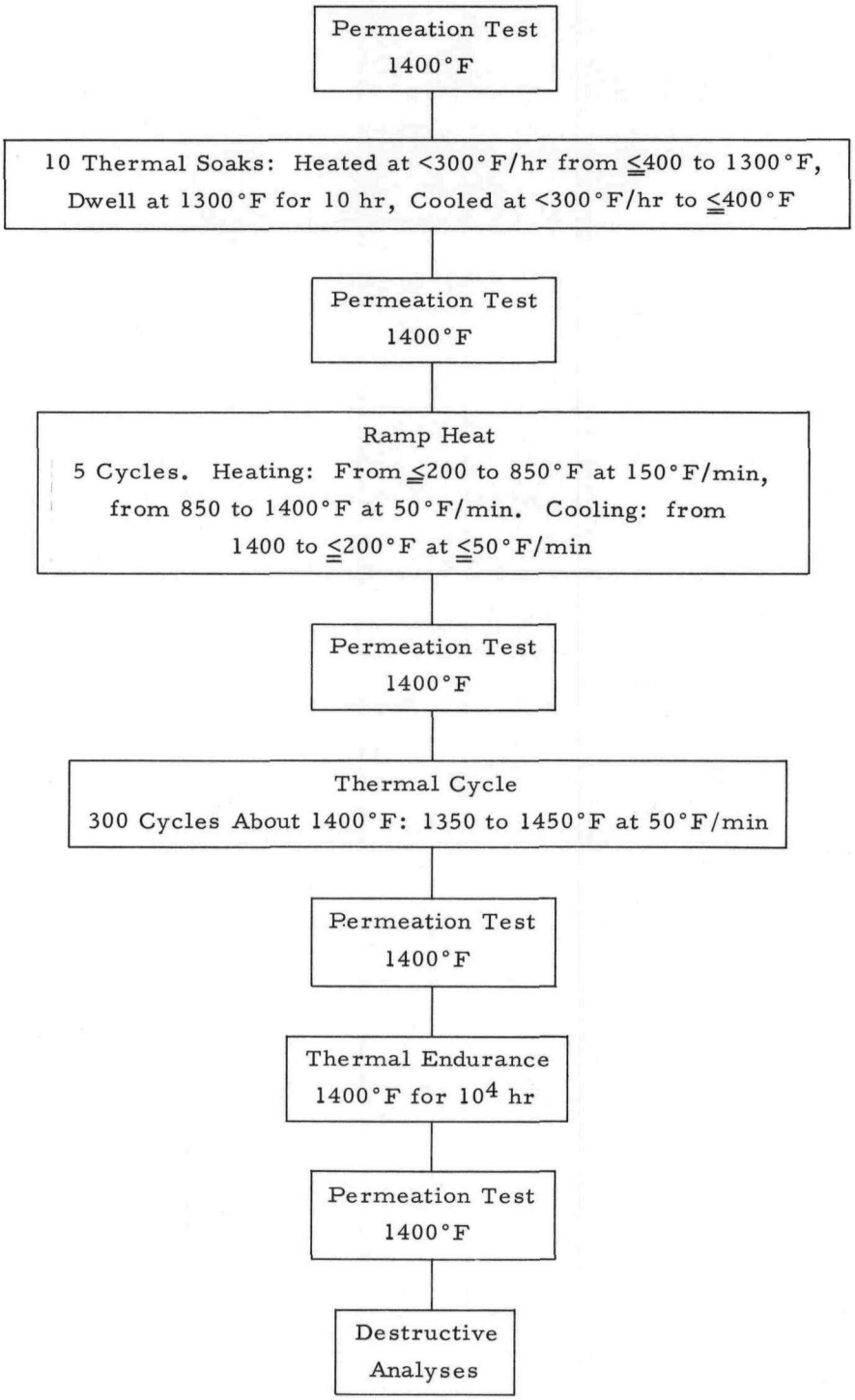

RESULTS: Tests not completed.

5.4.1.5 S8DS-1 Fuel Element Sequence[5.12]

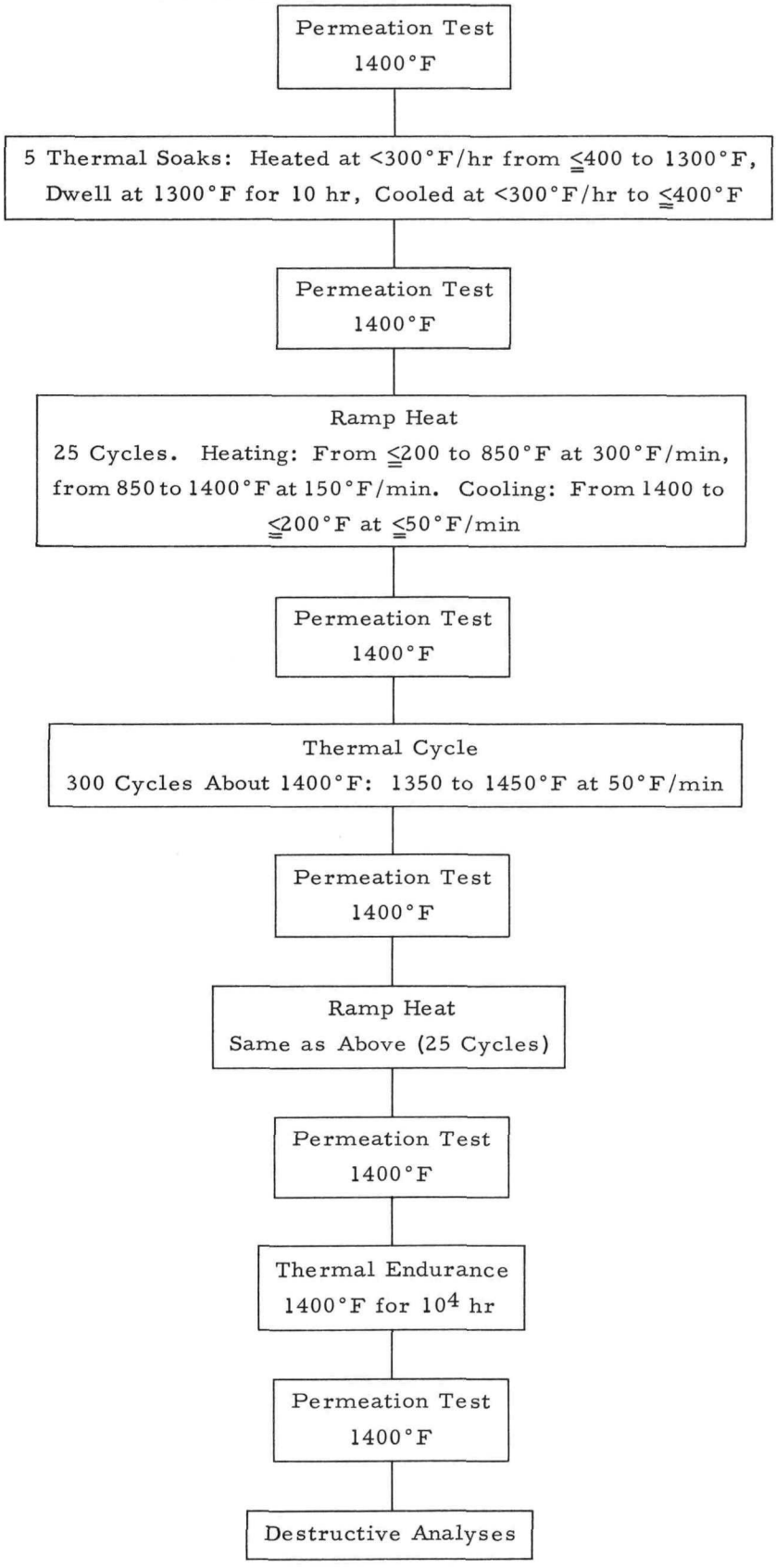

RESULTS: Design stage.

5.4.1.6 S8FS and S8FR-1 and -2 Fuel Element Sequence[5.12]

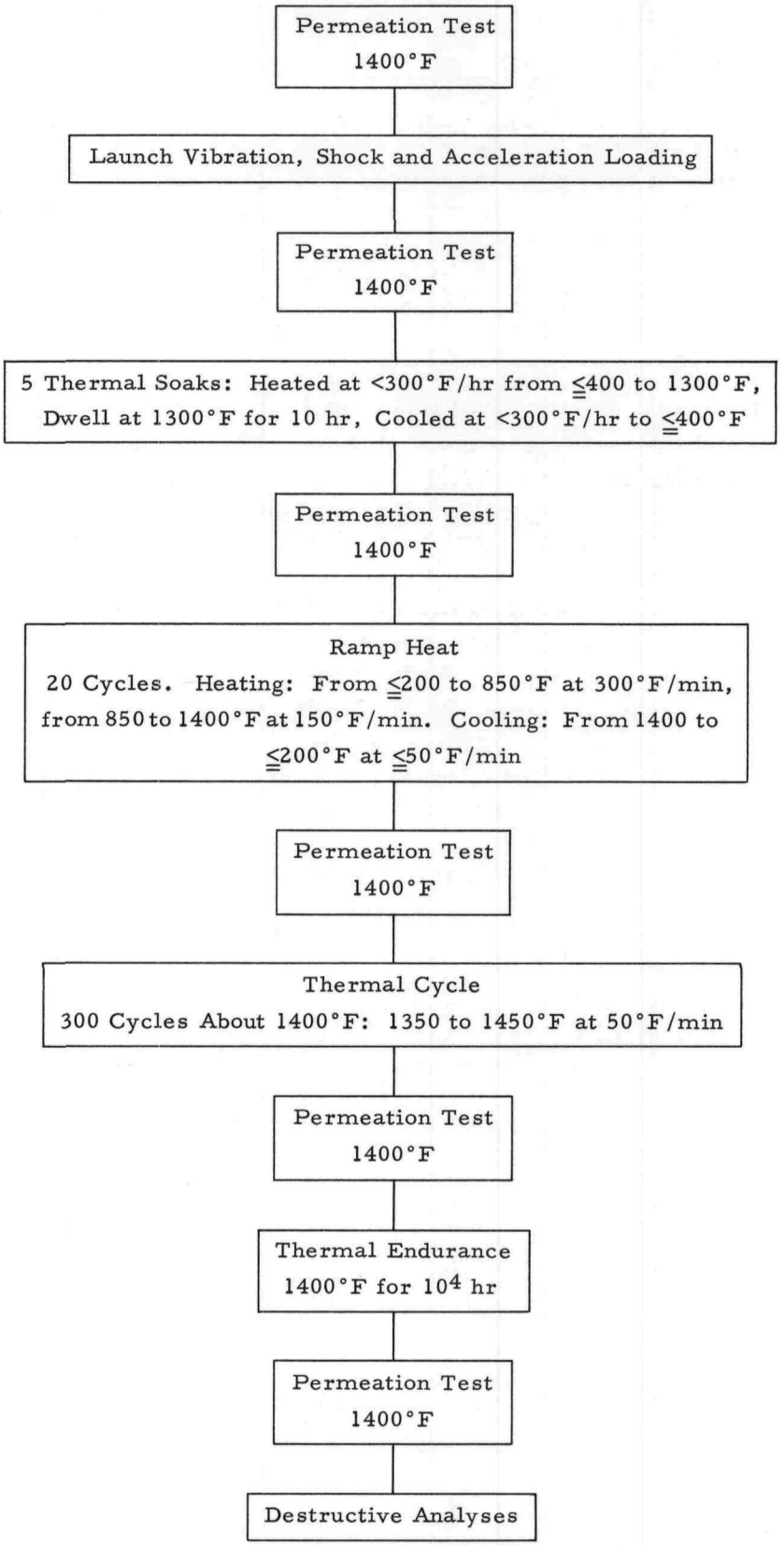

RESULTS: Design stage.

5.4.1.7 S8FR-3, -4, and -5 Fuel Element Sequence[5.12]

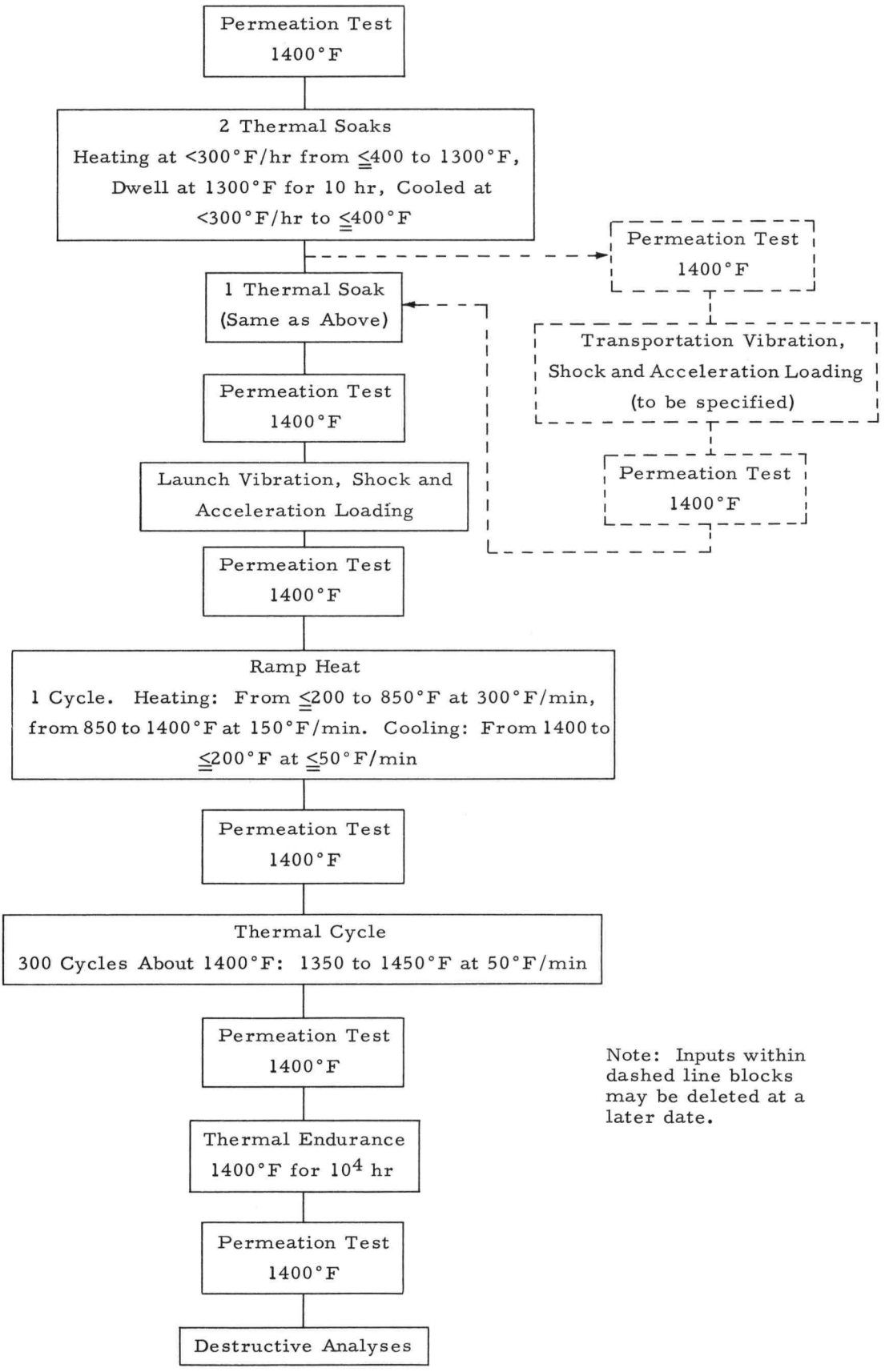

Note: Inputs within dashed line blocks may be deleted at a later date.

RESULTS: Design stage.

5.4.2 Environmental Testing

5.4.2.1 General Description

Environmental testing shall be done to establish the reliability of normal fuel elements and their components as a function of the severity of the environment, finally yielding the mode of failure and the ultimate capability of the fuel elements. Failure of a test element is defined as that point at which the hydrogen permeation rate exceeds the arbitrary value of 2.5 times the acceptance test limit.

5.4.2.2 SNAP 10A Fuel Element Sequence

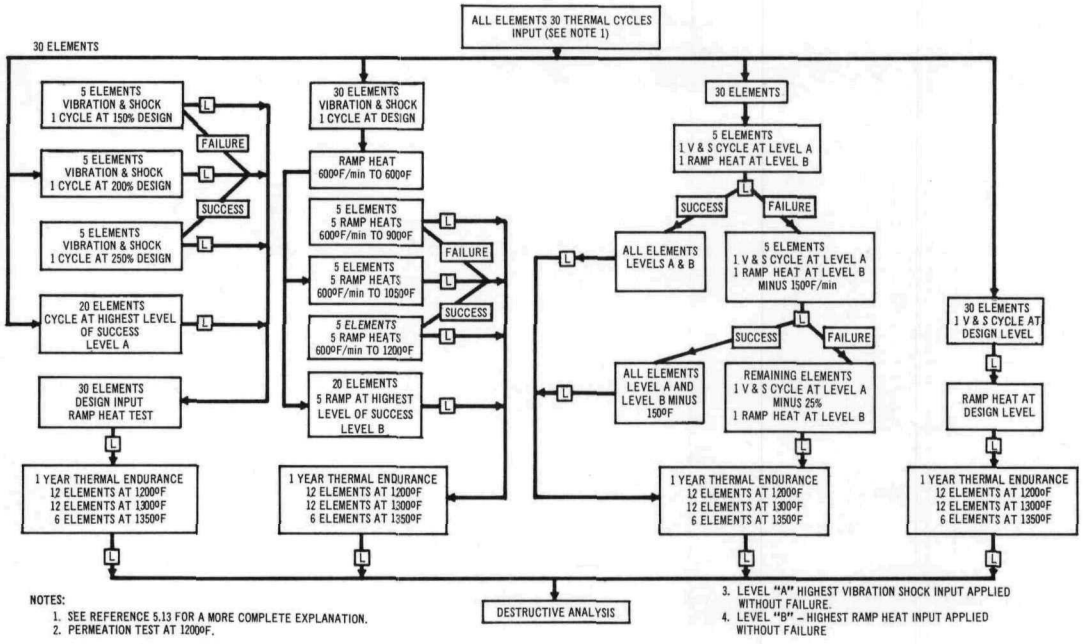

5.4.2.3 SNAP 8 Fuel Element Sequence[5.14]

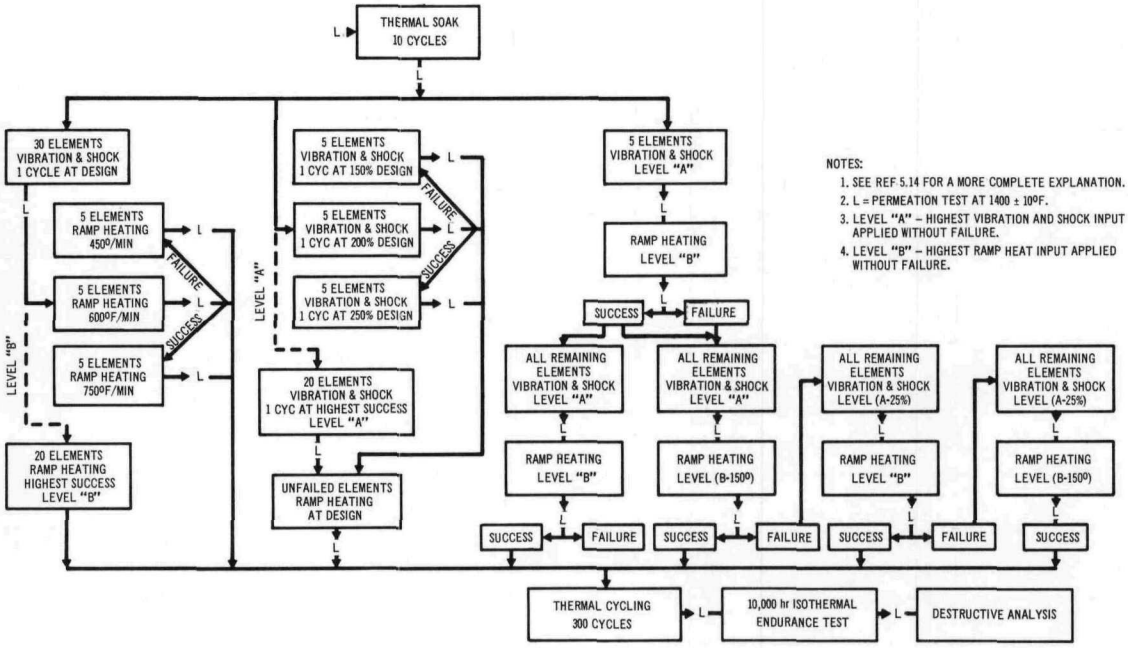

5.5 OPERATION

5.5.1 Irradiation Experiments [5.15]

5.5.1.1 Completed Experiments

Title	Purpose
1) NAA 26	Determine radiation effects on hydrogen dissociation pressure of hydrided zirconium fuel
2) NAA 43	Determine radiation stability of low N_H material as function of burnup level
3) NAA 53	Determine irradiation stability of SNAP 8 fuel as a function of temperature and burnup
4) AI 20	Determine the performance of SNAP 2 prototype elements under simulated reactor operating conditions
5) NAA 68-1	Determine the effect of neutron irradiation on hydrogen permeation through coatings by pre- and postirradiation permeation measurements

5.5.1.2 Experiments Being Performed

Title	Purpose
1) NAA 75	Determine the radiation stability of SNAP 4 fuel element configuration as a function of burnup at SNAP 4 operating temperature
2) NAA 77-1 through 4	Determine the effect of neutron irradiation on hydrogen permeation through coatings by in-pile permeation measurements
3) NAA 116	Determine the effect of composition variables on fission gas release and agglomeration by postirradiation annealing of fuel irradiated at low temperature
4) NAA 82-1	Determine the performance of SNAP 2 production elements under simulated reactor operating conditions
5) NAA 115-1	Determine the effect of temperature and major compositional variables on fuel element radiation stability at SNAP 8 burnup rate

5.5.1.3 Experiments to be Performed

Title	Purpose
1) NAA 82-2	Determine the performance of SNAP 2 production elements under simulated reactor operating conditions
2) NAA 115-2	Determine the effect of temperature and major compositional variables on fuel element radiation stability at SNAP 8 burnup rate
3) NAA 117	Determine the effect of temperature and major compositional variables on SNAP 8 fuel element radiation stability at an accelerated burnup rate
4) NAA 120	Determine the effect of temperature, burnup, and major compositional variables on fuel stability at high temperatures
5) NAA 121	Determine the performance of SNAP 8 production elements under simulated reactor operating conditions
6) NAA 77-5, -6	Determine the effects of neutrons on fission recoil on hydrogen permeation through coatings by in-pile permeation measurements.

5.5.1.4 Data on Completed Experiments

5.5.1.4.1 NAA 26*[5.15]

Test Number	3	4
Fuel Composition		
wt % Uranium	10	10
N_H	6.0	6.0
wt % Carbon	None	None
Specimen Description		
Size (Diameter x Length)	0.625 x 1	0.625 x 1
Number	2	2
Cladding	304 SS	304 SS
Coating	None	None
Instrumentation		
Temperature Control (Type)	Acme Thread	Acme Thread
Thermocouples (Number)	2	2
Pressure Transducer	Yes	Yes
Design Operating Conditions		
Total Radiation Exposure m at.%	0.04	0.04
Exposure Rate	-	-
Peak Surface Temperature, °F	-	-
Peak Center Temperature, °F	1300	1300
Reactor Facility	MTR	MTR
Data		
Avg. Central Temperature, °F	1285	1225
Avg. Surface Temperature, °F	1250	1190
Apparent Burnup, m at.%	0.027	0.034
Radiochem. Burnup, m at.%	0.022	0.028
Change in H_2 content, %	- 3.9	- 3.9
Dimensions	-	-
In-pile H_2 Pressure	Agreed with isochore plot[5.17]	

*NAA 26-1 and -2 aborted due to excessive temperature

5.5.1.4.2 NAA 43*(5.15)

Test Number	3	5	6
Fuel Composition			
wt % Uranium	10	10	10
N_H	3.8 to 4.0	3.8 to 4.0	3.8 to 4.0
wt % Carbon	none	none	none
Specimen Description			
Size (Diameter x Length)	0.187" x 2.50"		
Number	2	2	1
Cladding	304 SS	304 SS	304 SS
Coating	none	none	none
Instrumentation			
Temperature Control (Type)	none	none	none
Thermocouples (number)	6	6	3
Pressure Transducer	No	No	No
Design Operating Conditions			
Total Radiation Exposure m at.%	0.75	2.5	2.0
Exposure Rate, Fissions/cc-sec	4.2×10^{13}	4×10^{13}	4.2×10^{13}
Peak Surface Temperature, °F			
Peak Center Temperature, °F	650 to 1300	650 to 1300	1300
Reactor Facility	MTR	ETR	MTR
Data			
Avg. Fuel Central Temperature, °F	450 to 950	650	650
Radiochem. Burnup, m at %	0.95		

5.5.1.4.3 NAA 53(5.15, 5.21)

Test Number	1 Lower	1 Upper	2 Lower	2 Upper	3 Lower	3 Upper
Fuel Composition						
wt % Uranium	10					
N_H	6.0					
wt Carbon	None	None	None	None	0.5	0.5
Specimen Description						
Size (Diameter x Length)	.188 x 2.50					
Number	1					
Cladding	304 SS	304 SS	304 SS	304 SS	Hast N	Hast N
Coating	Solaramic S14-35A				8763D	8763D

*NAA 43-1 was irradiated to a design burnup of 0.25 m at.% and NAA 43-2 was irradiated to a design burnup of 0.50 at.% but were not examined because NAA 43-3, irradiated to a higher burnup, showed no major radiation damage. NAA 43-4 aborted on initial reactor insertion.

5.5.1.4.3 NAA 53[5.15, 5.21] (Continued)

Instrumentation						
Temperature Control (Type)	Heaters					
Thermocouples (Number)	8	8	8	8	8	7
Pressure Transducer	No	No	No	No	Yes	No
Design Operating Conditions						
Total Radiation Exp., m at.%	0.5	0.5	1	1	0.4	0.4
Exposure Rate, Fiss/cc-sec				3.6×10^{13}		
Peak Surface Temperature, °F	1150	1250	1150	1250	1200	1250
Peak Center Temperature, °F	1300	1500	1300	1500	1400	1500
Reactor Facility	MTR					
Data						
Avg. Central Temperature, °F	1472	1300	1213	1444	1411	1515
Avg. Surface Temperature, °F	1370	1226	1133	1359	1302	1409
Apparent Burnup, m at.%	0.69	0.60	1.13	1.26	0.43	0.43
Best Estimate Burnup, m at.%	0.52	0.68	1.03	0.97	0.30	0.36
Fission Gas Release, %	-	0.13	0.14	0.17	~0	-
$\Delta\rho/\rho$, %	-3.6	-1.3	-4.5(a)	-8.8	2.5	2.7
$\Delta L/L + 2\,\Delta D/D$, %	-	-	-	8.2/10.9(b)	2.8	2.4
$\Delta V/V$, %(c)	6.4	3.5	11.1	10.8	3.3	2.4

(a) Defect in cladding allowed NaK to leak in.
(b) 8.2% by caliper measurements, 10.9% by optical measurements.
(c) Assuming isotropic expansion, i.e., $\Delta V/V = 3\,\Delta D/D$.

5.5.1.4.4 AI 20[5.15]

Test Number	1	2
Fuel Composition		
wt % Uranium	10	10
N_H	6.5	6.5
wt % Carbon	None	None
Specimen Description		
Size (Diameter x Length)	1.212 x 10.0	
Number	1	1
Cladding	Hast N	Hast N
Coating	Solaramic S14-35A	
Instrumentation		
Temperature Control (Type)	Gas	Gas
Thermocouples (Number)	10	10
Pressure Transducer	No	No

5.5.1.4.4 AI 20[5.15] (Continued)

Design Operating Conditions		
Total Radiation Exposure, m at.%	0.05	0.05
Exposure Rate, Fiss/cc-sec	5.7×10^{11}	5.7×10^{11}
Peak Surface Temperature, °F	1200	1200
Peak Center Temperature, °F	1330	1330
Reactor Facility	WTR/GETR	GETR
Data	(b) (c)	(a)

(a) AI 20-2 aborted early in the first reactor cycle.
(b) AI 20-1 started irradiation in the WTR and was transferred to GETR after the WTR shut down operations.
(c) Aborted from reactor due to flux peaking and excessively high temperatures in the fuel element. Temperatures well in excess of 1500°F are expected to have occurred in unmonitored portions of the fuel element.

5.5.1.4.5 NAA 68-1[5.15, 5.21]

Test Number	1
Fuel Composition	None
Wt % Uranium	-
N_H	-
Wt % Additive	-
Specimen Description	
Size (diameter x length)	0.562 x 14.75 in.
Number	2
Cladding	Hastelloy N
Coating	AI8763D
Instrumentation	
Temperature Control (type)	Heaters
Thermocouple (number)	12
Design Operation Conditions	
Total Radiation Exposure	1.4×10^{21} nvt ($E_n > 1$ mev)
Exposure Rate	1×10^{14} nv ($E_n > 1$ mev)
Peak Surface Temperature	1200°F
Peak Center Temperature	-
Reactor Facility	ETR
Data	
Average Surface Temperature	1000°F upper
	1200°F lower
Accumulated time	~3700 hr
Radiation Dose	1×10^{21} nvt ($E_n > 1$ mev)
Results	(a)

(a) Permeation data and visual observation indicate no gross change to coating.

5.5.2 Reactor Operation

5.5.2.1 Summary of S2ER Operation[5.16]

Title	Results
Initial Fuel Loading	September 17, 1959
Final Shutdown	November 19, 1960
Elapsed time during testing (hr)	10,306
Reactor operating time (hr)	6,035
Operation at 50 kwt and 1200°F core outlet temperature (hr)	1,877
Operation at 50 kwt and less than 1200°F core outlet temperature (hr)	2,290
Operation at less than 50 kwt and less than 1200°F core outlet temperature (hr)	1,868
Reactor down time (hr)	4,271
Total Energy generated (kwh)	224,600
Equivalent time at 50 kwt (hr)	4,493

5.5.2.2 Summary of Postirradiation S2ER Fuel Element Examinations[5.16]

Type Examination	Comments
Number Examined	61 during disassembly; 6 for complete examination listed below.
Visual	Virtually unchanged; no compatibility problems.
Burnup Analyses	Gamma scanning and Cs^{137} analyses do not agree; Gamma scanning appears to be the most reliable.
Hydrogen Permeation	Permeation rate increased drastically probably due to rough handling after irradiation.
Dimensional Measurements	Diameter unchanged within experimental accuracy.
Density	One element was unchanged, another decreased in density, 0.6 to 1.5%, probably due to microcracking.
Fission Gas Release	Less than limits of detection.

5.5.2.3 Summary of S8ER Operation as of April 1, 1964[5.20]

Initial Fuel Loading (Dry)	May 19, 1963
(Wet)	June 2, 1963
Final Shutdown	-
Elapsed Time Since Startup (hr)	7,297
Reactor operating time (hr)	3,195
Operation at 600 kwt and 1300°F core outlet temperature (hr)	74
Operation at 450 kwt and 1300°F core outlet temperature (hr)	634.2
Reactor down time (hr)	4,102
Total Energy Generated (kwh)	959,996

REFERENCES

5.1 N. H. Katz, "SER Data Report," NAA-SR-MEMO-4722, December 10, 1959 (SRD)

5.2 P. S. Drennan and W. Sawicky, "Summary of Test Data for S-2 DR Fuel Elements," NAA-SR-MEMO 6745, September 15, 1961 (SRD)

5.3 C. J. Smiley, "SNAP 2 and 10A Fuel Elements," NE10FS1-18-001, March 12, 1962 (SRD)

5.4 M. A. Harten, "S8ER Fuel Element Assembly," 8ER1-100-001, March 12, 1962 (SRD)

5.5 H. Brager, "Specification for S8DRM1 Nuclear Element Assembly," NS8DRM1-18-001, April 4, 1963 (SRD)

5.6 "S8DS-1 Fuel Element Specification," NR 7568-07, unpublished (SRD)

5.7 D. C. Campbell, et al, "SNAP 10A FS-1 Fabrication Process Sheets and Auxiliary Forms," NAA-SR-MEMO-8272, February 15, 1963 (SRD)

5.8 C. R. Hoff and D. L. Henry, "Specification for SNAP Fuel Alloy Hydriding," NA0611-001, unpublished (SRD)

5.9 D. C. Campbell, et al, "SNAP 8ER Fabrication Process Sheets and Auxiliary Forms," NAA-SR-MEMO-8273, February 15, 1963 (SRD)

5.10 D. F. Atkins and D. L. Henry, "Specifications for S8DRM-1 Fuel Element Assembly," NA0622-001, August 8, 1963 (SRD)

5.11 T. G. Parker, Jr., "SNAP 10A Fuel Element Qualification Test Specification - Type 2", NA0422-008, May 7, 1963

5.12 A. J. Fitzgerald, "Procedures for Qualification Testing Fuel Elements for SNAP 8 Reactors," NA0210-001, March 26, 1963

5.13 D. H. Stone, "SNAP 10A Fuel Element Environmental Test Specification," NA0422-005, Revision A, March 10, 1964 (CRD)

5.14 D. H. Stone, "SNAP 8 Fuel Element Environmental Testing," NA0422-007, April 23, 1963 (CRD)

5.15 G. D. Calkins, to Those Listed, "SNAP Fuels Irradiation Experiments Summary," 64IL319, January 13, 1964 (SRD)

5.16 J. R. Miller, "Postirradiation Evaluation of SER Fuel Elements," NAA-SR-8090, May 1, 1963 (SRD)

5.17 D. F. Atkins, Dissociation Pressure of Hydrided Zirconium Uranium Alloys, NAA-SR-4245 (Del) 1960

5.18 M. E. Nathan to J. D. Watrous, Personal Communication, Atomics International, A Division of NAA, Canoga Park, Calif., November, 1963

5.19 H. A. Evans to G. F. Burdi, "Preliminary Investigation of SNAP 10A Fuel Rod Hydrogen Permeation Data," 64-IL-339, Atomics International, A Division of NAA, Canoga Park, Calif., July 1964 (SRD)

5.20 L. M. Fead to G. F. Burdi, Personal Communication, Atomics International, A Division of NAA, Canoga Park, Calif., April 3, 1964

5.21 R. C. Courtwright and C. J. Engberg, Personal Communication, Atomics International, A Division of NAA, Canoga Park, Calif., June 1, 1964